Fall 8-22-2017

CHARACTERIZATION OF ASPHALT HEALING AND INCORPORATION IN A FATIGUE DAMAGE MODEL

Umme A. Mannan
University of New Mexico

Recommended Citation

Mannan, Umme A.. "CHARACTERIZATION OF ASPHALT HEALING AND INCORPORATION IN A FATIGUE DAMAGE MODEL." (2017). https://digitalrepository.unm.edu/ce_etds/192

Umme Amina Mannan

Candidate

Civil Engineering

Department

This dissertation is approved, and it is acceptable in quality and form for publication:

Approved by the Dissertation Committee:

Rafiqul A. Tarefder, Chairperson

Tang-Tat Ng

Mahmoud R. Taha

Yu-Lin Shen

CHARACTERIZATION OF ASPHALT HEALING AND INCORPORATION IN A FATIGUE DAMAGE MODEL

by

UMME AMINA MANNAN

B. S. in Civil Engineering (2009)
Bangladesh University of Engineering & Technology (BUET), Dhaka, Bangladesh

M. S. in Civil Engineering (2012)
University of Akron, Akron, OH, USA

DISSERTATION

Submitted in Partial Fulfillment of the
Requirements for the Degree of

**Doctor of Philosophy in
Engineering**

The University of New Mexico
Albuquerque, New Mexico

December, 2017

DEDICATION

To my parents for their support and encouragement

ACKNOWLEDGEMENT

I would like to express my sincere gratitude to my dissertation committee chair and supervisor Dr. Rafiqul Tarefder, for his support, advice, guidance and encouragement throughout my Ph.D. study. It has been a great privilege to work with him. Dr. Tarefder gave me the confidence, opportunity and most importantly the freedom to explore on my own. Without his guidance and persistent help this dissertation would not have been possible.

I would like to extend my gratitude to my dissertation committee members: Drs. Tang-Tat Ng, Mahmoud R. Taha and Yu-Lin Shen. I appreciate their insight into my research and helpful suggestions. I would like to acknowledge Dr. Howard Schreyer, Professor Emeritus, UNM for sharing his knowledge on constitutive modeling and guiding me in developing the constitutive equations for the fatigue damage and healing in asphalt binder.

This study was funded by the New Mexico Department of Transportation (NMDOT). Also, I would like to thank Sharon Boyd from Department of Chemistry at UNM to help me in the Thin Layer Chromatography analysis of asphalt binder. I would like to acknowledge the academic support from the Civil Engineering department at University of New Mexico. Special thanks to all my colleagues, staff, faculty and friends at UNM for their help and encouragement.

Finally, I owe the greatest thanks to my family: my parents, my siblings and my husband for their unconditional support. A sincere thank you to my husband Mustafa Salman for his support, patience and encouragement during my difficult times; without his support, I could not have completed this dissertation.

Characterization of Asphalt Healing and Incorporation in A Fatigue Damage Model

By

Umme Amina Mannan

B.Sc., Civil Engineering, Bangladesh University of Engineering and Technology, 2009

M.S., Civil Engineering, University of Akron, 2012

Ph.D., Engineering, University of New Mexico, 2017

ABSTRACT

Healing is defined as the restoration of the material property during the rest period after damage. The healing property of the asphalt binder is opposite to fatigue damage, which occurs due to repeated traffic loading. On the other hand, healing occurs in the rest period between loading. Most of the existing methods for characterizing the fatigue damage and healing of asphalt are empirical in nature and do not consider the mechanism of healing. Although the asphalt concrete is a mixture of asphalt binder, fines and aggregates, most of the healing occurs in the asphalt binder. Therefore, it is important to understand the healing mechanism of the asphalt binder. In this study, the healing mechanism and the effects of several factors and asphalt chemistry are discussed. Then a constitutive fatigue damage model is developed with the incorporation of healing.

The overall healing has two parts: instant healing and long-term healing. Instant healing is defined as the instantaneous recovery of damage at the beginning of the rest period due to the wetting of the micro-crack surfaces. Wetting is the process of the crack surfaces coming in contact with each other. It depends on the cohesive strength of the asphalt binder. In this study, energy of separation from tack test is used as a measure of the

cohesive strength of the asphalt binder. It is observed that the instant healing is directly proportional to the energy of separation, which is correlated to the asphaltene and resin contents of the binder. Asphaltenes and resins represents larger molecules in the asphalt binder. An increase in the larger molecules in the binder reduces their mobility, which results in a decrease in wettability and instant healing. On the other hand, long-term healing is the time dependent recovery of damage over the rest period due to the inter-molecular diffusion at the micro-crack surfaces. The molecular diffusion rate depends on molecular chain length. In this study, molecular chain length is measured as the methylene to methyl ratio using Fourier Transform Infrared (FTIR). This study shows that the long-term healing rate of the asphalt binder is proportional to the molecular chain length.

The effects of aging and moisture conditioning on the healing of asphalt binder is also studied. Results showed that aging and moisture conditioning decrease both instant and long-term healing, resulting in a reduction in overall healing. The grade of the performance grade (PG) binders has significant effect on aging and moisture conditioning. The effects of different filler contents are studied for two different PG binders. Results showed that mastic healing is mostly controlled by the asphalt binder type. The instant and long-term healing of the mastics decrease with the addition of filler. This is expected since the addition of fillers decreases the molecular mobility by interrupting the continuous binder medium, resulting in a decrease in wettability and diffusion rate in the mastic.

In this study, a constitutive damage model is utilized to incorporate the healing and fatigue damage of the asphalt binder under cyclic shear loading with and without rest period. Healing is incorporated as a variable in this model. Shear loading is considered since previous studies showed that the force-interaction between the wheel and the

pavement generates shear stress, which affects the fatigue damage the most. Motivated by experimental observations, the proposed model divides overall damage evolution into two parts: recoverable and permanent damage. The micro-damage healing is captured by the decrease in recoverable damage during rest periods. At the same time, this damage and healing model is coupled with the viscoelastic and viscoplastic model to simulate the non-linear behavior of the asphalt binder. For continuous loading, initially the permanent damage is almost close to zero. It accumulates with continuous loading which eventually results in the failure of the material. For loading with rest period, the recoverable damage heals during the rest period, resulting in a reduction in overall damage. However, after repetitive loading-rest period sequences the healing decreases and permanent damage becomes larger. The model prediction agrees with the experimental measurements under cyclic loading with and without rest periods. Thus, the model developed in this study can capture the overall response of the asphalt binder under cyclic or repetitive loading with and without rest period. The incorporation of healing in the damage model will provide an accurate measure of fatigue damage in the asphalt binder.

TABLE OF CONTENT

LIST OF FIGURES

LIST OF TABLES

CHAPTER 1

INTRODUCTION

1.1 Problem Statement

Healing is defined as the restoration of the material property during the rest period after damage. It is necessary to define damage first in order to understand healing. This study focuses on repetitive cyclic loading, therefore fatigue damage will be defined instead. Fatigue damage is a phenomenon in which material properties degrade due to repeated loading. Under repeated loading, asphalt binder can show elastic, viscoelastic and viscoplastic deformations, which cause fatigue damage in the binder. During the rest period, viscoelastic recovery and healing of the micro-damage occur simultaneously. However, viscoelastic recovery occurs at any loading level with or without damage whereas healing only occurs if there is some damage. To this day, only the viscoelastic recovery has been considered in the constitutive equation, but healing has not been considered in the constitutive equation. It needs to be incorporated in the constitutive equation of damage to accurately measure the fatigue damage in the asphalt material, which is the focus of this study.

Previous studies showed that the fatigue performance obtained from the laboratory testing of the asphalt concrete (AC) is significantly different from its field fatigue performance (Bateman 2012; Little et al. 1999; Tarefder et al. 2013). This difference, which varies by a factor between 3-100, is probably because part of the fatigue damage heals. In the field, when any point of the pavement section goes under repetitive traffic loading, there is always a rest period between loads. If these two loads are from the two sets of tires (front, rear) of the same vehicle, then the rest period depends on the axle distance between them and the speed of the vehicle. If these two loads are from two different vehicles (e.g., from the rear tire of one vehicle and the front tire of a second vehicle), then the rest period depends on the frequency of traffic. Thus, in the asphalt pavement, traffic loading with variable rest period is controlled by the vehicle speed, loading, axle distribution and gap between one traffic to the next. During these rest periods, healing occurs and causes recovery of damage (Carpenter and Shen 2006). Most of the previous studies used fatigue testing without any rest period simply to reduce the testing time (Bateman 2012; Mannan et al. 2015a). As a result, the laboratory-predicted fatigue damage is 3 to 100 times higher than the field fatigue damage. A study by Maillard et al. (2004) using ultrasonic waves through an asphalt film showed that a considerable amount of healing occurred after each loading cycle. Nishizawa et al. (1997) concluded that at low magnitude of loading, minor fatigue cracks can heal completely. Since healing of the fatigue damage is found to be significant in evaluating the fatigue performance of the asphalt pavements, it is highly desirable to quantify the amount of healing and incorporate it into the fatigue damage model of asphalt.

Asphalt concrete consists of three components: binder, mastic (mixture of fillers/fines and asphalt binder), and aggregate. Performance of AC is essentially the combined performance of all three components. Figure 1.1 shows a laboratory compacted AC sample and a schematic of the AC components. Previous studies identified that healing mostly occurs in the asphalt binder and mastic as these components work as a cohesive medium in AC (Cheng et al. 2002; Little et al. 1997). However, why or how healing occurs in the binder and mastic is not clear from the past studies. Asphalt binder has a very complex chemical composition which affects the overall mechanical behavior of the asphalt and therefore controls the performance of AC. To understand healing, it is necessary to find if the chemical composition and rheological properties of asphalt affects the healing. Aging and moisture conditioning of the asphalt binder can change the chemical orientation of the bonds inside the asphalt molecular structure, which may affect healing. The effects of different factors such as temperature, damage level and rest period on healing have been previously studied by comparing the experimental data (Bhasin et al. 2008; Little and Bhasin 2007; Shen et al. 2010). Therefore temperature, rest period and damage level will not be examined in this study. However, little is understood about the effects of aging and moisture on healing of the binder and have not been studied yet. Therefore, these factors will be investigated in this study.

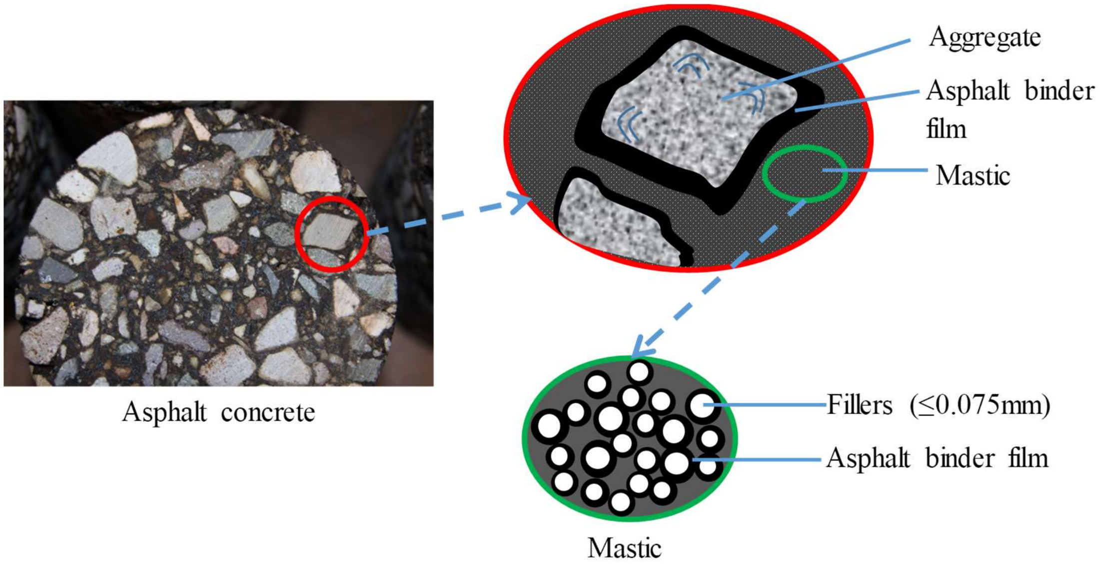

Figure 1.1: Asphalt Concrete (AC) components

It is very important from the safety and economic point of view to understand how much healing occurs in the binder and the mastic. If the mastic heals less than the binder, the asphalt production industry can simply design an asphalt mix containing smaller amount of mastic. Similarly, one can try to reinforce the binder portion more than the other components to increase healing. Very little has been done to identify to what extent the binder chemistry is affected by the amount of filler content which may reduce the healing capacity of AC. Therefore, healing of mastic is also studied in this dissertation.

Previous studies have coupled viscoelastic-viscoplastic models with the damage model by Schapery (1975) to predict fatigue damage (Bai et al. 2014; Darabi et al. 2012; Gibson 2006; Kim and Little 1990; Lee et al. 2000; Levenberg 2009; Park et al. 1996; Park and Schapery 1999). However, healing was not included in these damage models and only tensile loading conditions were considered. Whereas in realistic loading case, fatigue damage occurs due to the development of shear stress in the asphalt binder and mastic. Therefore, a novel damage and healing model coupled with viscoelastic–viscoplastic model is developed in this dissertation.

1.2 Hypothesis

1.2.1 Hypothesis One

Previous studies have attempted to study the effects of temperature, damage level etc. on the healing of the asphalt binder. However, how the asphalt chemistry and other factors such as aging and moisture affect the healing has not been studied so far. It is hypothesized that asphalt binder healing is affected by asphalt chemistry and several factors such as aging, moisture and filler content in mastic.

1.2.2 Hypothesis Two

There has been a considerable gap between the field and laboratory fatigue damage. In the field healing occurs which reduces the fatigue damage compared to the laboratory-predicted fatigue damage. It is hypothesized that the incorporation of healing in the damage model can provide more accurate prediction of fatigue damage in asphalt.

1.3 Scope and Objectives

The scope of this research is to investigate healing in the asphalt binder and mastic through laboratory testing and incorporate the healing in a fatigue damage model for accurate prediction. Specific objectives are:

1. Determination of the effects of healing in fatigue damage of asphalt.
2. Identification of the healing mechanisms by relating the asphalt binders' chemical and physical properties.
3. Determination of the effects of aging, moisture and filler contents on the asphalt binder and mastic healing.
4. Development of a damage model considering healing coupled with viscoelastic–viscoplastic material properties.

1.4 Outline of the Dissertation

This dissertation is divided into eight chapters. Chapter 1 summarizes why this study is important, the research hypothesis and objectives. Chapter 2 provides the current pool of literature on the healing and fatigue damage. Chapter 3 shows the effects of healing on the fatigue damage of asphalt. Chapter 4 discusses the chemical composition of asphalt binders. Chapter 5 discusses the healing mechanism from the mechanical and chemical point of view. Chapter 6 shows the effects of aging, moisture and filler content on healing of the asphalt binders and mastics. Chapter 7 develops a damage and healing constitutive model coupled with viscoelastic–viscoplastic model using experimental data. Chapter 8 summarizes the main findings of this study and provides a few recommendations for future work.

CHAPTER 2

LITERATURE REVIEW

2.1 General

Literature related to the healing of the fatigue damage in asphalt binder and asphalt concrete is documented in this chapter. Healing in the asphalt pavement has been studied for over two decades and many studies have tried to incorporate healing in the asphalt concrete experiments. However, most of the work related to healing have been done in the last five years, with the purpose of quantifying healing from the experimental results and instead of understanding the healing mechanism. Also, there has been more work on the healing of asphalt mixtures rather than asphalt binders. This chapter first provides a review of the different constituents in the asphalt binder structure and the effects of these constituents on the binder's overall mechanical properties. Then, a comprehensive literature review on the healing in asphalt is presented.

2.2 Asphalt Binder Chemistry and Structure

Asphalt binder is a complex blend of different hydrocarbon molecules, which contain small amounts of heteroatoms such as nitrogen (≤1%), oxygen (≤1%), sulfur (≤ 5%) and metals (e. g. nickel, vanadium, iron) (Robertson et al. 1991). Although the presence of heteroatoms is very small in percentage, the polarity in the asphalt binder is induced by these. One molecule of asphalt binder contains carbons between 20 to 110, which plays a significant role in the molecular weight and physical properties (Redelius and Soenen 2015). At the molecular level, the asphalt binder is a mix of high boiling point hydrocarbons: aliphatic, aromatic and a mixture of both aliphatic and aromatic (Robertson et al. 1991). Thus, asphalt binder can be separated into four generic fractions based on polarity as: saturates, aromatics, resins and asphaltenes (SARA) (Figure 2.1) (Groenzin and Mullins 2000; Lesueur 2009). The molecular weight of the fractions increase as saturates ≤ aromatics ≤ resins ≤ asphaltenes (Masson 2008).

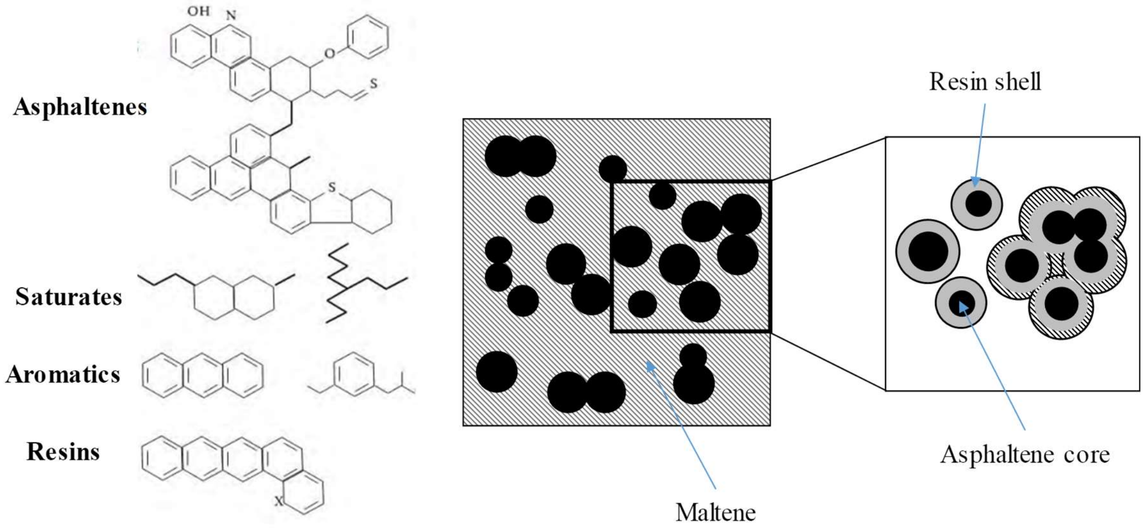

Figure 2.1: Molecular structure of the asphalt binder's four generic fractions (Lesueur 2009; Masson et al. 2001)

Due to this complex molecular structure of the asphalt binder, it is impossible to conduct a detailed chemical analysis with identification of one single molecules. Previous studies tried to identify the chemical composition and functional groups using ultraviolet spectroscopy (UV), infrared spectroscopy (IR), nuclear magnetic resonance (NMR) and mass spectroscopy (MS) (Branthaver et al. 1993a; Redelius and Soenen 2015). However, all of these techniques failed to explain the relationship between the chemical and physical properties, except the IR. Studies showed that IR can identify asphalt binder aging by indicating carbonyl and sulfoxide groups (Abbas et al. 2013; Mannan 2012). This is because asphalt binder aging is basically the oxidation at the molecular level, due to this oxidation the carbonyl and sulfoxide groups increases in the aged binder. Therefore, some researchers developed fractionization of the asphalt binder into different chemical fractions to understand it's chemical properties (Redelius and Soenen 2015). SARA analysis is the most commonly used separation technique, which separates the asphalt binder into four generic fractions based on their polarity (Jones 1993; Schmidt and Santucci 1966). In SARA analysis, first the asphaltenes and the maltenes are separated by dissolving the asphalt binder in n-alkanes (i.e. n-heptane, n-pentane). The non-soluble fraction in n-heptane is separated as asphaltenes. Maltenes consist of saturates, aromatics and resins. Afterwards saturates, aromatics and resins are separated using chromatography. Saturates contains paraffin, naphthene or a mixture of both. Aromatics contains paraffin, naphthene and aromatics with sulfur. Resin has a molecular structure with multi rings and more heteroatoms. Asphaltenes consist of polycycles of paraffin, naphthene, aromatics and heteroatoms (Schmidt and Santucci 1966). Previous studies showed that the chemical composition of the asphalt drives the binder's physical properties. For example, the asphaltene is responsible for viscosity, glass transition temperature and hardness of the binder (Puig et al. 2004; Storm et al. 1996). The properties of each of these fractions are discussed below:

Saturates: Saturates are colorless or lightly colored liquid at room temperature, typical PG grade asphalt binders contains 5-15% of saturates (Corbett 1969). Their average molecular weight is about 600 g/mol and they are mainly aliphatic. Their density at 20°C is around 0.9 g/cm^3 (Corbett 1969).

Aromatics: Aromatics are yellow to red liquid at room temperature and typically asphalt binder contains 30-45 % of aromatics (Corbett 1969). Their average molecular weight is about 800 g/mol and their density is close to 1 g/cm^3 at 20°C (Corbett 1969).

Resins: Resins are black solid at room temperature and typically found 30-45 % in the asphalt binder depending on the solvent used for separation (Corbett 1969). The composition of resins is close to that of the asphaltenes except that resins has lower molecular weight approximately 1,100 g/mol. Their density at 20°C is about 1.07 g/cm^3 (Corbett 1969). As asphaltenes are surrounded by resins, thus resins play very important role in the stability of asphalt binder.

Asphaltenes: Asphaltenes are black powder at room temperature and typical asphalt binders contains about 5 to 25 % of asphaltenes (Corbett 1969). Asphaltenes are the most studied fraction in the binder as they are responsible for the viscosity of the asphalt binder. Their average molecular weight is approximately 800-3,500 g/mol (Dickie and Yen 1967; Speight 2014; Speight and Plancher 1991). Their density at 20°C is close to 1.15 g/cm^3 (Corbett 1969). Asphaltenes play a significant role in building up the hardness and viscosity of the asphalt binder whereas maltenes develop the ductility and facilitate adhesion.

Different models have been proposed to explain the complex structure of the asphalt binder in past studies. Among these, the colloidal model proposed by Nellensteyn in 1924 is most commonly used (Lesueur 2009; Nellensteyn 1924). In this model, the higher-molecular weight asphaltenes are dispersed in lower-molecular weight maltenes. This model presents a two-phase system where the asphaltene micelles surrounded by the resins are dispersed in a continuous oily medium composed of the saturates, aromatics and dispersed part of the resins. If the asphaltene micelles are not interconnected, then the binder is sol-type binder and if the micelles are interconnected then the binder is gel-type binder (Pfeiffer and Saal 1940). The sol-type binder has a higher fraction of aromatic and saturates to disperse asphaltenes, and possess no network of micelles agglomeration. They show high ductility, low complex flows, and lower rates of age hardening. On the other hand, the gel-type asphalts have low ductility, increased elasticity and higher rate of age hardening. However, majority of the asphalt binders show a behavior between sol and gel type defined as sol-gel binder. Thus, this sol-gel structure of the asphalt binder can capture most of the rheological behavior. The gel-type binder shows interconnected molecular structure which results in less molecular mobility. Conversely, the sol-type binder shows more dispersed structure resulting in higher molecular mobility. As the mobility of the molecular structure is the most important part in healing, the sol-gel type binder may play a significant role in the asphalt binder healing.

2.3 Healing in Polymers

Self-healing is a well-known term in polymer science. Prager and Tirrell (1981) provided the definition of healing in polymers as follows: “When two pieces of the same amorphous polymeric material are brought into contact at a temperature above the glass transition, the junction surface gradually develops increasing mechanical strength until, at long enough contact time, the full fracture strength of the virgin material is reached. At this point the junction surface has in all respects become indistinguishable from any other surface that might be located within the bulk materials: we say the junction has healed.” Factors that affect the healing potential of any self-healing polymer are: temperature, rest period, damage level, aging and physical and chemical properties of the material (Wool 2008).

Self-healing polymers have the capability to repair damage without any external influence. Therefore, the self-healing polymers are mostly used for applications which involve exposure to fatigue loading (Jones and Dutta 2010). Several researchers have evaluated the self-healing ability of the polymer by conducting fatigue testing. In those fatigue tests, healing was quantified as the recovery of lost stiffness due to damage induced by cyclic loading (Kessler et al. 2003). They showed that healing extends the fatigue life of the polymer during the fatigue loading. Jones and Dutta (2010) presented two fatigue life models: one is a phenomenological model and the other one is a mechanics based fatigue model. In their study, they proposed a crack growth rate equation which is the difference between damage rate and healing rate.

Healing mechanism was found by Elber and Wolf (1971; 1970) based on crack closure of 2024-T3 aluminum alloy. Suresh (1991) categorized the healing mechanisms which promote retardation of fatigue crack growth. Healing can occur during both the loading and the rest period, but mostly occurs during the rest period. As the external load is removed, two processes take place: viscoelastic recovery and micro-cracks healing. The viscoelastic recovery happens due to the rearrangement of molecules in the material, while crack healing is the result of wetting (crack closure) and the inter-diffusion between the crack faces.

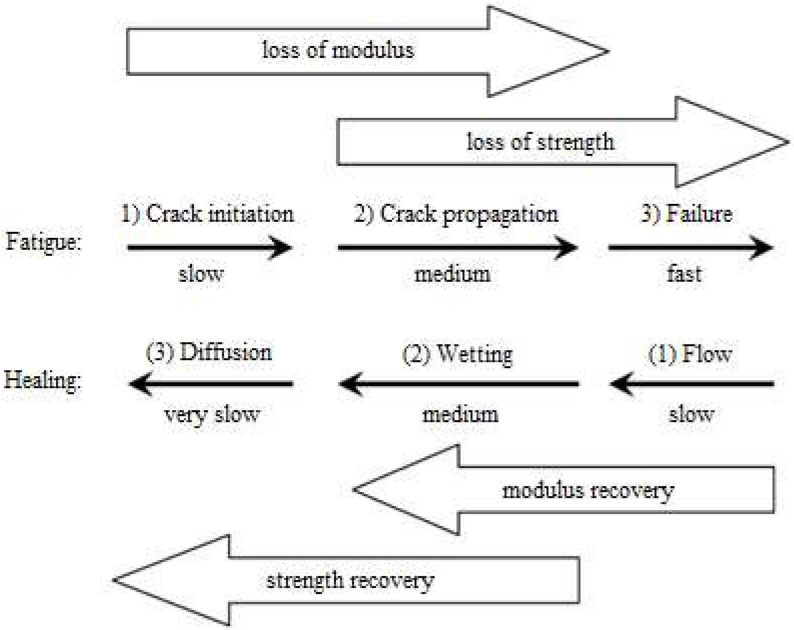

Figure 2.2: Steps in the fatigue and healing process (Phillips 1998)

Philips (1998) proposed a three-step process in the healing of asphalt binders as follows: wetting of the two faces of the crack (adhesion of crack faces due to the surface free energy), diffusion of the molecules between crack faces and complete recovery of strength and other mechanical properties due to the randomization of the diffused molecules. Figure 2.2 shows the steps in the fatigue damage and healing process. The wetting is believed to be the fastest among these and causes the stiffness and strength recovery in the material (Phillips 1998; Wool and O’connor 1981). Healing in polymer is a common phenomenon. However, healing is not commonly considered in asphalt, even though it may have a significant impact on the fatigue damage of the asphalt.

2.4 Healing in the Asphalt Concrete

This section provides a brief literature review of the previous works by other researchers on asphalt healing. Most of the research done so far is on asphalt concrete and only based on the laboratory testing. Since the beginning of the 1960s, many researchers have been trying to identify the healing phenomenon by conducting various kind of laboratory tests. A laboratory based research by Deacon (1965) showed that a reduction in the rest period time has a significant effect on the fatigue life. Other studies showed that longer rest period on damaged specimens increases the fatigue life of the samples (Bazin and Saunier 1967; Van Dijk and Visser 1977). Raithby and Sterling(1970) varied the rest period in an axial loading test and found that applying rest period of 40 ms to 800 ms increases the fatigue life of the specimens by five times on average. They also suggested an optimum rest period length beyond which no significant increase in the fatigue life would occur. Another research done by Raithby and Sterling (1972) showed that for rest periods greater than ten times the loading time, the fatigue life of the mixtures does not increase significantly. Bonnaure et al. (1982) used pulse-rest healing test to investigate fatigue life changes due to the rest period at different temperatures. They found that the rest period increases the fatigue life.

Lee and Kim (1998a) proposed a viscoelastic continuum damage (VECD) based constitutive model for the asphalt concrete that can be used for modeling the micro-damage healing as well as the rate dependent damage growth. To represent the induced damage in a specimen under cyclic fatigue test an internal state variable (ISV) is calculated from a rate type damage evolution law. Using controlled-strain tensile uniaxial cyclic tests with different strain amplitudes, they were able to derive the VECD model parameters. They also successfully verified the model by showing that their model was able to predict the damage growth and healing in the asphalt concrete.

Daniel et al. (2001) used third-point bending beam fatigue and impact resonance tests together to evaluate the effects of the mixtures type and temperature on micro-crack healing. To indicate the level of damage in the specimen pseudo stiffness and an internal state variable (ISV) from the viscoelastic continuum damage (VECD) theory were used. The horizontal shift from the dynamic modulus vs. number of cycle curve, indicate the increase in the fatigue life due to the rest period (Figure 2.3). The recovery after rest period was measured with respect to the modulus loss due to previous repetitive cycles.

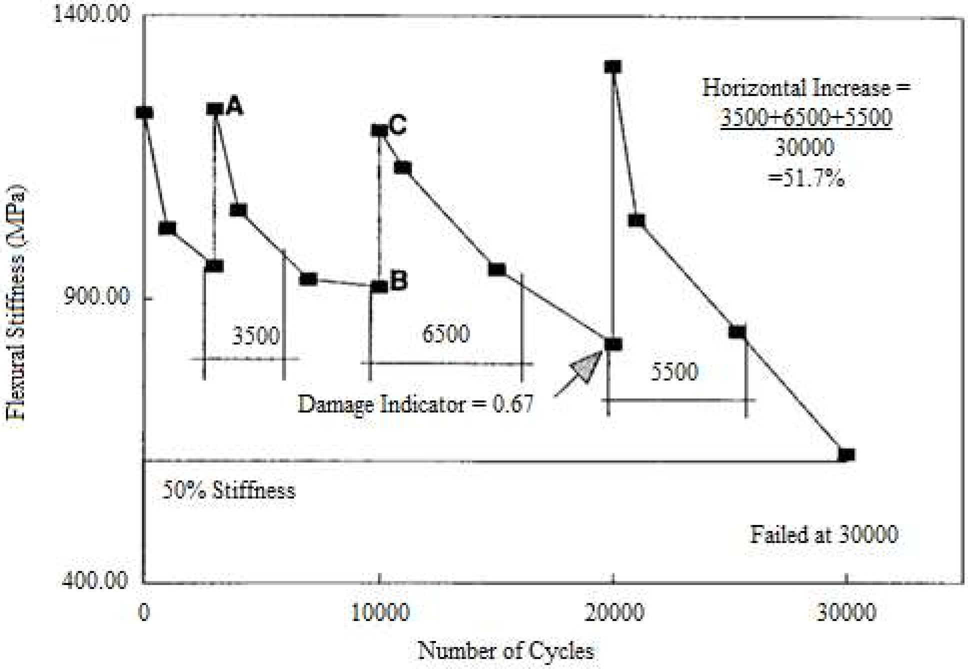

Figure 2.3: Graphical representation of Daniel's healing test result (Daniel and Kim 2001)

Zhang et al. (2001) used indirect tensile test (IDT) to investigate the effects of healing. In their study, both group-rest (12 hours rest) and pulse-rest (haversine load with 10 Hz frequency followed by a 0.9 second rest) were applied to the specimen. To prove that healing exists, they used a threshold concept based on the dissipated creep strain energy limit. Assuming that if the dissipated creep strain energy limit exceeds the threshold, macro-cracks may not heal. Grant (2001) also conducted IDT on two Superpave mixtures with fine blend and coarse blend at the temperatures of 10°C and 15°C. In his study, loading sequence was 0.1 second haversine load followed by a 0.9 second rest period. The results indicated that the healing rate was much higher at 15°C and in coarse mixture than that of at 10°C and in fine mixture, respectively.

Si et al. (2002) considered pseudo-stiffness to calculate the healing index. Healing index was defined as the increase in pseudo stiffness after each rest period. They used controlled strain repeated cyclic uniaxial tensile fatigue test with four different rest periods of 2, 5, 10, and 30 minutes. All the rest periods were applied after 1000 cycle intervals to investigate the effects of healing on micro-cracks. They showed that there is a healing effect in pseudo stiffness due to the rest periods which causes fatigue life extension.

Kim et al. (2002, 2003) used three different damage parameters to monitor damage and healing. Those parameters were: pseudo stiffness, dynamic modulus and dissipated strain energy. They used dynamic mechanical analysis (DMA) controlled-strain testing on two different sand asphalt mixtures. It was found that all the parameters were very useful for monitoring the healing. Their work also showed that the healing effect is most prominent when rest periods are applied at lower damage level (Figure 2.4).

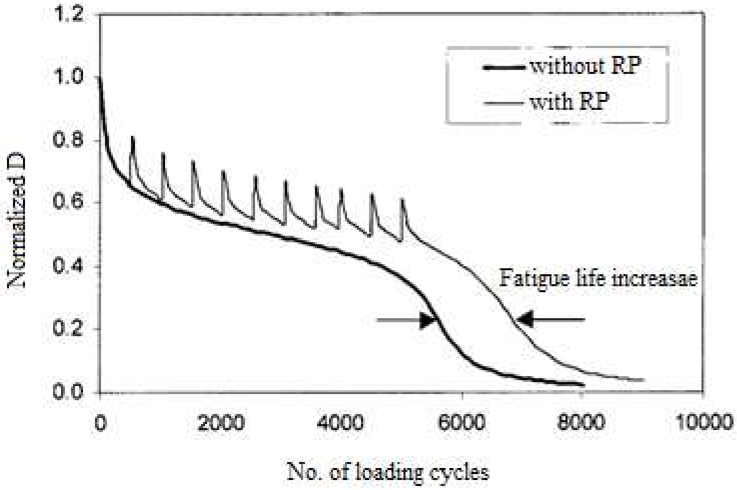

Figure 2.4: Normalized dynamic modulus vs. number of cycles (Kim et al. 2003)

Kim et al. (2006) studied healing characteristics of the asphalt binders in different asphalt mixtures in terms of the recovered dissipated creep strain energy per unit of time. Their study revealed that the total dissipated energy during the cyclic loading should not be used to calculate the fatigue damage because it includes both the irreversible (viscous) and reversible (elastic) dissipated energy. Only the irreversible dissipated energy contributes to the damage. They calculated the irreversible dissipated energy by using the rheological parameters obtained from static creep test data.

Castro and Sanchez (2006) carried out three-point flexural fatigue tests on beam specimens at controlled-displacement sinusoidal loading mode and defined the failure point when the final force was equal to half of the initial force. They conducted both continuous fatigue tests without rest periods and pulse-rest healing tests (a sinusoidal load for 0.1 second followed by a rest period of 1 second). They concluded that the healing during the rest period resulted an increase in the fatigue life by five to ten times.

Carpenter and Shen (2006) conducted intermittent pulse loading (figure 2.5) tests to observe healing by using four-point bending beam fatigue equipment. Their results showed that healing exists. The effects of healing on the fatigue life was measured by the energy recovered per second of rest period. They also concluded that the effect of healing is more prominent at low strain levels or long rest periods. At low strain, healing dominates compared to damage, so in this case full damage recovery is possible. This full recovery of energy explains the fatigue endurance limit.

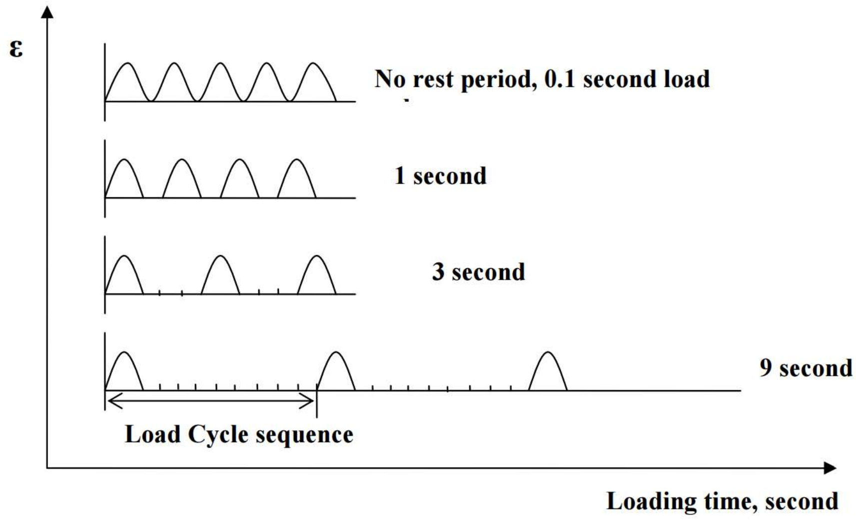

Figure 2.5: Load pulse sequence of fatigue-healing test (Carpenter and Shen 2006)

Little and Bhasin (2007) presented the healing mechanism using the phenomenological model. They suggested that healing is the cumulative effects of the wetting and the inter-diffusion of a crack. To quantify healing, they used the healing index defined as the ratio of change in the pseudo-strain energy to the pseudo-strain energy after the rest period. To incorporate the healing effects in the prediction of fatigue life of real pavements, they suggested an empirical equation which relates the measured fatigue life of the mixture in the lab to the one in the field by using a shift factor multiplier.

A study conducted by Liu et al. (2011) showed the induction heating can heal the broken sample under fatigue loading. They conducted their study on mastic beam samples. This study concluded that the induction heating causes an increase in the fatigue life as well as the healing rate of the asphalt mixtures. The authors believed that the induction heating caused the flow of the asphalt binder between the two cracked faces and thus the healing and strength recovery were achieved.

In a study conducted by Mamlouk et al. (2012), hot mix asphalt (HMA) fatigue and healing properties were investigated using four-point bending beam fatigue test. Tests were conducted at deflection-controlled mode with a loading frequency of 10 Hz, two strain levels and at three test temperatures (4°, 21° and 38°C). Both haversine and sinusoidal loading patterns with 5 and 10 second rest periods were applied on beam specimens. They concluded that the sinusoidal load pattern is more consistent and accurate because maintaining the haversine shape for stresses and strains during a test is not possible due to the permanent deformations.

Several researchers investigated the effects of inductive heating on the healing of asphalt mixtures in recent years (Ajam et al. 2016; Norambuena-Contreras and Garcia 2016; Zhu et al. 2017). All these studies defined healing as the stiffness or modulus of asphalt mixture before and after healing. Ajam et al. (2016) concluded that both electromagnetic induction and infrared radiation methods show about 90% healing rate.

The acoustic emission (AE) method was used by Seo and Kim (2008) in order to monitor damage accumulation and healing in the cyclic fatigue tests of the asphalt concrete.

Uniaxial tensile fatigue tests were conducted with and without rest periods at 20°C temperature. The results showed that the AE energy and AE counts obtained from sensors attached to the middle of specimens can identify the fatigue damage growth and quantify the healing effects in the asphalt concrete. Lee et al. (2011) conducted fatigue tests with rest periods on asphalt concrete slabs using third scale model mobile loading simulator (MMLS3) and evaluated the fatigue damage growth and the healing effect. Two nondestructive evaluation (NDE) techniques used in his study were stress wave velocity test and ultra-sonic pulse velocity test. Results showed that with an increase in the wheel application the phase velocity reduces and during the rest period it increases. They also concluded that most of the healing occurs during the initial 30 minutes of the rest period.

2.5 Healing in Asphalt Binder and Mastics

The healing of asphalt binder has been investigated by several researches based on the work done on polymer healing. Different methods have been developed to quantify healing. Bahia et al. (1999) applied cyclic loading on the asphalt binder using dynamic shear rheometer (DSR) and then rested the sample for 1 hour, 2 hours, and 12 hours at temperatures ranging from 20 °C – 40 °C to evaluate the effects of rest period on healing. However, such loading with long rest periods is not typical in the real field. Therefore, Carpenter and Shen (2009) proposed an intermittent loading sequence by applying short rest periods (2-9 seconds) after every loading cycle to the asphalt binder by using DSR test. Lytton, et al. (2001) proposed a micromechanics fracture and healing model for the asphalt based on the rate of change in the dissipated pseudo strain energy and the cohesive surface energy. Damage and healing were monitored using X-ray CT and Dynamic Mechanical Analyzer (DMA). Their continuum and micromechanics damage models pointed out three primary healing processes for asphalt: (1) wetting of the two faces of a nano-crack; (2) diffusion of molecules from one face to the other; (3) randomization of the diffused molecules in an attempt to reach the level of strength of the original material (Little and Bhasin 2007; Song et al. 2005).

A study conducted by Shen et al. (2010) investigated the fatigue and healing of the asphalt binder using a DSR. Stress-controlled test (60 kPa, 70 kPa, 180 kPa and 230 kPa) at one frequency (10 Hz) and three different rest periods (2 sec, 4 sec and 6 sec) were performed. The ratio of dissipated energy change (RDEC) approach was used as the fatigue and healing criteria. They concluded that the asphalt binder healing affects the fatigue performance in both qualitative and quantitative ways. Their study also evaluated the effects of temperature, stress level and binder type on healing. They demonstrated that healing increases with temperature increment and stress reduction. Additionally, modified binder has more healing potential than unmodified binder. Shan et al. (2010) used dynamic viscosity criteria to characterize fatigue and healing of the binder. Different terminal dynamic viscosity (20%, 40% and 60% of the initial value), different rest periods (1 hour, 6 hours, 12 hours, 24 hours and 48 hours) at 25 °C were used to evaluate the healing efficiency. Results showed that binder fatigue performance improves after a rest period and long rest periods accelerates the improvement.

A research group from Delft University worked recently on healing phenomena of binder, mastic, fine aggregate mixture (FAM) and asphalt mixture (Qiu et al. 2009, 2010, 2012). Qiu et al. (2009) investigated the healing potential in the asphalt binder. They used three different self-healing test procedures. In those three tests the crack was introduced in the body of the asphalt binder samples by using a knife (tests 1 and 3) or originally two samples of the binder were faced and pushed together to join with each other (test 2). For each test, the following equations were developed to quantify the cohesive healing:

$$P_{ductility}\% = \frac{L_{healed}}{L_{original}} * 100\% \tag{2.1}$$

$$P_{DSR}\% = \frac{M_{healed}}{M_{original}} * 100\% \tag{2.2}$$

$$P_{DTT}\% = \frac{S_{healed}}{S_{original}} * 100\% \tag{2.3}$$

where

$P_{ductility}\%$ = Ductility self-healing test

$P_{DSR}\%$ = Dynamic shear rheometer (DSR) self-healing test

$P_{DTT}\%$ = Direct tensile self-healing test (DTT)

L = Length of the sample;

M = Measured stiffness (modulus)

S = Measured maximum strength

Another study by Qiu et al. (2010) used DTT testing with healing and reloading to investigate the healing capacity of the asphalt mastic. They programmed the DTT machine to stop at predefined target elongations (TE) in the tested specimen in order to apply healing procedure and investigate self-healing capability of the specimen at different crack phases. Qiu et al. (2012) developed a test to investigate healing in asphalt mixtures. A beam on elastic foundation (BOEF) setup was sequentially loaded-healed-reloaded. Strength recovery and residual crack opening displacement (COD) recovery were used to quantify the healing phenomena in asphalt mixes.

Bhasin et al. (2011) used molecular dynamics (MD) simulation to investigate healing in the asphalt binders. They demonstrated the self-diffusivity of asphalt molecules across the crack interface which is one of the mechanisms of healing and is dependent on the chain length and degree of chain branching of the binder molecules. Lu (2013) investigated the asphalt healing at molecular level using molecular dynamics (MD) simulation. He concluded that the movements of the molecules quantify the diffusivity. In addition, it was showed that smaller cracks healed easily when the simulation systems contain the same number of molecules.

Palvadi et al. (2012) presented a new method for healing quantification in asphalt concrete using cylindrical FAM specimens. They used viscoelastic continuum damage (VECD) theory which was also successfully used for modeling fatigue damage growth in the asphalt mixtures by Lee and Kim (1998b). The FAM specimens (100 mm diameter and 75 mm height) were subjected to controlled-stress sinusoidal cyclic torsional loading tests with rest period (5, 10, 20 and 40 minutes) at 25°C and frequency of 10 Hz using DSR. Rest periods were applied to the specimen at 20%, 30% and 40% damage respectively. Figure 2.6 shows a typical curve for the fatigue test with a single rest period. Internal state variable (S) is an indicator of the fatigue damage growth and defined in VECD theory by Lee and Kim (1998b). Using the pseudo stiffness from the test result, the internal state variables after the rest period (S_f) and internal state variables before the rest period (S_i) were calculated. Then the percent healing was calculated using the following equation:

$$\%Healing\ (C,t) = \frac{S_f - S_i}{S_i} * 100 \qquad (2.4)$$

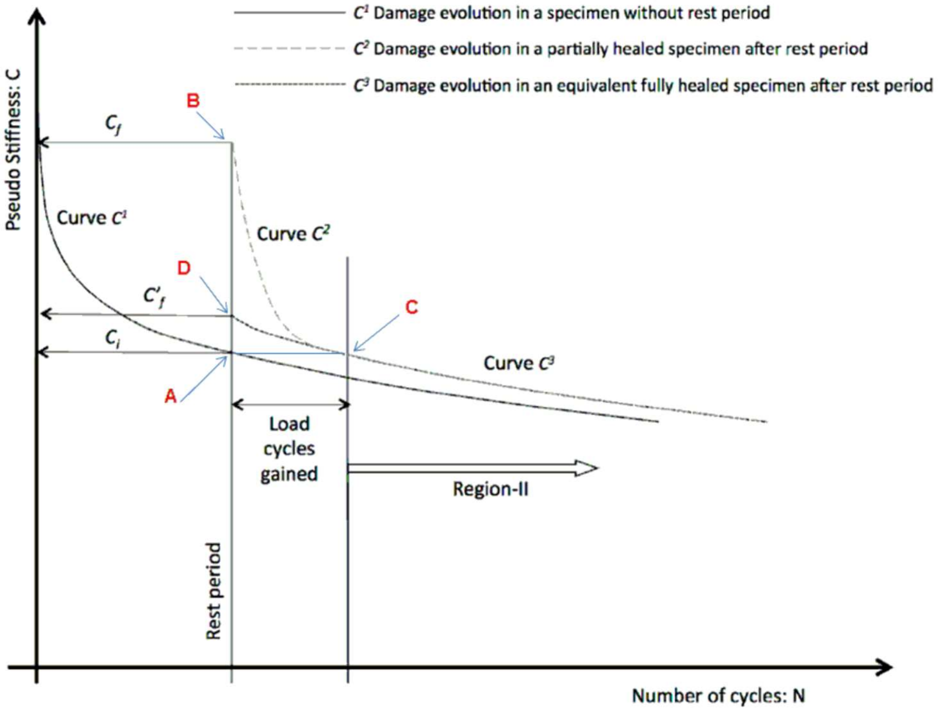

Figure 2.6: Single rest period applied in the middle of a fatigue test (Palvadi et al. 2012)

2.6 Self-Healing Models

In the literature two types of self-healing models can be found for polymer and asphaltic materials. One of them is called the physical-chemical healing model, which is a conceptual model to explain the healing phenomenon using physical and chemical theories. The other one is called the mechanics based healing model, which is a regression model based on continuum damage state. Details of these two models are discussed below:

2.6.1 Physico-Chemical Based Healing Model for Polymer

Healing of polymers has been the subject of extensive research since the 1980s. Research showed that if two pieces of the same polymer are brought into contact at a temperature above its glass transition temperature (Tg), then the interface gradually disappears. Also, the mechanical strength at the interface increases as the crack heals. Wool and his colleagues proposed five-step healing model as shown in the Figure 2.7. The steps are: surface rearrangement, surface approach, wetting, diffusion and randomization (Kim and Wool 1983; Wool and O'connor 1981).

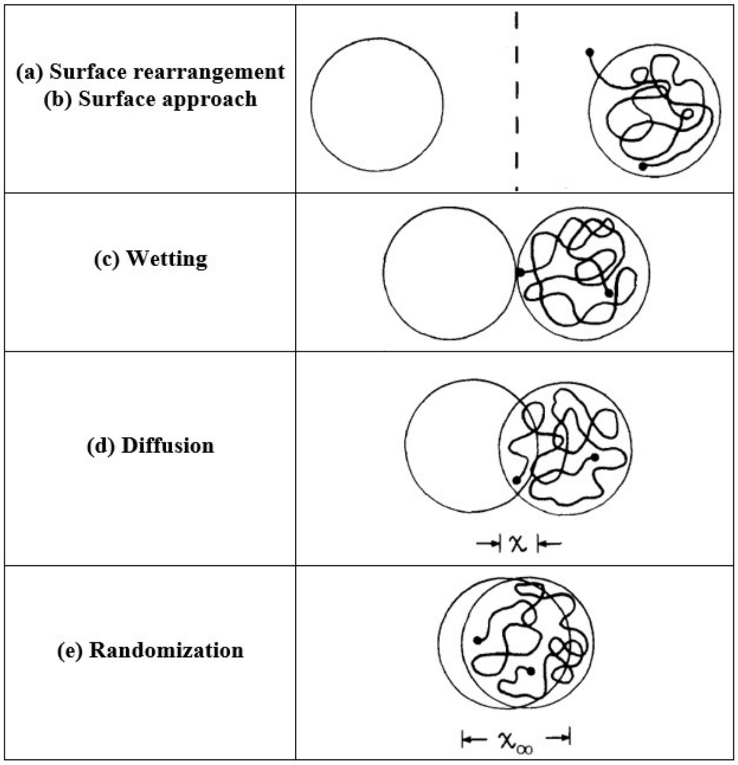

Figure 2.7: Schematic diagram of the five-step crack healing of a physico-chemical based healing model (Kim and Wool 1983; Wool and O'connor 1981)

These researchers concluded that most of the recovery of the mechanical strength take place in the wetting and diffusion stages. They proposed an equation for healing which includes intrinsic healing ($R_h(t)$) and wetting function ($\varphi(t)$) as follows:

$$R = \int_{-\infty}^{t} R_h(t-\tau)\frac{d\varphi(\tau)}{d\tau}d\tau \tag{2.5}$$

They estimated the intrinsic healing functions for strength, elongation at break, impact energy, and fracture parameters as a function of time, molecular weight, temperature, pressure, and processing conditions using Eq. (2.5). For all these cases, the results agreed with the theory. They also concluded that the wetting function depends on the cohesion and surface energy.

Thixotropy is defined as the continuous decrease in viscosity with time when subjected to flow and the recovery of viscosity with time when the flow is stopped (Shan et al. 2011). Thixotropy is an inherent material property of the asphalt binder and has a significant effect on the rheological properties of the binder (Mouillet et al. 2011). Thixotropy is related to the colloidal nature of binder, and depends on the source of the binder, the degree of processing and the temperatures. Thixotropy also relate the changes in the microstructure of a material, as it decreases the viscosity by applying flow (Shan et al. 2011). If rest period is applied, then the material regains its structure and its viscosity increases to the initial value due to the movement of the molecules. Verstraeten (1991) related the thixotropic effects to the decrease in stiffness during fatigue tests and its recovery during rest periods. Based on the results he proposed that at temperatures higher than 25 °C, the fatigue of the asphalt mixtures is mainly caused by the thixotropic effect. He also concluded that if the rest time is sufficiently long, then full recovery is possible. However, at low temperatures (less than 5°C), the fatigue damage is due to the structural damage and thus the recovery is partial. Di Benedetto et al (2011) concluded that thixotropy influences the real fatigue performance of the asphalt concrete and it can be modelled using an equivalent temperature increase. Shan and her colleagues (2010) introduced the Cox-

Merz relationship of the thixotropy model to characterize the fatigue and healing behavior using the break-down and build-up coefficients of the microstructure.

Both the multi-step healing model and the thixotropic model explain the recovery process during rest periods. However, the multistep healing model explains the healing of micro-damage that occurs during the loading, and the thixotropy model explains the recovery process that occurs due to the molecular motion at high temperature. From the above discussion, it can be seen that physico-chemical based healing model appears adequate for discussing the healing mechanism and finding out the existence of healing in the asphalt. However, it is very difficult to relate these healing models to the fatigue models, because all the currently available fatigue models are empirical models. Therefore, these healing models are best to use when the healing mechanism is investigated.

2.6.2 Mechanics Based Healing Model

2.6.2.1 VECD Model

Since asphalt concrete is a viscoelastic material, the creep behavior due to constant loading and the relaxation behavior due to constant strain have to be considered while modeling the material (Kim et al. 1997). It indicates that during a simple strain controlled direct tension test, the stress-strain relationship obtained is a combination of two things: the damage development and relaxation due to viscoelasticity. Kim et al. (1997) developed a VECD model for fatigue damage using Schapery’s elastic-viscoelastic correspondence principle (CP) by using the so-called pseudo strain variables which can be applicable to both linear and nonlinear viscoelastic materials (Schapery 1984). In VECD model damage is defined as all structural changes in the material that results in a reduction in stiffness or strength during loading. The predicted damage parameter (S) is then compared using the

C-S relationship. This model on damage and healing characterization of asphalt concrete, during monotonic and fatigue tests was reported by several researchers (Daniel and Kim 2002; Kim et al. 2003; Lundström 2004). During fatigue testing, the slope of the stress-pseudo strain loop appears to decrease, which is developed as the function C_1 (S_1) to represent the damage accumulation. Another parameter called pseudo stiffness S^R, is defined as the slope of the stress-pseudo strain loop. Lee and Kim (1998b) defined the micro-damage healing function H for asphalt mixture. Although this model has been used to explain the experimental results, it model does not give a constitutive equation for damage and healing relating the stress and strain which could be used in the damage model to predict the asphalt material fatigue damage.

2.6.2.2 PANDA Model

Abu Al-Rub et al. (2010) developed and validated a micro-damage model which improves the ability of an integrated nonlinear viscoelastic, viscoplastic, and viscodamage constitutive model based on continuum damage mechanics for predicting the fatigue life of the asphalt mixtures. This is a three-dimensional computational code called the Pavement Analysis Using Nonlinear Damage Approach (PANDA). The code is written in the user material (UMAT) subroutine under a commercial finite element software ABAQUS. Abu Al-Rub and his colleagues indicated that the healing (h) is a function of the rest period (or healing time), temperature, level of damage and the history of healing. They proposed a procedure to identify the healing model parameters using the repeated creep-recovery tests with different recovery periods only. However, their model was developed for static loading only. Their model did not investigate the healing mechanism during the cyclic strain controlled tests. The cyclic loading condition has significant importance for developing the fatigue model. Also, their study considered only the axial loading. However, in the field, shear stresses may be dominant and significantly affect the occurrence of the fatigue damage.

2.6.2.3 Partial Healing Model

Pronk proposed a partial healing (PH) model to describe the evolution of the stiffness modulus due to reversible and irreversible damage in a bending fatigue test (Pronk 2000; Pronk and Cocurullo 2009). Pronk assumed that the damage is related to the dissipated energy per cycle and the asphalt mixture can heal during rest and loading periods. In this model, the loss and storage modulus is calculated for each cycle and before and after rest period. At rest period, it is assumed that the loss modulus is zero as no energy will be dissipated during rest period. Thus, the loss modulus is divided in to two parts: reversible and non-recoverable. The loss modulus was defined as:

$$S_{mix} sin\varphi = F\{t\} = F_o - \int_0^t \left[F\{\tau\}\left(\alpha_1 e^{-\beta(t-\tau)} + \gamma_1\right)\right] d\tau \qquad (2.6)$$

where $\alpha_1, \alpha_2, \gamma_1, \gamma_2$ and β are the products of material constants. Because no energy is dissipated during a rest period, the function $F\{\tau\}$ in the integral equals to zero during the rest period. When a rest period (t_1) is applied the loss modulus equation becomes as follows:

$$F\{t\} = F_o - e^{-\beta t} \int_0^{t_1} \alpha_1 F\{\tau\} e^{+\beta\tau} d\tau - \int_0^{t_1} \gamma_1 F\{\tau\} d\tau \qquad (2.7)$$

The second term on the right-hand side represents the reversible damage (R_{L1}) and the third term the non-recoverable damage (P_{L1}) which is equal to the accumulation of the permanent damage in the load period. Thus, the evolution of the loss modulus during the rest period is as follows:

$$F\{t\} = F_o - R_{L1}e^{-\beta(t-t_1)} - P_{L1}\text{ , for } t \geq t_1 \quad (2.8)$$

The evolution of damage is calculated based one the change in the overall modulus over the cycles. PH model predicts the evolution in modulus and phase lag for continuous loading but fails to do so for discontinuous loading. Thus, it can be concluded that the healing of damage cannot be captured accurately using this model.

2.7 Remarks

Fatigue damage and healing occurs simultaneously in the asphalt. The chemical properties of the asphalt binder play a significant role in identifying and understanding healing. A review of past literatures reveal that healing in asphalt binder and asphalt concrete have been studied for several years. However, most of the studies are focused on factors such as: temperature, rest period and damage level affecting the amount of healing. Effects of aging and moisture on the healing capability have not studied yet. Most of the research did not develop a model for asphalt binder healing. Some empirical fatigue damage models are available for asphalt mixtures. Yet the key factors that influences asphalt healing, contribution of asphalt cohesive healing to material performance, and a way to link healing to pavement design have not been studied. Following are the important aspects required to be investigated:

- Investigation of the effect of healing on the asphalt binder fatigue damage criteria in fatigue curve.
- Examination of the effects of various factors such as aging, moisture and different types of modifications in the asphalt binder healing by studying the physical and

chemical properties of the asphalt binder. Investigation of the effects of fillers in the healing of mastics using the proposed physico-chemical model.

- Development of a constitutive model for damage incorporating healing of the asphalt binder and validation of the model.

CHAPTER 3

FAILURE CRITERIA FOR FATIGUE DAMAGE CONSIDERING HEALING

3.1 General

This chapter presents the effects of healing on fatigue damage. A review of different fatigue failure criteria (both energy based and traditional) are conducted and then different fatigue failure criteria are evaluated to understand their applicability using fatigue data from asphalt binders under strain controlled loading. The stiffness reduction criteria can be used as a simple but reasonable fatigue criterion, which basically captures the transition from micro-crack initiation to propagation. The traditional 50% initial modulus reduction criterion is used as the fatigue failure criteria in this study. The fatigue curves have been constructed for both the fatigue (without rest period) and the healing tests (with rest period). Then both curves are compared to understand the effect of healing.

3.2 Background

To understand the effect of healing on fatigue damage of the asphalt material it is very important to define the fatigue failure criteria for laboratory testing. Defining fatigue failure is very difficult for laboratory fatigue testing samples. Specifically, for the strain controlled testing where no catastrophic failure is noticed as can be seen in the stress controlled testing. Traditionally in the asphalt industry, fatigue failure is defined as the number of cycles required to reduce the modulus or stiffness of asphalt to 50% of its initial modulus (N_{f50}). However, this criterion has always been challenged due to its arbitrary assumption. Over the years many different fatigue failure criteria have been developed to understand the fatigue damage of asphalt, among which the dissipated energy ratio is a notable one. Hopman et al. (1989) developed the energy ratio parameter for strain controlled test based on the assumption that the dissipated energy changes due to the fatigue damage. Later Pronk and Hopman (1990) introduced the dissipated energy ratio (DER) concept using the accumulative dissipated energy to determine the fatigue life of asphalt mixtures and binders. Also, Carpenter and his research team (2003; 1997; 2006) developed another DER concept based on the change of dissipated energy. They later modified this approach and renamed it as the ratio of dissipated energy change (RDEC) approach (Carpenter et al. 2003; Carpenter and Shen 2006). This RDEC approach is mostly used for the macroscopic failure in the asphalt mixture as it can identify the starting of macro crack propagation. In addition to the energy criteria there are some other approaches to define the fatigue damage failure in asphalt, such as the maximum phase angle criterion by Reese (1997) and the 50% loss in pseudo stiffness suggested by Lee et al. (1995).

As the dissipated energy approach is well accepted as a fundamental property to define the fatigue damage, this chapter provides a comprehensive review of various energy-based fatigue failure criteria. Experimental data from both the fatigue and the healing tests are utilized to evaluate the suitability of different approaches in analyzing the binder fatigue under strain controlled loading.

3.3 Existing Fatigue Failure Criteria

Two approaches were used for defining fatigue failure of asphalt binders from the test data, which includes the traditional stiffness reduction and dissipated energy approach. Among the dissipated energy approach, many different criteria exist, however in this study only two of them are discussed.

3.3.1 Stiffness Reduction Approach

The most commonly used fatigue failure criterion is 50% reduction of the initial stiffness/modulus. Sample stiffness at the 50th cycle is defined as the initial stiffness. Figure 3.1(a) shows a typical plot of stiffness ratio (S) per loading cycle and the determination of fatigue life (N_f) based on 50% stiffness reduction. The stiffness ratio (S) is calculated as follows:

$$S = \frac{S_i}{S_{initial}} \tag{3.1}$$

where S_i is the stiffness at cycle i and $S_{initial}$ is the initial stiffness.

3.3.2 Dissipated Energy Ratio (DER) Approach

The formula to calculate the dissipated energy ratio is shown in Eq. (3.2).

$$W_i = \pi \sigma_i \varepsilon_i \sin \delta_i \tag{3.2}$$

where W_i is the dissipated energy at cycle i, $\sum_{i=1}^{n} W_i$ is the cumulative dissipated energy up to a loading cycle n. For strain control test Eq. (3.2) can be rewritten as Eq. (3.3)

$$W_i = \pi (\varepsilon_i)^2 S_i \sin \delta_i \tag{3.3}$$

where S_i is the stiffness at cycle i and ε_i is the applied strain. The DER is defined as the ratio between the cumulative dissipated energy up to cycle n and the dissipated energy at cycle n as shown in Eq. (3.4).

$$DER = \frac{\sum_{i=1}^{n} W_i}{W_n} \tag{3.4}$$

Figure 3.1(b) shows a typical plot of the dissipated energy and DER with the number of loading cycles. It is shown that initially DER increases linearly, but then deviates as damage accumulates due to the increase in the loading cycle. The fatigue indicator N_{p20}, is defined based on the DER deviation from the initial straight line. N_{p20} is the number of cycles at which the DER deviates 20% from no damage straight line (Bonnetti et al. 2002).

3.3.3 Ratio of Dissipated Energy Change (RDEC) Approach

As mentioned earlier, the $RDEC$ method is mostly used to define the macro crack. Several researchers have shown that as the damage starts to accumulate the dissipated energy changes gradually with the number of cycles (Bonnetti et al. 2002; Carpenter et al. 2003; Carpenter and Jansen 1997; Carpenter and Shen 2006; Hopman et al. 1989; Rowe and Bouldin 2000). Therefore, change in the dissipated energy is considered as the failure criterion rather than the dissipated energy itself. $RDEC$ is calculated as following equation:

$$RDEC_a = \frac{DE_a - DE_b}{DE_a(b-a)} \tag{3.5}$$

where a and b are two consecutive loading cycles; $RDEC_a$ is the average ratio of dissipated energy change at cycle a with respect to the next cycle b ; DE_a, DE_b are the dissipated energy at cycle a and b respectively. For strain control testing, the typical plot for the $RDEC$ vs the number of loading cycles for the asphalt binder is shown in Figure 3.1(c). It shows three distinctive regions: initially the RDEC decreases and then it becomes constant and then it starts to increase dramatically. The point where the RDEC starts to increase is termed as the initiation of macro cracking. The constant value of RDEC is called the plateau value, where the micro-cracks starts to develop. Once these micro-cracks start to propagate, then the third region begins and eventually the samples fail. The number of cycles where the shift from plateau value occurs is assumed to be the number of cycles to failure (N_{fl}).

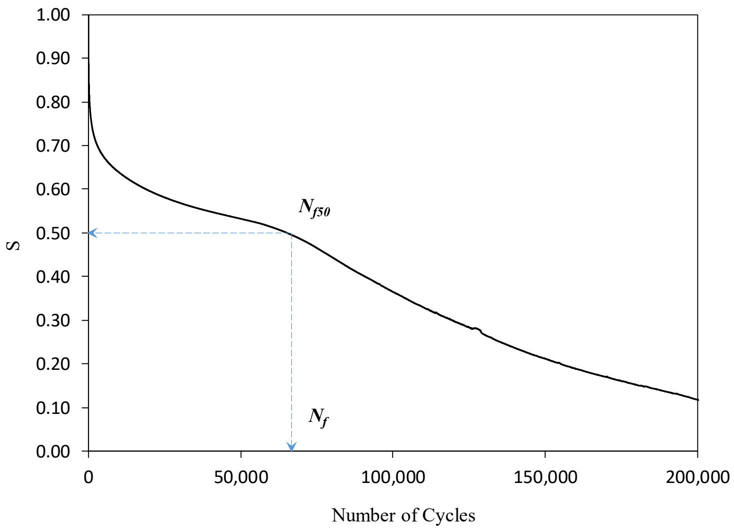

(a) Stiffness reduction approach

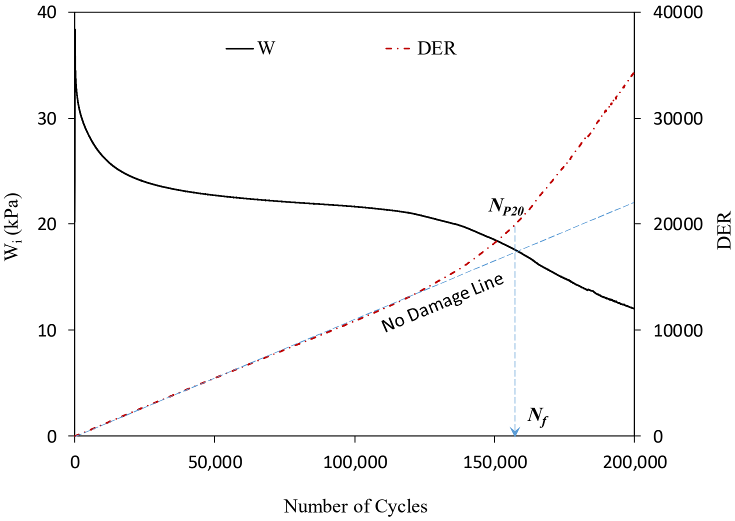

(b) Dissipated energy ratio approach

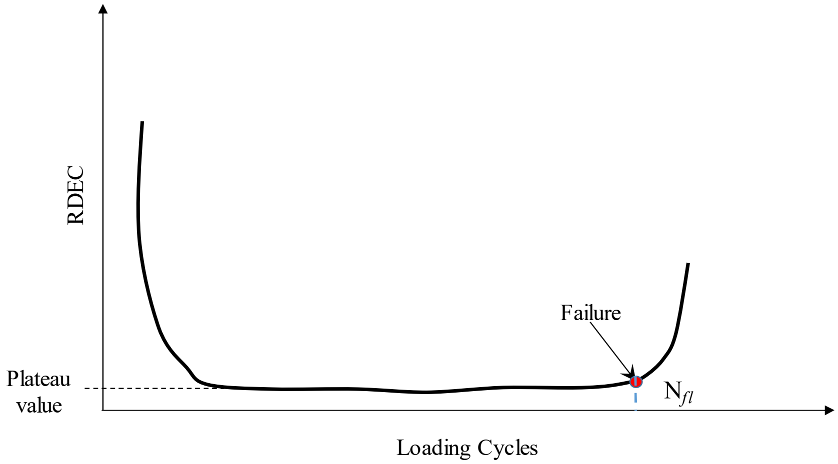

(c) Ratio of dissipated energy change approach

Figure 3.1: Schematic representation of different fatigue criteria

3.4 Experimental Plan

3.4.1 Materials

Three different performance grade (PG) binders were collected from a local plant in Albuquerque, NM. They are: PG 58-22, PG 64-22 and PG 70-22 binders.

3.4.2 Testing Conditions

All the binders were tested in dynamic shear rheometer (DSR) under pure shear deformation. Fatigue and healing tests were performed by subjecting the asphalt binder to a sinusoidal deformation and measuring the resulting mechanical response (torque) as a function of time. Shear loading was considered because the force-interaction between the wheel and the pavement generates shear stresses, which cause most of the fatigue damage in the pavement. Both fatigue and healing tests were conducted in strain control mode. This is because fatigue cracking is a problem in thin pavement and it is mainly strain controlled. Also, in the stress control test the increase in temperature due to the change in dissipation energy is more prominent than the strain control test under cyclic loading. Therefore, it is difficult to conduct a constant temperature fatigue testing under the stress control mode. Hence, strain controlled tests were performed.

Binders were tested at 10Hz frequency. To determine the linear viscoelastic (LVE) strain limit, a strain sweep test was conducted using DSR. In this test, at 10Hz frequency the applied strain was increased from 0.01% strain to 100% strain and the resulting stresses were recorded. Then the dynamic shear modulus (*G**) was calculated. Figure 3.2 shows the stress vs. strain and *G** vs. strain curves. From Figure 3.2(a) it appears that at lower strain level the stress increases linearly, which is called damage-free strain level. After this region, the increment of stress becomes nonlinear with the increase of strain, which is defined as the initiation of micro-damage. Then at higher strain levels, the stress starts to decrease, which is defined as the starting point of the micro-cracking in the material. All of the binders reach their ultimate strength at three different strains, 20.1%, 16% and 12.6% strain for PG 70-22, PG 64-22 and PG 58-22 respectively. Figure 3.2 (b) shows the *G** vs. strain curves, where the linear and nonlinear regions can be easily identified. For all three binders, the transition between the linear and nonlinear region starts at about 2.5% strain. Johnson, et al. (2008) considered the strain at which dynamic shear modulus reduces to 5% of its initial value as the LVE strain limit. According to this concept, all three binders also showed a LVE range of about 2.5%.

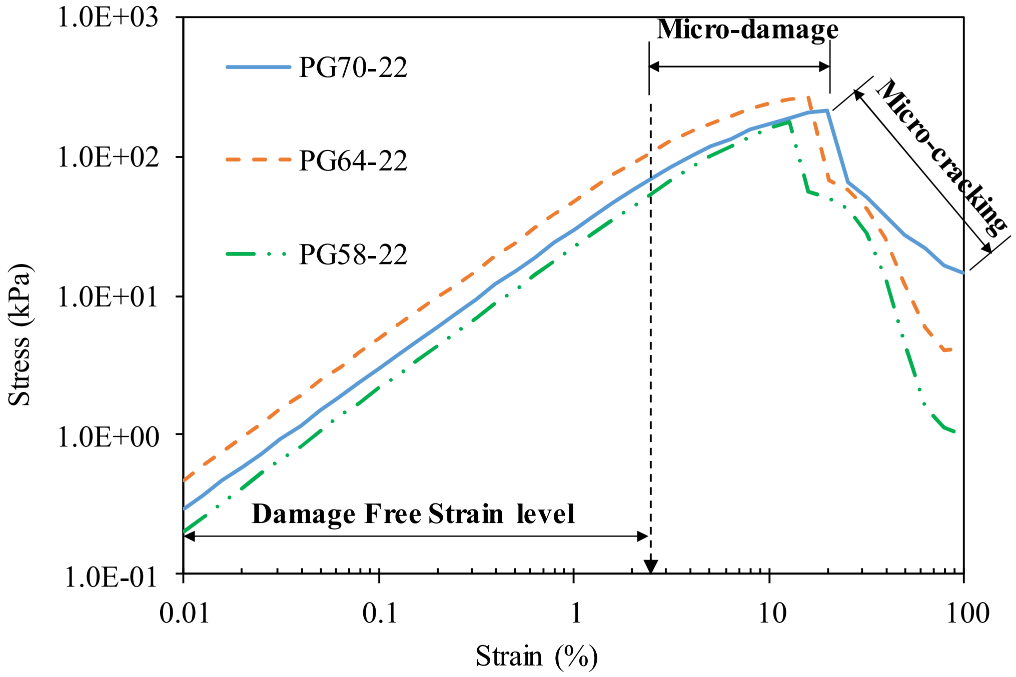

(a) Stress vs. Strain plot for all binders

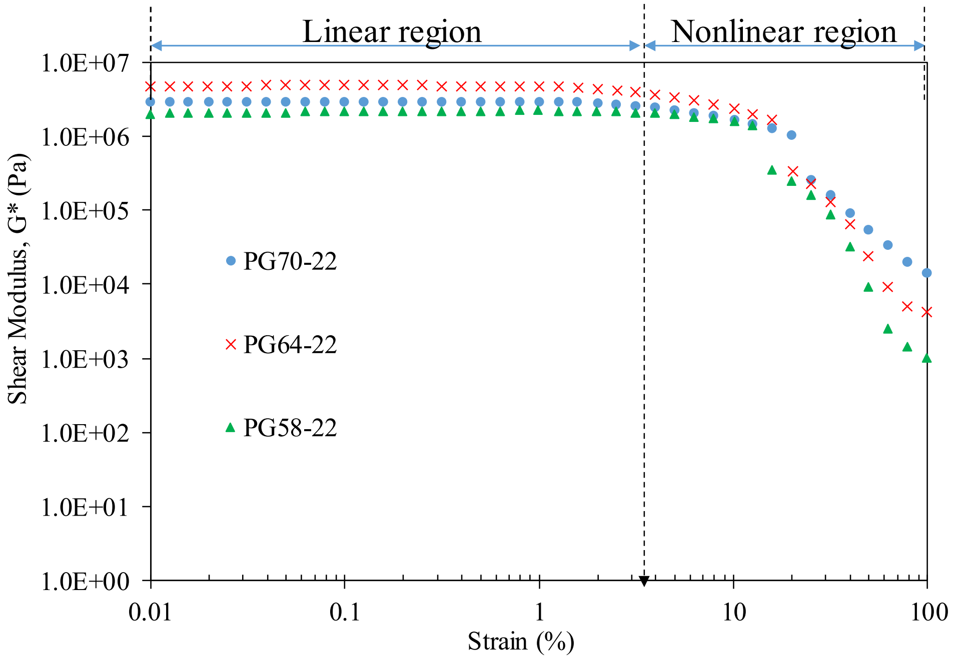

(b) Modulus vs. Strain to determine LVE range

Figure 3.2: LVE range for three binders

Once the LVE range was determined, the testing strains for the fatigue and healing tests were selected by including strains both at the LVE limit and out of the linear range, thus the strain levels selected for the fatigue and healing test were: 2.5%, 5%, 8% and 10%. The nonlinear range of strain was chosen because at higher strain damage accumulation is faster and thus the failure occurs faster compared to that at lower strain levels. Then, time sweep test with and without rest period was conducted on the asphalt binder to understand the effect of healing on the fatigue damage of binder. The time sweep test without rest period is denoted as the 'fatigue test' and time sweep test with rest period is denoted as the 'healing test'. The loading pattern for both fatigue and healing test is shown in Figure 3.3. For all tests three replicates were tested.

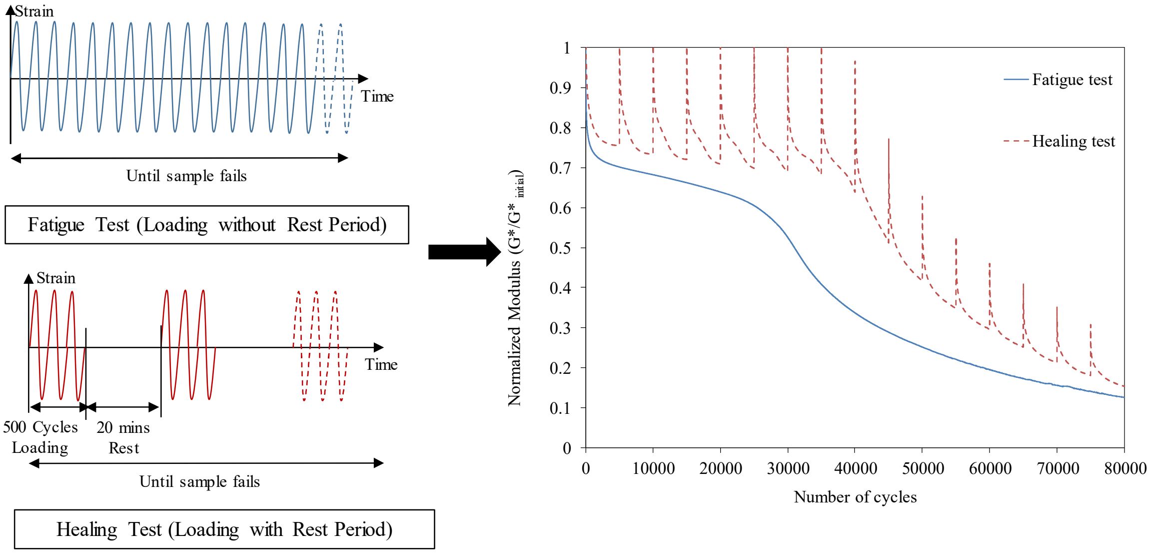

Figure 3.3: Schematic representation of fatigue and healing test

3.5 Results and Discussions

3.5.1 Comparison of Fatigue Failure Criteria

Three different binders were tested at three different strain levels with and without rest period (RP). For the comparison of the above discussed fatigue failure criteria, only healing test with 500 secs of loading and 20 minutes of rest period were considered. Both the fatigue and the healing tests were conducted at 20°C and 10Hz frequency. The number of cycles to failure based on the above three criteria are shown in the Table 3.1 for both fatigue and healing tests. Here, N_{f50}, N_{p20} and N_{fl} represents the number of cycles to failure (N_f) by 50% stiffness reduction, DER and RDEC approach respectively. Figure 3.4 shows the fatigue and healing test results for PG 70-22 binder at 5% strain level. It shows that the shear modulus (G*) decreases over the loading cycle. This reduction in G* is caused by the damage accumulation of the material under cyclic loading. This plot can be divided into three phases: firstly, in phase 1, the reduction in modulus has a faster rate (steep slope); followed by phase 2, with a gradual reduction of modulus (constant slope); and finally, more severe types of damage appear in phase 3, where the modulus decreases drastically and finally results in failure. This behavior implies that initially the damage accumulates slowly over the loading cycles. However, with the increase in the loading cycle the damage accumulation rate increases which eventually causes failure of the materials. The end of the second phase is called the transition point. In this figure, the N_{f50}, N_{p20} and N_{fl} points for both fatigue and healing test are shown. Note that for all three approaches, N_{fl} is near the transition point of phase 2 to phase 3. This transition point can be defined as the point where the micro-cracks start to connect and propagate. Also, for the healing test the transition point shifted toward higher loading cycles resulting in an increase in the number of cycles to failure for all the criteria. It can be seen from Table 3.1 that there is no specific pattern for these three different approaches irrespective of the binder type and strain level. However, for all the binders and all the criteria, the number of cycles to failure is higher in the healing test compared to the fatigue test. Also, the determination of N_{p20} and N_{fl} is very difficult for the healing test, whereas, determining N_{f50} is very easy. Therefore, statistical analysis is done to find out whether the fatigue failure determined using these three approaches are significantly different or not. The analysis of variance (ANOVA) test is used to analyzed the data in Table 3.1.

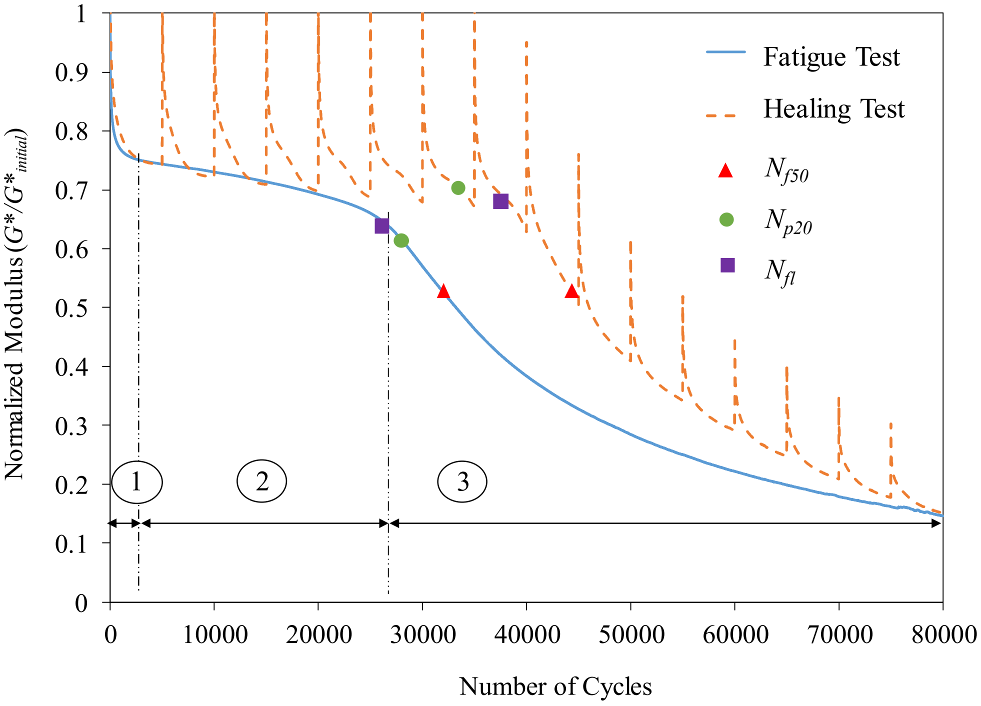

Figure 3.4: Typical plot for fatigue and healing test results for PG 70-22 binder

Table 3.1: Comparison of N_{f50}, N_{p20} and N_{fl} for different binder type

Binder type	**Test type**	**Strain (%)**	N_{f50}	N_{p20}	N_{fl}
PG 70-22	Fatigue	2.5	356730	280010	280000
		5	33230	26487	27357
		10	2516	2120	2000
	Healing	2.5	786850	545945	1099034
		5	46220	34020	35000
		10	5680	6000	6050
PG 64-22	Fatigue	2.5	146000	125000	100000
		5	24960	23510	21000
		10	3530	3500	3200
	Healing	2.5	205020	137000	120000
		5	30010	26000	24500
		10	4010	3800	3350
PG 58-22	Fatigue	2.5	26760	20000	15000
		5	5780	5200	4900
		10	940	950	700
	Healing	2.5	46910	35000	32000
		5	6220	5650	5200
		10	1250	1100	1000

Analysis of variance (ANOVA) is conducted on the values presented in Table 3.1 to identify the significance level of the influential factors. Here the dependent variables are the fatigue life calculated using three different approaches. There are three independent variables: fatigue criteria, strain level and binder type. The null hypothesis (H_0) for the analysis is that, the mean fatigue life is same for all independent variable categories. The significance level (α) is 0.05, which is the probability of rejecting the null hypothesis given that it is true. *P-value* is used for testing the hypothesis, if *P-value* is greater than α then the null hypothesis cannot be rejected. Then it can be concluded that there is no significant difference in the fatigue life at various level of the independent variables.

Table 3.2 presents a summary of the results from the ANOVA test using the experimental data. The independent variables that are significant at 0.05 level in the prediction of the fatigue life are strain level and binder type. The ANOVA analysis shows that the *P-value* for the fatigue failure criteria is greater than 0.05, which means that the null hypothesis cannot be rejected. It means that there is no significant difference between the fatigue life calculated using these three different approaches. Therefore, fatigue life calculated using energy based fatigue failure criteria and the stiffness change criteria do not have any statistical difference.

Both N_{p20} and N_{fl} represent the start of the micro-cracks propagation and it represents the transition point in the dissipated energy vs. loading cycle plot. Statistical analysis shows that there is no significant difference between the energy based approaches and traditional approach. Most importantly, N_{f50} is easy to determine for both the fatigue and healing tests. Therefore, using N_{f50} as a fatigue criterion is a simple and fast way to assess the fatigue behavior of asphalt.

Table 3.2: ANOVA tests to evaluate influence of different fatigue criteria

Variable	**Fatigue**			**Healing**		
	F-value	**P-value**	**Reject H_0**	**F-value**	**P-value**	**Reject H_0**
Fatigue Criteria	0.16	0.851>0.05	No	0.2	0.8215>0.05	No
Strain Level	14.55	**0.0001**<0.05	Yes	7.63	**0.0034**<0.05	Yes
Binder Type	6.02	**0.009**<0.05	Yes	4.63	**0.0223**<0.05	Yes

3.5.2 Fatigue Curve for the Fatigue and Healing Tests

Based on the stiffness reduction method, the fatigue curves are plotted for both the fatigue and healing tests. Figure 3.5 shows the strain vs. N_{f50} plot for three different binders. This figure shows that N_{f50} decreases with the increase of applied strain for both the fatigue and healing test. The log-log plot shows a linear relationship between strain and N_{f50}. There is a horizontal shift in the fatigue curve due to the 20 min rest period in the healing test. Therefore, it can be concluded that the incorporation of rest period increases the fatigue life of the binder and shifts the overall fatigue curve towards the higher loading cycles values. The shift factor due to healing is higher at low strain and lower at high strain. Also, for the hard binder, the shift factor is higher than that of the soft binder. For all the binders, shift factor due to healing ranges from 1.07 to 2.20. Previous studies showed that the fatigue data of the asphalt binder best fitted to the power law model (Airey and Brown 1998; Al-Khateeb et al. 2009; Mannan et al. 2015a). The experimental data are fitted in the power law model to obtain the equation of the fatigue curve for different binders using the following equation:

$$N_f = a\varepsilon^b \tag{3.6}$$

where N_f= Fatigue life

ε = Applied strain

a, b = Regression coefficients

The regression coefficient b is the material parameter that depends on the loading frequencies. The regression coefficients and the coefficient of determination (R^2) for all binders are showed in Table 3.3. For all the tests the R^2 value is close to 1 which indicates that the power model fits the data very well. Using these equations, the fatigue endurance limit (FEL) (the value of strain at 50 million loading cycle is defined as FEL) is calculated, which basically represents the strain level below, which there is no fatigue damage occurring in the material (Bateman 2012). The calculated FEL values for fatigue tests are 0.11%, 0.29% and 0.49% for PG 58-22, PG 64-22 and PG 70-22 binders respectively. It means that the harder binder can withstand more strain than the softer binder. Also, due to the 20 minutes of rest period higher FEL is observed for all the binders. The FEL increases about 50%, 26% and 21% for PG 58-22, PG 64-22 and PG 70-22 binders respectively in the healing test compared to the fatigue test. Therefore, it can be said that due to healing, the binder can withstand more strain and the fatigue life of the binder also increases. Furthermore, healing has less influence on FEL for the harder binder compared to the softer binder.

Table 3.3: Fatigue equations and fatigue endurance limits for fatigue test and healing test

Binder type	Fatigue test			Healing test		
	Fatigue equation	R^2	FEL (%)	Fatigue equation	R^2	FEL (%)
PG 58-22	$N_f = 2.57\times10^5 \varepsilon^{-2.416}$	0.998	0.11	$N_f = 4.81\times10^5 \varepsilon^{-2.615}$	0.996	0.17
PG 64-22	$N_f = 2.0\times10^6 \varepsilon^{-2.685}$	0.999	0.29	$N_f = 3.0\times10^6 \varepsilon^{-2.838}$	0.999	0.36
PG 70-22	$N_f = 1.22\times10^7 \varepsilon^{-3.82}$	0.977	0.63	$N_f = 1.66\times10^7 \varepsilon^{-3.46}$	0.989	0.76

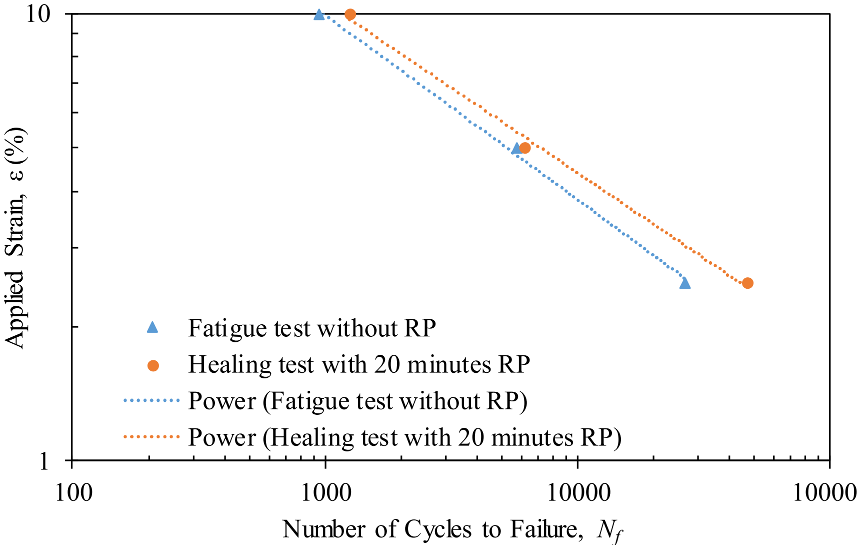

(a) PG 58-22

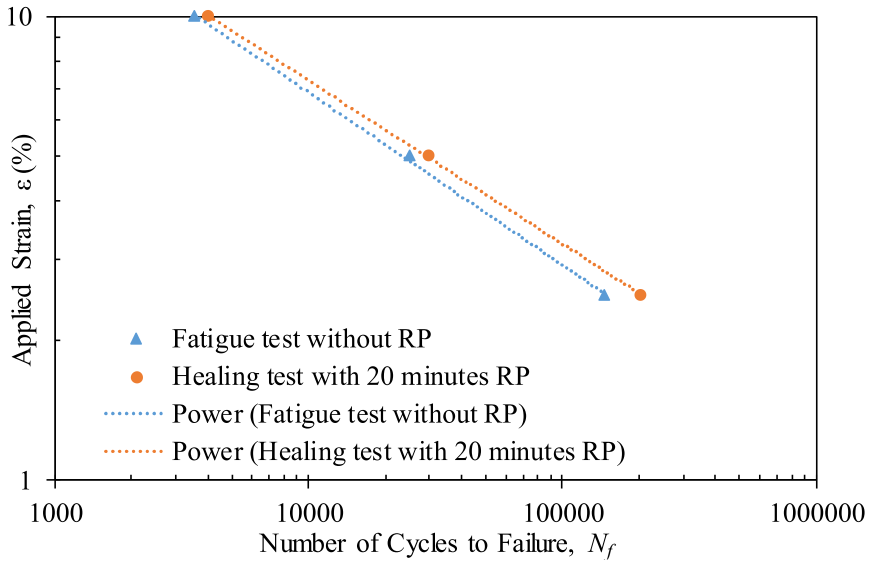

(b) PG 64-22

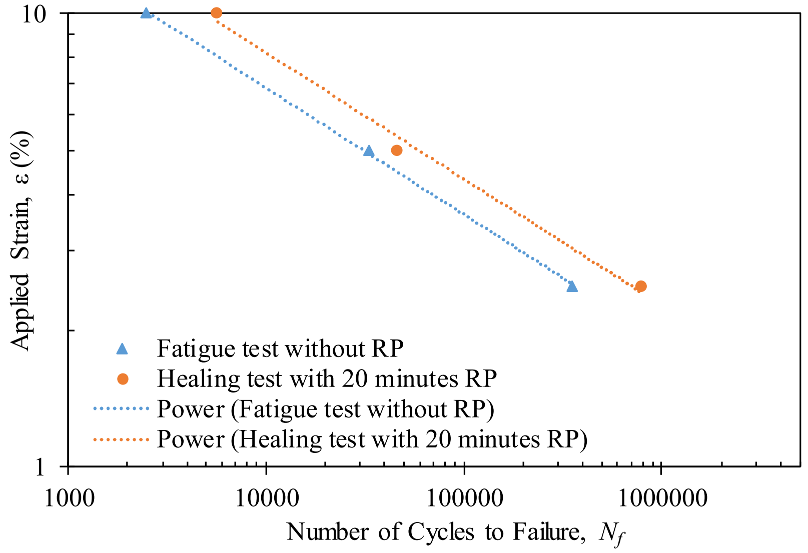

(c) PG 70-22

Figure 3.5: Fatigue curve for both the fatigue and healing tests

3.5.3 Effects of Healing on the Fatigue Curve

Healing test was conducted for different rest periods to observe the effects of the rest period on the fatigue curve. Only PG 70-22 binder was tested at four different strain levels and four different rest periods. The strain levels were 2.5%, 5%, 8% and 10%. Rest period of 2, 5, 10 and 20 minutes were applied after each 500 secs of loading. Then the fatigue curves are constructed for all these tests using the stiffness reduction criteria and then compared with the no rest period fatigue curve.

Figure 3.6 shows the fatigue curves for the different rest periods of PG 70-22. It shows that due to healing over different rest periods, the fatigue curves shift to the right in the plot. It means that healing increases the overall fatigue life. The asphalt binder heals more under long rest period and the fatigue curve shifts further from the no-rest-period curve. Thus, it clearly shows that healing increases the fatigue life and the rest period is directly proportional to the healing of the binder. Longer rest periods show higher healing resulting in an increase in the fatigue life.

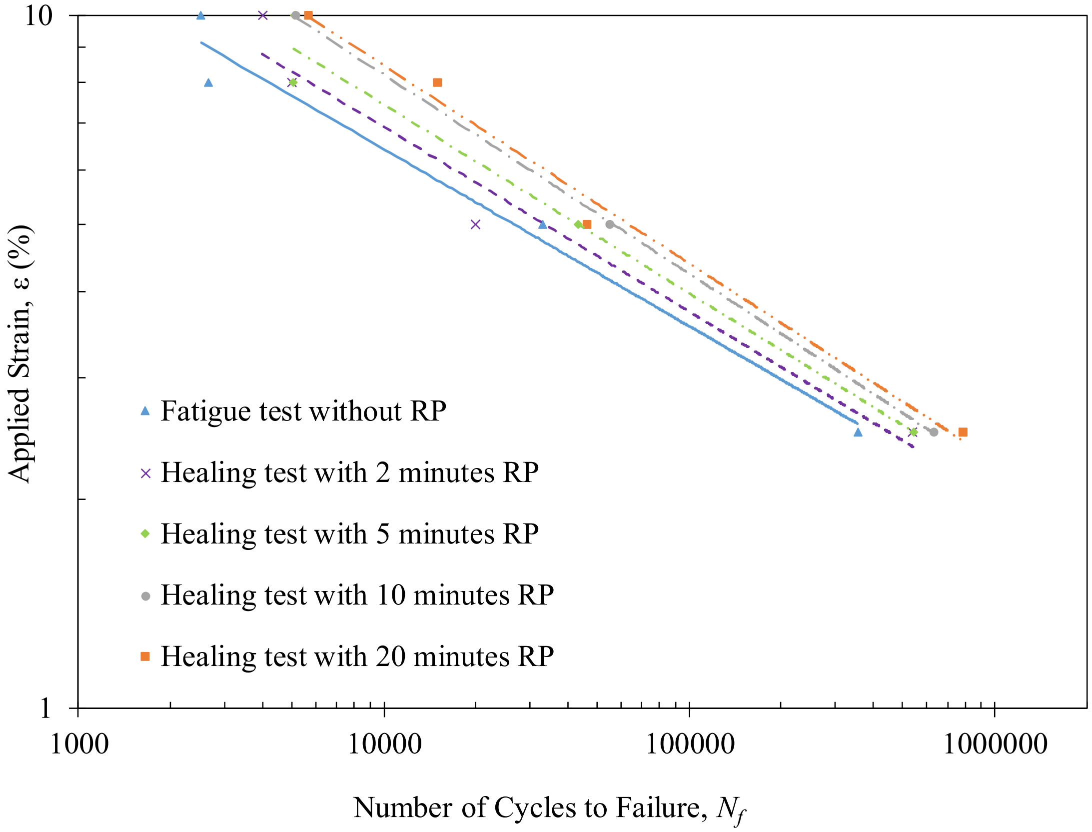

Figure 3.6: Fatigue curve for different rest periods

Fatigue equation is developed for all the rest periods and then the shift factor is calculated for different rest periods. Table 3.4 shows fatigue equations for different rest periods. The coefficient of determination (R^2) for all the equations are close to 1 which means the fitted model strongly agree with the actual data. Figure 3.6 shows that due to the rest period the fatigue curve horizontally shifts towards higher loading cycles, this is the shift factor in the binder due to the healing. The shift factor (SF) is defined as the ratio of fatigue life with and without rest period.

$$\begin{aligned} N_{f(with\,rest)} &= SF \times N_{f(without\,rest)} \\ SF &= \frac{N_{f(with\,rest)}}{N_{f(without\,rest)}} \end{aligned} \tag{3.7}$$

Table 3.4: Fatigue equations for different rest periods for PG 70-22 binder

Rest Period (mins)	Fatigue equation	R^2
0	$N_f = 1.22\times10^7 \varepsilon^{-3.82}$	0.977
2	$N_f = 1.13\times10^7 \varepsilon^{-3.63}$	0.966
5	$N_f = 1.37\times10^7 \varepsilon^{-3.59}$	0.978
10	$N_f = 1.52\times10^7 \varepsilon^{-3.48}$	1
20	$N_f = 1.66\times10^7 \varepsilon^{-3.46}$	0.989

Figure 3.7 (a) shows the calculated SF over the rest periods for different strain levels. As the rest period increases the SF also increases. At 2.5% strain, the change in SF over the rest period is very little, however for 10% strain the SF increases at a faster rate for

increase in the rest period. Therefore, SF is dependent on rest period (RP) and strain level (ε) and all the SF are fitted into a multi-variable equation using MATLAB curve fitting toolbox to obtain an equation for SF. Here rest period (RP) and strain (ε) is assumed as the independent variables and fatigue life is assumed as the dependent variable. The proposed equation for SF is as follows:

$$SF = m_1 \times \exp^{\left(-1/\varepsilon\right)} \times \left(RP + 1\right)^{m_2} \tag{3.8}$$

where m_1 and m_2 are the fitting parameters. For PG 70-22 binder, the value of m_1 and m_2 are found to be 1.027 (0.9118, 1.143) and 0.3908 (0.3466, 0.435) respectively. The (R^2) value for this equation is 0.9684, which means that the fitted model strongly agrees with the actual data. Figure 3.7 (b) shows the 3D plot of the predicted SF for the PG 70-22 binder. Figure 3.7 (c) is the plot of the predicted vs. measured fatigue life of the PG 70-22 binder. This figure shows that all the points are closer to the line of equality (LOE). It implies that the predicted fatigue life from using the predicted SF is almost the same as the measured fatigue life from the test. Therefore, the fatigue life of the binder increases with the rest period due to healing, which can be seen by the shift in the fatigue curve. Thus, the final equation for the fatigue curve with consideration of healing for asphalt binder will be as follows:

$$\begin{aligned} N_{f(with\ rest)} &= SF \times N_{f(without\ rest)} \\ N_{f(with\ rest)} &= m_1 \times \exp^{\left(-1/\varepsilon\right)} \times \left(RP + 1\right)^{m_2} \times N_{f(without\ rest)} \end{aligned} \tag{3.9}$$

This equation provides an empirical way to incorporate healing into the fatigue damage, where SF ranges from 1 to 3.5. However, this does not consider any mechanistic feature. Also, this equation does not explain the healing mechanism in the binder. Therefore, more realistic model considering the chemical and mechanical characteristics is required to understand healing in the asphalt binder.

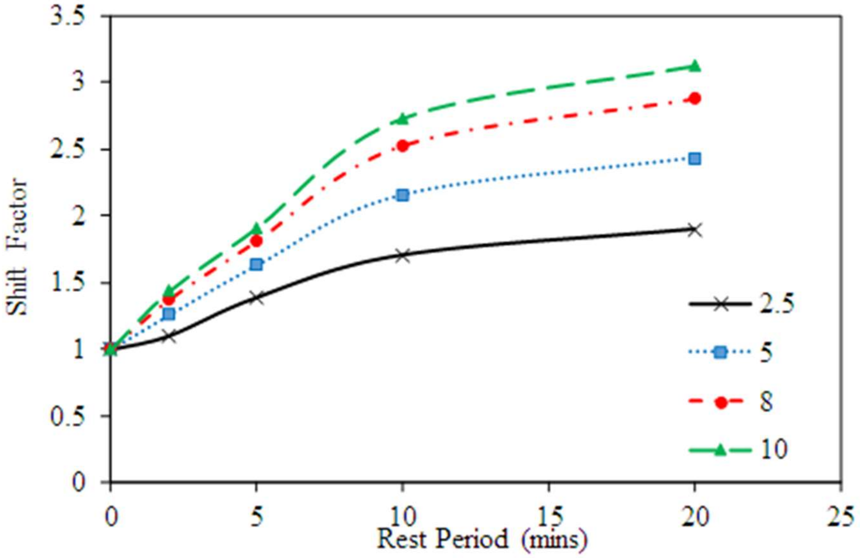

(a) Shift factor vs. rest period

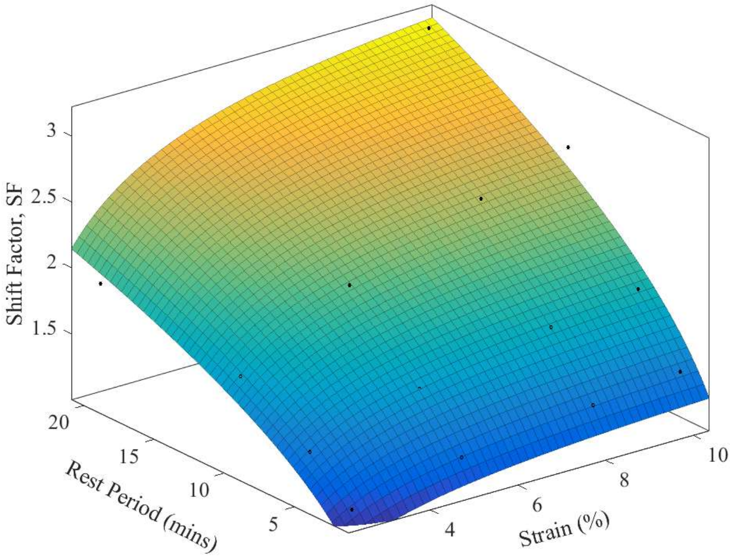

(b) 3D plot of shift factor vs. rest period, strain

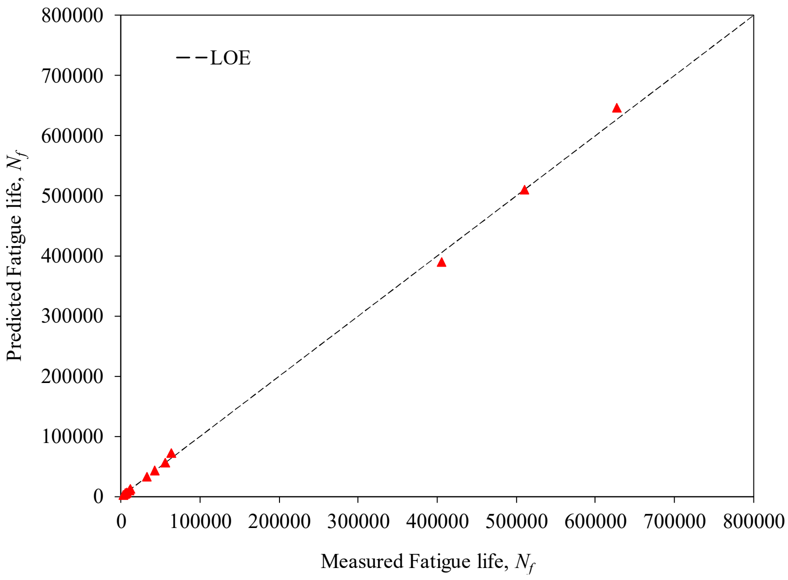

(c) Comparison between the measured fatigue life and predicted fatigue life

Figure 3.7: *SF* calculation for healing test and the predicted fatigue life using *SF*

3.6 Remarks

This chapter presented a comprehensive review of different fatigue approaches: energy based (N_{p20} and N_{fl}) and traditional (N_{f50}) approaches for the fatigue and healing tests. N_{f50}, N_{p20} and N_{fl} are calculated from both the fatigue and healing tests and then are statistically compared. Also, the fatigue curve is constructed for both tests and then the effects of healing on the fatigue damage of the binder is investigated. Based on the review and evaluation of this chapter, the following findings and conclusions are drawn:

- Statistical analysis showed that there is no significant difference between the dissipated energy based criteria ($\boldsymbol{N_{p20}}$, and $\boldsymbol{N_{fl}}$), and the traditional stiffness reduction criterion ($\boldsymbol{N_{f50}}$). The dissipated energy based fatigue failure criteria ($\boldsymbol{N_{p20}}$, and $\boldsymbol{N_{fl}}$) basically capture the initiation of micro-crack propagation, which represents the shift in the energy vs loading cycles curve. Results show that the $\boldsymbol{N_{f50}}$

values for different binders represents the second transition point of the slope in the modulus vs. loading cycle. Therefore, the traditional stiffness reduction criteria can be used as the fatigue failure criteria for both the fatigue and healing test. Thus, in the later chapters the fatigue damage is defined as the reduction of the modulus.

- For the fatigue and healing tests, the cycles required to failure increases due to the rest period during the fatigue loading. The fatigue curves for healing test shift toward the higher loading cycles due to the rest period. For different strain levels, the shift factor for healing ranges from 1.07 to 3.5. An empirical equation is proposed to predict the shift factor in the fatigue life due to healing, which appears to be in good agreement with the measure data.
- It is shown that healing in the binder delays the fatigue damage under cyclic loading and thus increases the overall fatigue life of the asphalt binder. An empirical shift factor can predict the delay in fatigue damage due to healing, however it fails to explain the healing mechanism and the mechanics behind the damage-healing. Thus, in the next chapters, healing mechanism and a mechanistic damage-healing model is discussed.

CHAPTER 4

CHEMICAL CHARACTERIZATION OF THE ASPHALT BINDER

4.1 General

The chemical property of the asphalt binder is key to understanding, modifying and designing the macroscopic properties. As seen in the literature review, asphalt chemistry is too complex to discuss it at the molecular level. However, without understanding the asphalt chemical behavior it is impossible to understand the healing mechanism. Therefore, this chapter presents chemical properties and analysis of the binders that have been used in the later chapters to understand the healing mechanism. These chemical properties will later be used in Chapter 5 to explain healing mechanism.

4.2 Asphalt Chemistry and Healing

Healing of the asphalt binder depends on the chemical composition and structure of the asphalt binder. Healing occurs in two parts: first the wetting of the micro-crack surfaces and then the molecular diffusion of the crack surfaces. Both are dependent on the chemical composition of the binder. Wetting depends on the cohesive strength of the material, which basically depends on the colloidal structure of asphalt. Thus, the quantification of the asphalt binder generic fractions may help to understand the wetting and cohesive strength of the binder. The molecular diffusion part in healing depends on the molecular chain length. Some previous studies have tried to relate the chemical composition of the asphalt binder with over all healing. Kim et al. (1990) proposed a molar ratio of the hydrogen atom and the carbon atom in methyl and methylene (MMHC) from NMR to relate the chemical composition with the healing ability of asphalt. They concluded that higher value of MMHC decreases the healing ability of asphalt. Santagata et al. (2009) tried to relate the ratio of the saturates and aromatics (S/Ar) with the asphalt binder healing. They found that if S/Ar increases then the healing in the binder also increases. However, without studying the chemical properties of the asphalt binder and their effects on asphalt physical properties, these indications are not enough to understand healing.

Asphalt binder chemistry has been studied extensively by utilizing many different techniques over the past few decades. Many researches were conducted to learn the elemental composition. Elemental analysis showed that the asphalt binder mainly consists of carbon (80-88 wt.%) and hydrogen atoms (8-12 wt.%). Thus, the binder has a hydrocarbon content which is more than 90%, which results in a hydrogen-to-carbon molar ratio (H/C) around 1.5. This H/C ratio is in between the aromatics (H/C = 1) and saturates (H/C = 2) (Branthaver et al. 1993b; Read and Whiteoak 2003). In addition, some heteroatoms such as sulfur, nitrogen and oxygen are also present in the binder. The average molecular weight of the asphalt binder falls typically in the range 600-1,5000 g/mol depending on the experimental set-up (Barth 1962; Branthaver et al. 1993b; Traxler 1961). Based on this an average molecular structure of the asphalt binder is shown in Figure 4.1 (Jennings et al. 1992). Asphalt binder is not a macromolecule like the polymer therefore, care should be taken to compare the properties of the polymer to that of the binder. Particularly, elemental analysis and molecular weight is not sufficient when it comes to understanding the properties of the binder. Rather, separating the asphalt binder into different fractions based on the solubility and polarity provides more information about the chemical properties of the asphalt binder.

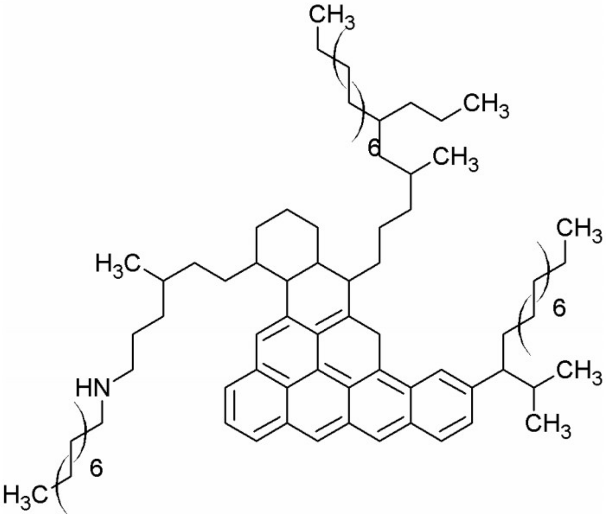

Figure 4.1: Average molecular structure for asphalt binder (Jennings et al. 1992)

SARA analysis is the most widely used method for analyzing asphalt binder into four generic fractions based on polarity: saturates, aromatics, resins and asphaltenes. It is apparent from the above discussion that asphalt healing depends on the chemical property of the binder and the chemical composition drives the physical properties of the binder. Therefore, the chemical composition should be studied before relating them to the healing mechanism of the asphalt binder. In this chapter, SARA analysis of asphalt is conducted using Thin Layer Chromatography (TCL) to investigate the chemical composition. The functional groups in the asphalt binder are determined using Fourier Transform Infrared Spectroscopy (FTIR). Then the chemical composition of the binder is related to the functional groups of the asphalt binder to later relate with the healing mechanism. FTIR of damaged and healed binder are also conducted to determine the change in the functional groups due to damage and healing.

4.3 SARA Analysis

Richardson separates asphalt binder into two fractions asphaltenes and maltenes based on the solubility of the asphalt components in n-heptane (Richardson 1905). It was found that, separating the binder into only two fractions is not satisfactory as maltenes has numerous components. Thus, maltenes are divided into three more fractions. Corbett proposed an elution-adsorption liquid chromatography method on the active alumina with solvents of increasing polarity and aromaticity (Corbett 1969). This method is now the reference method for separating the maltenes into saturates, aromatics and resins, according to their elution in different solvents. Using this method, the composition of the asphalt binder is usually given in terms of the SARA fractions for saturates, aromatics, resins and asphaltenes respectively.

Nowadays, the separation method by Corbett is modified due to the safety reasons and convenience. The standard method for crude oil is the ASTM D-4124 (ASTM 1988), which is also quite similar to the Corbett procedure. This study uses the Thin Layer Chromatography (TLC) to separate the three fractions from maltenes using different solvents. Figure 4.2 describes the overall SARA analysis method used in this study.

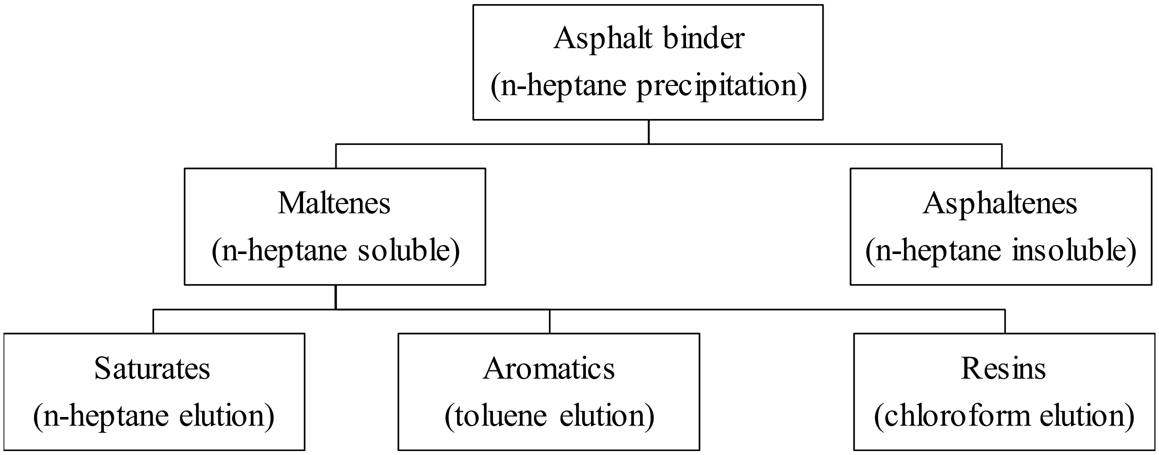

Figure 4.2: SARA analysis of the asphalt binder using TLC

The overall procedure of SARA analysis used in this study is as follows:

1. 50-100 mg of the asphalt binder was weighted into a small container. Then 3 ml of n-heptane (99 %) was added to the container and the solution was stirred for 3-5 mins to dissolve the maltenes.
2. The insoluble asphaltenes were filtered off using vacuum, a fritted filter funnel (15 ml, type B) and a 50 ml filter flask.
3. Then asphaltenes was transferred to another tared small container using chloroform (3-5 ml) and the chloroform was allowed to evaporate overnight. The container was weighted to determine the quantity of asphaltenes.
4. TLC plate was prepared as follows: four lines at 3 cm (a), 8 cm (b), 14 cm (c) and 19 (d) cm from the bottom of the plate was drawn. The top 1 cm was removed from the plate by scraping it off with a razor blade as shown in Figure 4.3.
5. The filtrate with n-Heptane + maltenes was then applied uniformly to the 20 x 20 cm silica gel TLC plate on the 3-cm line (a) using the capillary spotter. Several

successive applications were required and the layer was allowed to dry in between applications.

6. A TLC developing chamber was prepared by placing ~100 ml of n-Heptane into the TLC chamber that was lined with a paper towel. After waiting for 20-30 minutes to make the chamber saturated, the prepared TLC plate was placed into the chamber.
7. The plate was left in the chamber until the n-Heptane solvent reaches to the top of the plate (point d). Then the TLC plate was removed from the chamber and allowed to dry. This step separates out the saturated component of the asphalt binder.
8. The solvent in the developing chamber was replaced with toluene and the chamber was again saturated. Then the plate was placed in a developing chamber until the solvent reaches 14 cm line (point c). Then the TLC plate was removed from the chamber and allowed to dry. This step separates out the aromatic component of the asphalt binder.
9. The solvent in the developing chamber was replaced with chloroform and the chamber was again saturated. Then the plate was placed in a developing chamber until the solvent reaches the 8 cm line (point b). Then the TLC plate was removed from the chamber and allowed to dry. This step separates out the resin component of the asphalt binder.
10. Once all the components were separated, each section was scraped off the TLC plate with a razor into a tared and labeled beaker. The weight was recorded.
11. The components were removed from the silica using a 1:1 methanol: chloroform solution. After stirring the silica for 5-10 min, the solvent was removed by vacuum

filtration using a fritted funnel and a filter flask. The filtrate and the silica were each placed in a tared beaker and dried overnight. This was done for all three components.

12. The final weight of the filtrate residue and the silica is determined and used to calculate the percentages by weight of the four components of the asphalt binder.

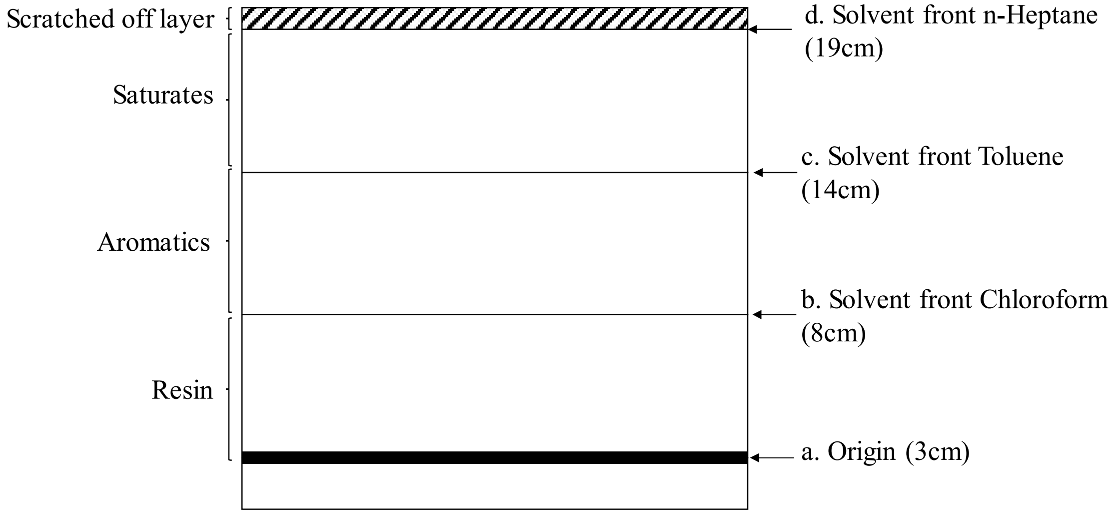

Figure 4.3: Schematic picture of TLC layer development and chamber solvent for different layers

4.4 FTIR Analysis

The asphalt binder has a very complex chemical composition, containing various functional groups (Table 4.1), such as hydrocarbons (C-H), carbonyls (C=O), sulfoxide (S=O). FTIR spectroscopy characterizes the chemical composition of a material by using the infrared (IR) absorption ability of the chemical bonds (Chen et al. 2014; Mannan 2012; Painter et al. 1981). Therefore, FTIR will be used to determine the chemical functional groups in the binder. Later these functional groups will be related to the healing of the binder to understand the role of binder functional groups in healing.

The spectrum from FTIR provides crucial information about the functional groups of the organic compounds such as aromatic, aliphatic, carbonyl and hydroxyl groups. FTIR provides qualitative (through fingerprinting), semi-quantitative, and quantitative information about the chemical composition of the materials. However, it has been mostly used for the qualitative analysis of polymer and different organic and inorganic materials. Several FTIR related studies derived indices or semi-quantitative ratios to characterize coal, minerals, meteorite, starch and different bio polymers (Capron et al. 2007; Chen et al. 2012; Lyons et al. 1995; Mastalerz et al. 2013; Warren et al. 2016; Yesiltas and Kebukawa 2016). Most of these studies used integrated peak areas of the major functional groups, where as some of them used the peak height of the functional groups. A study by Chen et al. (2012) used the functional groups ratios by utilizing the integrated areas of selected functional groups of different coal. The aromaticity ($AR = A_{3000}/A_{2800}$) and aliphatic chain length ($ACL = A_{2915}/A_{2975}$) are some indices which has been defined to understand the composition of coal. Materials such as cutinite and alginate shows negligible value of AR as they are highly aliphatic (Vasconcelos et al. 2012). Asphalt binder shows may different functional groups, some of the important groups and their wavenumber are shown in Table 4.1. As the wavenumbers ranging from 500 to 2000cm^{-1} are known as the fingerprint wavenumber for the asphalt binder, therefore the indices are calculated only for the strong absorbance peak between 500 to 2000 cm^{-1}. The area of an absorbance peak indicates the concentration of a specific molecular component in the sample. For a specific asphalt binder, the ratio of the area under two peaks represents the molecular components present in asphalt. These ratios between the peaks are always reproducible irrespective of the number of IR scan and change in thickness of the sample.

Table 4.1: Characteristic bands of the functional groups in the asphalt binder (Coates 2000)

Functional groups	Wavenumber (cm^{-1})
νO-H bond	3400-3700
νC-H Aliphatic	2924, 2853
νC=O Carbonyls	1700
νC=C Aromatic	1600
δC-H Aliphatic index ($-(CH_2)_n-$)	1455
δC-H Aliphatic branched ($-CH_3$)	1375
νS=O Sulfoxide	1030
Stretching vibration of Benzene	866, 812
γwC-H Aliphatic index ($-(CH_2)_n-$)	724

PerkinElmer FTIR with the Universal Attenuated Total Reflectance (UATR) accessories was used for the analysis. The spectra were recorded with a horizontal ATR accessory and a DiComp crystal (composed of a diamond ATR with a zinc selenide focusing element). A small amount ($\approx$ 1 g) of asphalt binder was placed directly on the ATR plate and a fixed load was applied to the sample to ensure full contact with the crystal and even thickness. For each sample, six scans were collected at a resolution of 1 cm^{-1}. For all binder samples spectra were measured from a range of 4000 to 400 cm^{-1} wavenumbers. Chemical bonds have different regions in the IR spectrum: single bond region (600-1500 cm^{-1}), double bond region (1500-2000 cm^{-1}) and fundamental vibrations (2700-4000 cm^{-1}) (Stuart 2005). Single bond region contains C-C, C-O, C-N; double bond region contains

C=C, C=O, C=N, N=O; and fundamental vibration contains C-H, N-H, O-H functional groups.

4.5 Materials

Five different performance grade (PG) asphalt binders are collected from the same source and then their chemical composition and structure is determined using SARA analysis and FTIR. The PG binders tested in this study are PG 52-22, PG 58-22, PG 64-22, PG 70-22 and PG 76-22. This study focuses on the change in the chemical composition for different PG grades. These binders are chosen because they are most commonly used non-modified binders in the USA.

4.6 Chemical Characterization

4.6.1 Component Analysis

A total of five PG binders were analyzed using TLC to determine the SARA fractions of the asphalt binders. The results are given in Table 4.2. For all the binders, the typical yield lies in between the 87-102% range. It is assumed that most of the loss during the SARA analysis is due to the evaporation during solvent removal. Radke et al. (1980) showed that the loss was primarily due to the evaporation of the saturates. Therefore, the binder which showed low yield has been corrected to 100% by adjusting the saturate values. Figure 4.4 presents all four fraction for all five binders. For all the binders, aromatics are the dominating component ranging from 52 to 63% wt. of the binder. Saturates in all the binders remains between 5-7% wt. of asphalt. Note that with higher PG grade the % aromatics in the binder decreases and the sum of the asphaltenes and resins increases. Due to this increase in asphaltenes and resins, the binder hardness increases with the PG grade. Previous studies showed that asphaltenes are the main reason for the viscosity of asphalt binders (Pfeiffer and Saal 1940; Speight 2014; Speight and Plancher 1991). Also, the asphalt colloidal system shows that if the asphaltenes and resins content increase in binder, then they construct an interactive gel-type structure. This results in more viscosity and less flow in asphalt binder. But more aromatics causes asphaltenes to float separately in the binder molecule resulting in a sol-type structure. Thus, aromatics in the binder makes the binder more flowable or less viscous. Whereas, asphaltenes and resins make the binder stiffer and more viscous.

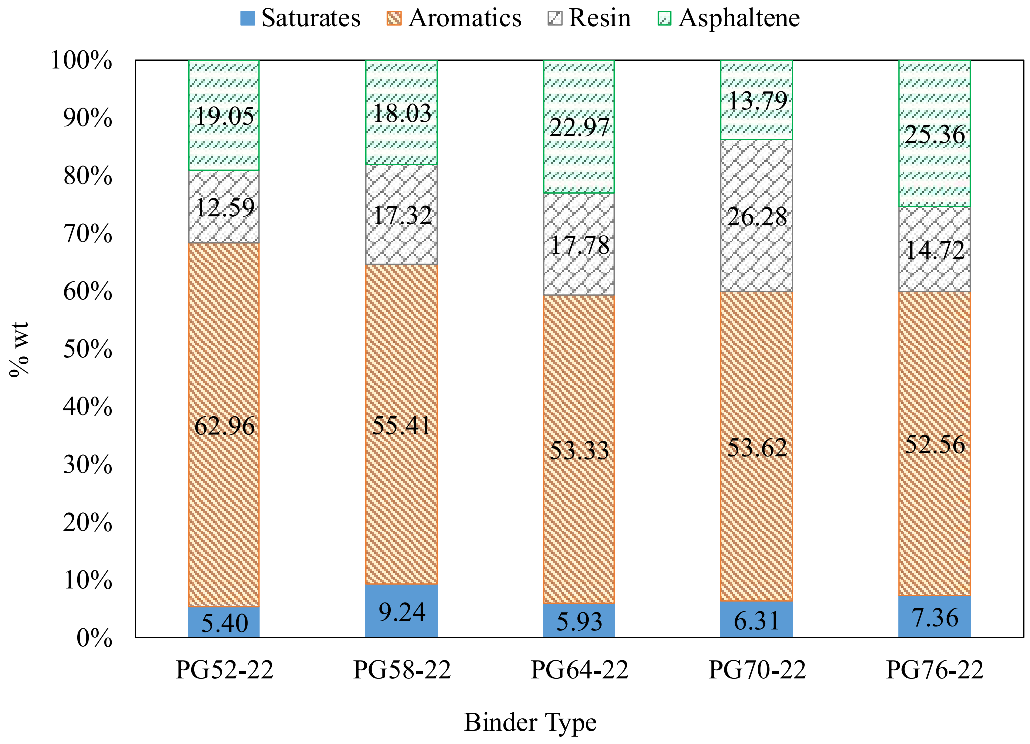

Figure 4.4: SARA fractions of five PG binders

After quantifying the fraction for each binder, (*As*+*R*), *S/Ar* ratio and the colloid instable index ($CII = \frac{(A_s + S)}{(R + A_r)}$) were calculated and showed in Table 4.2. The (*As*+*R*) represents the content of large molecules in the binder and the *S/Ar* ratio reflects the ratio of the long molecules to the ring-shaped molecules. The higher the *S/Ar* ratio the longer is the molecular structure. *CII* characterizes the stability of the binder structure. A smaller *CII* results in a sol-type more stable binder. Table 4.2 presents *S/Ar*, (*As* + *R*) and *CII* values for all five binders. It is found that with the increase of the PG grade of the asphalt the content of large molecular (*As* + *R*) increases, which explains the increase in hardness with the PG grade. Also, PG 76-22 binder has the highest *CII*, meaning this binder is more of a gel-type binder. This also means that PG 76-22 binder has more unstable colloidal system with more asphaltenes and resins network in it. PG 58-22 has highest *S/Ar* ratio, which means that it has longer molecular structure than ring shaped structure, which increases the mobility of the asphalt molecules.

Table 4.2: SARA fractions for the five PG binder (SARA fractions are normalized to 100 wt %)

Binder	Saturates (wt %)	Aromatics (wt %)	Resins (wt %)	Asphaltenes (wt %)	Yield (%)	*As* + *R*	*CII*	*S/Ar*
PG 52-22	5.40	62.96	12.59	19.05	90	31.64	0.32	0.09
PG 58-22	9.24	55.41	17.32	18.03	93	35.35	0.37	0.17
PG 64-22	5.93	53.33	17.78	22.97	87	40.75	0.41	0.11
PG 70-22	6.31	53.62	26.28	13.79	98	40.08	0.25	0.12
PG 76-22	7.36	52.56	14.72	25.36	102	40.08	0.49	0.14

Once the fractions are separated from the asphalt binder, they are analyzed by FTIR and shown in Figure 4.5. To further investigate the chemical composition and microstructure of the asphalt binder, the functional groups present in the SARA fractions are should be investigated. Figure 4.5 shows that all the SARA fractions show strong peaks at 2850–2960 cm^{-1} (stretching), indicating that they contain mostly saturated hydrocarbons. Figure 4.5 (a) and (b) shows that the absorbance peaks of saturates and aromatics are similar, indicating both contain similar functional groups. However, their intensities of absorbance peaks are different. The IR spectrum shows different branching structures and some long aliphatic chains. Saturates show higher intensity at 2850–2960 cm^{-1} compared to the aromatics, which indicates that the saturates has higher saturated hydrocarbons than the aromatics (Jiang et al. 2012). Whereas aromatics show higher peak intensities at 1360-1470 cm^{-1} (deformation vibration) and 841-765 cm^{-1} (rocking vibration) wavenumbers, indicating that it has more unsaturated hydrocarbons than the saturates. Figure 4.5 (c) and (d) show that the absorbance peaks of resins and asphaltenes are similar, indicating that both contain similar functional groups. However, the intensities of the absorbance peaks are different. Both show a peak at 1600 cm^{-1}, which represents the C=C bonds. Asphaltenes shows strong and district peaks at 975, 899 and 810 cm^{-1} which are also present in the asphalt binder spectrum (Figure 4.6 (a)). Also, asphaltenes show the stretching vibration of the S=O bonds at band 1023 cm^{-1} as shown in Figure 4.5 (d). The resins show a peak at 1700 cm^{-1}, which indicates the C=O bonds (Figure 4.5 (c)). Figure 4.6 (a) shows the FTIR spectrum for the asphalt binder. It appears that the functional groups of the asphalt binder are a combination of the functional groups in all four fractions. However, the functional groups in the asphalt binder is primarily dominated by the groups in the asphaltenes and saturates. Therefore, in the asphalt binder the functional groups of the resins and aromatics are absorbed by asphaltenes and then asphaltenes get packed by saturates (Lesueur 2009).

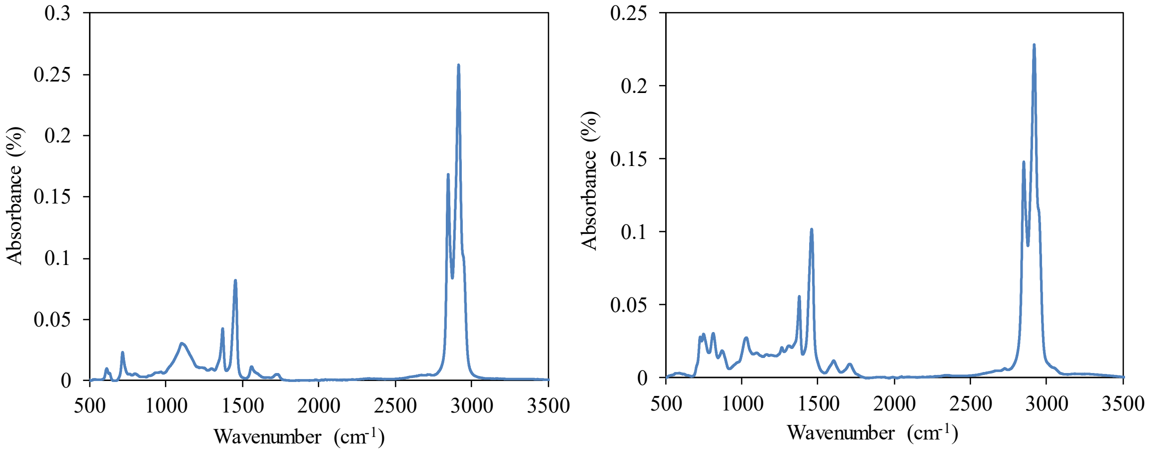

(a) Saturates (b) Aromatics

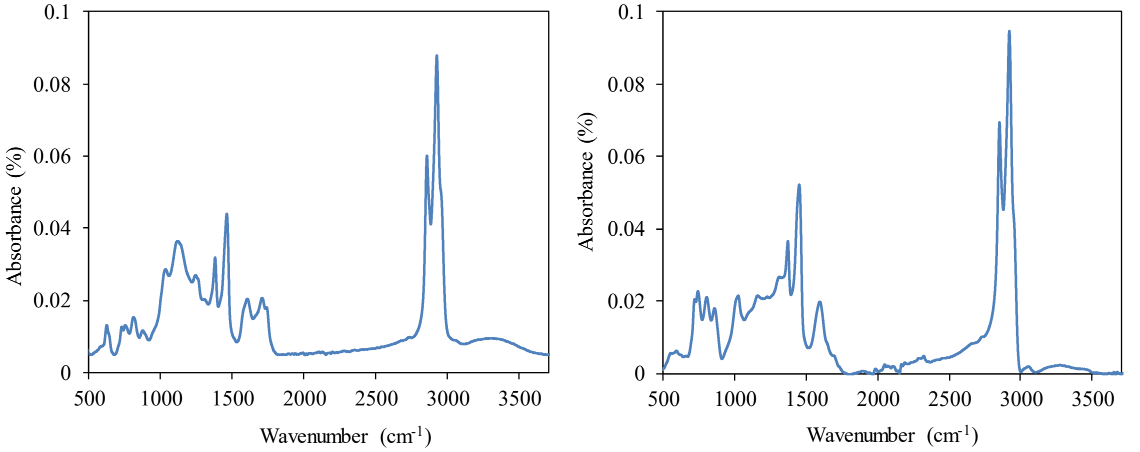

(c) Resins (d) Asphaltenes

Figure 4.5: FTIR spectra of the SARA fractions separated from asphalt binders

4.6.2 Functional Group Analysis

FTIR absorbance vs. wavenumber spectra of five asphalts are shown in Figure 4.6 (a). It appears that the asphalt binder spectrum is essentially the combination of asphaltenes and saturates spectrum shown in Figure 4.5. As the asphalt binder is an organic material with different functional groups, FTIR can be used to characterize the molecular nature of the material. Therefore, Figure 4.6 (b) shows the region from 1750 to 650cm^{-1}, where the differences between asphalt binders are mostly seen. Note that all the binders show similar functional groups. However only PG 64-22 and PG 70-22 show a very small carbonyl (C=O) peak at 1700 cm^{-1}. Figure 4.6 (c) shows the first-order differentiated spectra for all the PG binders. The first derivation is a useful tool for separating overlapping bands in a peak as at the narrow peaks the spectrum suddenly changes from a positive slope to a negative slope. The differentiated spectrum shows maximum positive and minimum negative going through zero at each peak, which basically distinguishes the overlapping peaks. Thus, using the first derivation of the spectrum the overlapped peaks are separated and then the area under the peaks are calculated. Figure 4.6 (c) shows that all the peaks labeled in Figure 4.6 (b) do not have any overlapping peaks all of them are individual peaks. In the differentiated spectra of all the binders, the spectral differences are diminished for most of the functional groups, but the difference in the methylene, methyl and sulfoxides absorption patterns for all the samples can still be easily observed. Later in this section, the integrated area under these peaks are calculated for determining the functional indices.

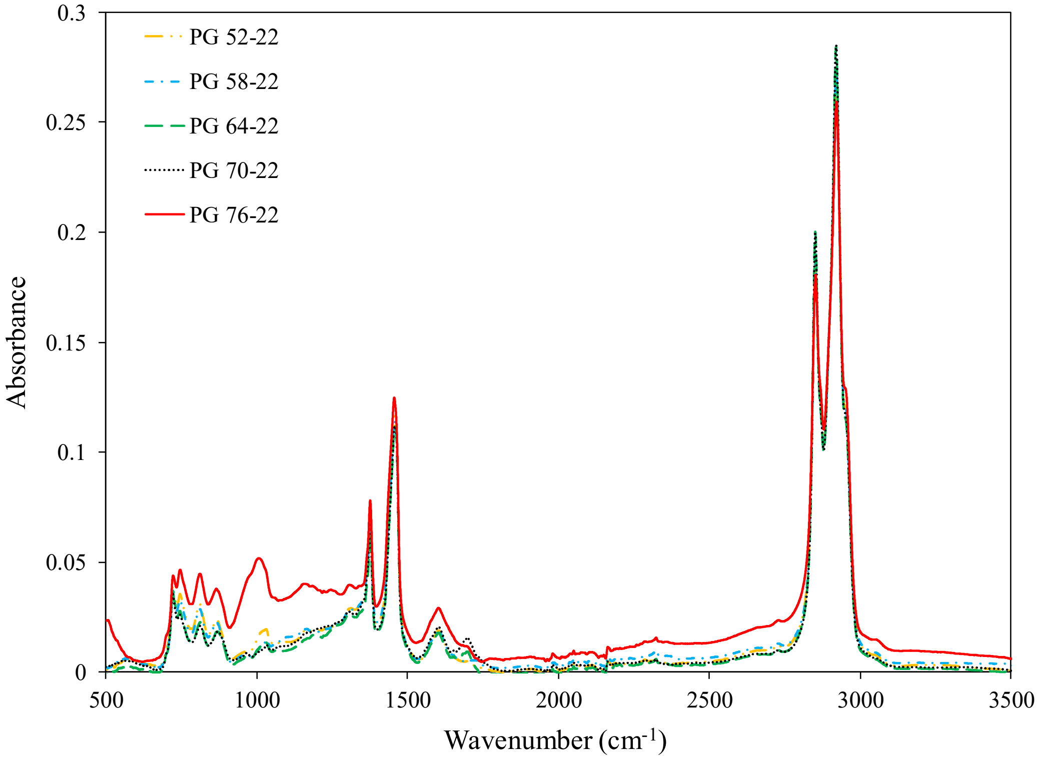

(a) FTIR spectra for five different PG binders

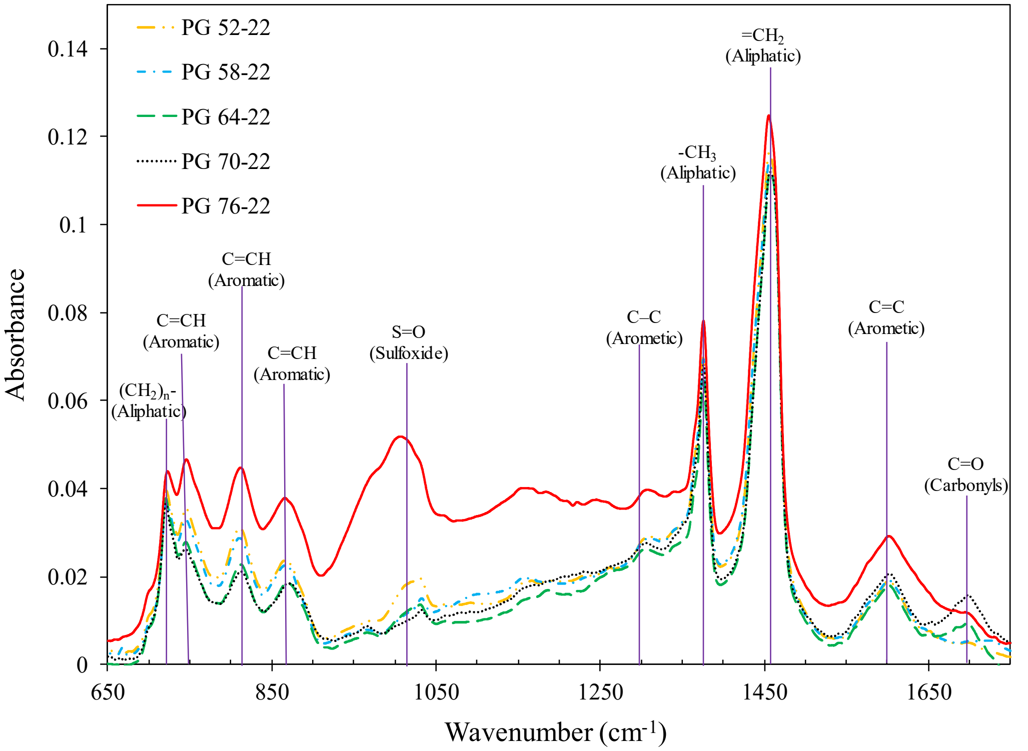

(b) Part of the FTIR Spectra for five binders indicating all the functional groups

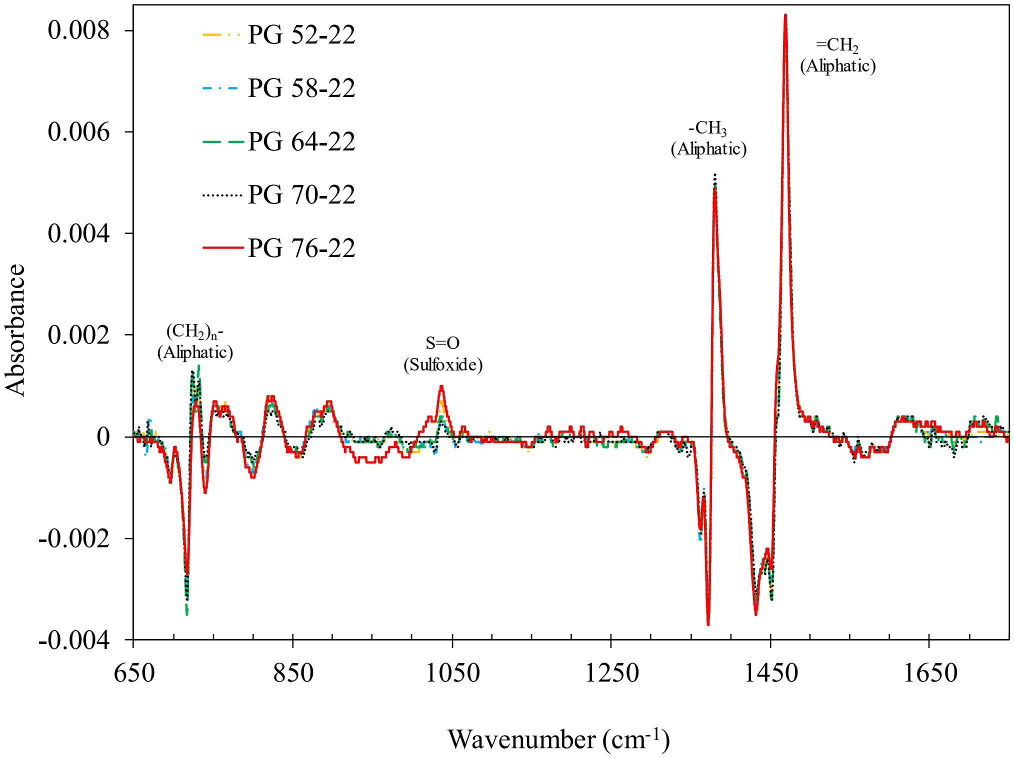

(c) Part of the first-order differentiated FTIR spectra for all binders

Figure 4.6: FTIR analysis of binders

The integrated peak areas of the major functional groups of the asphalt binder are calculated and then the functional group ratio (or functional index) is determined. These functional indices provide quick and reliable information about the aromatic structures, aliphatic structures, and oxygenated functions in the material (Gong et al. 2017). In this study, aliphatic chain length or methylene to methyl ratio ($\frac{=CH_2}{-CH_3}$), aliphatic index (I_{al}), aromatic index (I_{ar}), carbonyl index ($I_{C=O}$), sulfoxide index ($I_{S=O}$), branched alkane index (I_{branch}) and long chain alkane index (I_{long}) are calculated.

$$\frac{=CH_2}{-CH_3} = \frac{A_{1455}}{A_{1375}} \tag{4.1}$$

$$I_{al} = \frac{A_{1455} + A_{1375}}{\sum A} \tag{4.2}$$

$$I_{ar} = \frac{A_{1600}}{\sum A} \tag{4.3}$$

$$I_{C=O} = \frac{A_{1700}}{\sum A} \tag{4.4}$$

$$I_{S=O} = \frac{A_{1030}}{\sum A} \tag{4.5}$$

$$I_{branch} = \frac{A_{1375}}{A_{1455} + A_{1375}} \tag{4.6}$$

$$I_{long} = \frac{A_{724}}{A_{1455} + A_{1375}} \tag{4.7}$$

where $\sum A = Area\ under\ 2000\ and\ 600\ cm^{-1} = A_{1700} + A_{1600} + A_{1455} + A_{1375} + A_{1030} + A_{866} + A_{812} + A_{724}$

Table 4.3 shows all the indices values for five PG binders. The methylene to methyl ratio ($\frac{=CH_2}{-CH_3}$) reparents the length and degree of branching of the aliphatic side chain, high value of $\frac{=CH_2}{-CH_3}$ means that the binder has long aliphatic structure without branching (Kebukawa et al. 2013; Matrajt et al. 2013). The I_{al}, I_{ar}, $I_{C=O}$ and $I_{S=O}$ quantify the aliphatic, aromatics, carbonyls and sulfoxides in asphalt binder respectively. The I_{branch} and I_{long} represent the branched and chained alkanes in asphalt binders. Table 4.3 clearly shows that the five asphalts binders differ with each other in their functional groups. PG 52-22 and PG 58-22 have high aliphatic index and long chain alkane, but the lowest aromatic and carbonyl indices. PG 64-22 has the highest methylene to methyl ratio. PG 70-22 has the highest aliphatic and carbonyl indices, but the lowest sulfoxide and long chain alkane indices. Meanwhile PG 76-22 has the highest aromatic, branched and sulfoxide indices, but the lowest methylene to methyl ratio and aliphatic index. From the perspective of functional groups, it can be said that PG 52-22 and PG 58-22 binders have similar structure and only differ in the sulfoxide groups and the branching of the alkane. PG 76-22 binder has higher sulfoxide and aromatic indices; from the SARA analysis, it was also found that it has the highest asphaltenes content. From FTIR analysis, it appears that the functional groups and the calculated indices provide many important clues about the microstructures of the asphalt binder. Some of the indices might be related to the asphalt component and others might not be related at all. However, the mechanism and relationship is not clear among the functional groups and the components of asphalt binders. In the following section, a relationship is established between these indices and the asphalt components.

Table 4.3: Indices of functional groups and structures from FTIR test

Binder Type	$\frac{=CH_2}{-CH_3}$	I_{al}	I_{ar}	$I_{C=O}$	$I_{S=O}$	I_{branch}	I_{long}
PG 52-22	4.033	0.630	0.080	0.000	0.036	0.199	0.255
PG 58-22	3.912	0.644	0.086	0.000	0.016	0.204	0.248
PG 64-22	4.226	0.636	0.086	0.032	0.025	0.191	0.264
PG 70-22	3.632	0.659	0.091	0.049	0.012	0.216	0.241
PG 76-22	3.176	0.536	0.113	0.000	0.060	0.239	0.344

4.6.3 SARA Fractions and Functional Groups Relationship

FTIR is a quick and reliable way of obtaining information about the functional groups in the material. Although the SARA analysis is a long and complicated procedure, it fractionalizes the asphalt binder into four generic groups upon which the binder's physical properties depend. Therefore, the results from the FTIR test might be related to the SARA fractions and can provide details on asphalt component and functional groups. Pearson's correlation coefficient is determined for all 14 variables from SARA and FTIR analysis by paired comparison to determine the correlation. Figure 4.7 shows the correlation matrix of the Pearson's correlation coefficients among each pair of all 14 variables. This figure shows that some pairs have strong negative correlation, such as: asphaltenes and I_{al} , CII and I_{al} , resins and $I_{S=O}$, aromatics and I_{ar} . Others show strong positive correlation: resin and $I_{C=O}$, asphaltenes and $I_{S=O}$, asphaltenes and I_{long} , CII and I_{long} . Also, another interesting observation is that $\frac{=CH_2}{-CH_3}$ shows strong negative correlation with both I_{branch} and I_{ar} , which means that as the branching and atomicity increases in the binder the aliphatic chain length or methylene to methyl ratio decreases. From the correlation analysis, it can be said that as the asphaltenes in the binder increases the $I_{S=O}$ also increases and I_{al} decreases. It means that, high sulfoxide functional groups represent high asphaltene contents in the binder. A study by Branthaver et al. (1993a) observed that the sulfur content are strongly correlated with the asphaltenes content. Thus, the sulfoxide index can represent the asphaltenes content in the asphalt binder. Therefore, asphaltenes content is directly proportional to the sulfoxide and inversely proportional to the aliphatic groups in the binder. Similarly, resin increases with the increase of $I_{C=O}$ and aromatic decreases with the increase of I_{ar} . Thus, these functional group indices provide important and useful information about the asphalt components or SARA fractions.

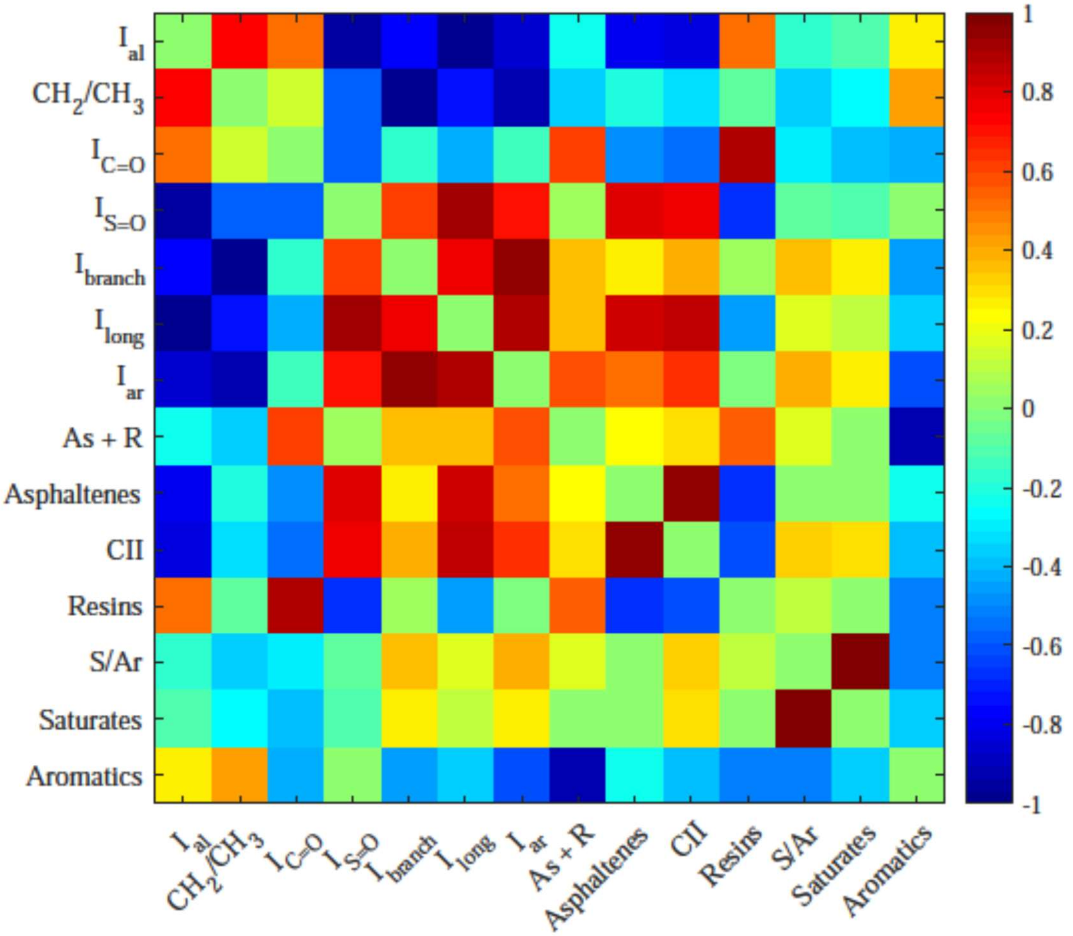

Figure 4.7: Correlation between the SARA fractions and functional groups

4.6.4 FTIR of the Damaged and Healed Asphalt Binder

In this section, the spectral changes for damaged and healed asphalt binder is quantified by the change in the absorbance peak area. For this, only three PG binders are studied: PG 58-22, PG 64-22 and PG 70-22. Initially, all binders are damaged up to 90% under cyclic loading and then the damaged binder sample is tested using FTIR. Another sample is damaged similarly under cyclic loading and then undergoes 5 hours of rest period to provide maximum healing of the damaged sample. After that FTIR is used to analyze the functional groups of the damaged and healed binders. In the FTIR spectrum for damaged and healed binder, no significant difference was found among the functional groups, except the absorbance peaks at 1375 cm^{-1} (methyl) and 1455 cm^{-1} (methylene) wavenumber. Therefore, in Figure 4.8 only the spectrum between 1300 to 1500 cm^{-1} wavenumber is shown. It can be seen that, the change in absorbance is more visible for PG 58-22 binder than PG 70-22 due to damage and healing. Both peaks at 1300 to 1500 cm^{-1} wavenumber decreases due to damage and increases due to healing. Then the area under these functional groups are determined and the change in absorbance due to damage and healed compared to undamaged spectrum is calculated. Table 4.4 shows the area under the peaks and the percentage changes in the absorbance area of the damaged and healed compared to the undamaged binder for different functional groups. All three PG binders showed a decrease in the methylene group due to damage and increase due to healing. Thus, it can be concluded that the due to the damage and healing the area under the methylene group absorbance peak changes. Damage decreases the methylene groups, however after healing the methylene groups increase. As the methylene groups represents the long chain structure in the asphalt binder, therefore during fatigue damage the long-chained molecule breaks and the after healing the long chain molecules are reconstructed fully or partially.

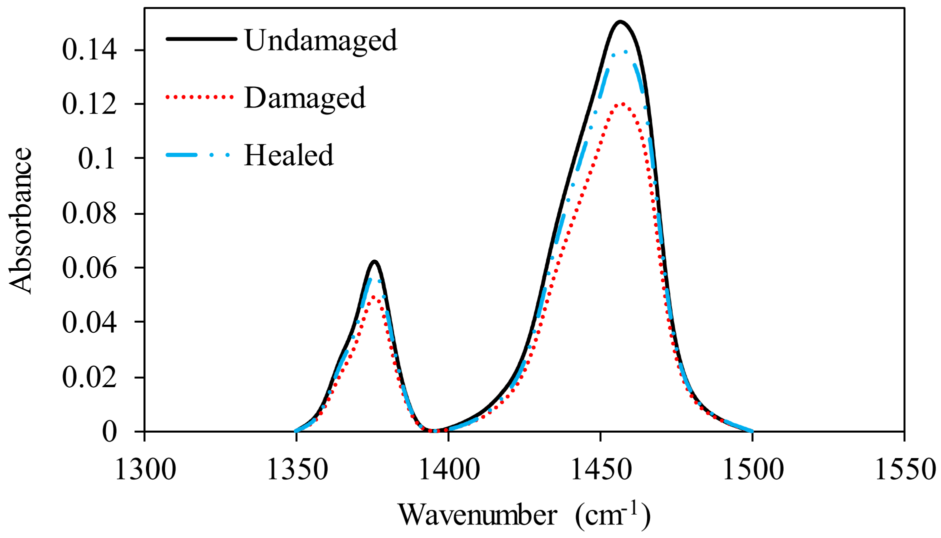

(a) IR spectrum for PG 58-22

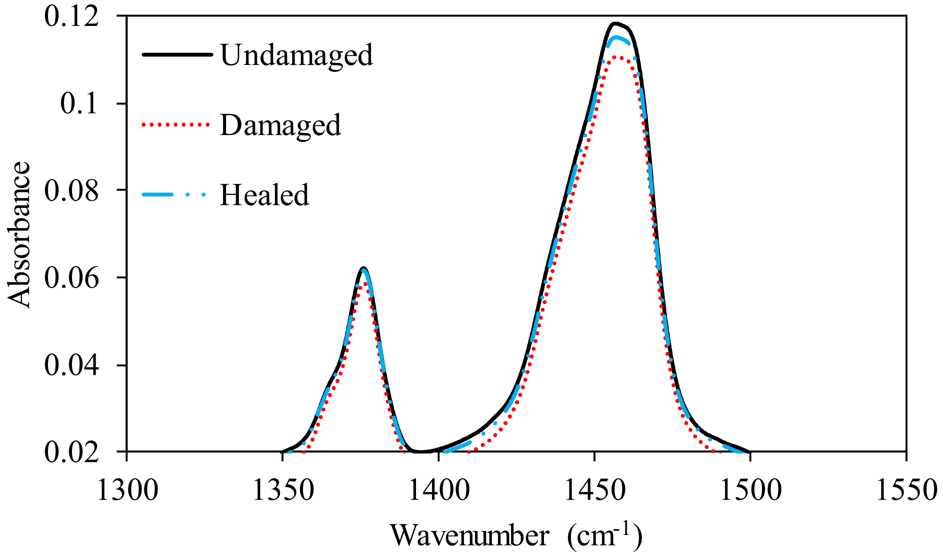

(b) IR spectrum for PG 64-22

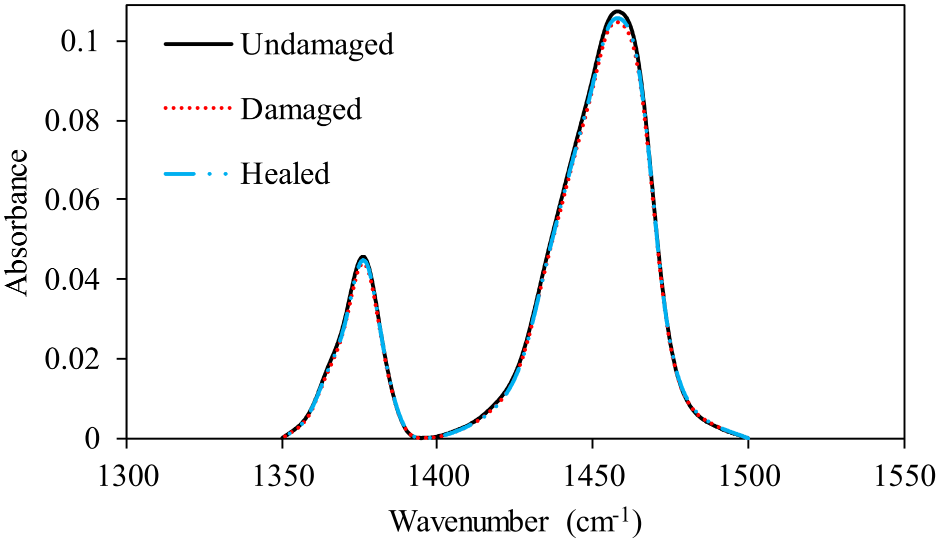

(c) IR spectrum for PG 70-22

Figure 4.8: FTIR spectrum for undamaged, damaged and healed binder

Table 4.4: Percentage changes in the absorbance area for different functional groups

Binder Type	**Condition**	**Area under the Peak**		**Change in absorbance area** $\Delta A = \frac{(A_{un} - A_{d/h})}{A_{un}} \times 100\%$	
		Methylene (=CH_2)	Methyl (CH_3)	Methylene (=CH_2)	Methyl (CH_3)
PG 58-22	Undamaged	5.42	1.08		
	Damaged	4.32	0.85	**20.30**	21.30
	Healed	5.02	0.99	**7.38**	8.33
PG 64-22	Undamaged	3.43	0.66		
	Damaged	3.26	0.66	**4.96**	0
	Healed	3.35	0.67	**2.33**	-1.52
PG 70-22	Undamaged	3.71	0.77		
	Damaged	3.6	0.74	**2.96**	3.90
	Healed	3.64	0.75	**1.89**	2.60

4.7 Remarks

Five different asphalt binders were characterized in terms of SARA analysis and FTIR methods to study the properties of the asphalt chemical structure. SARA analysis provides the generic components of the asphalt binder to understand the colloidal microstructure of the binder, whereas FTIR provides information about the chemical bonds which exist in the binder. This chapter characterizes the chemical composition and structure of the asphalt binder using the data gathered by SARA analysis and FTIR analysis.

- SARA analysis showed that the asphalt binder is a blend of four generic fractions and mutual interactions of these molecules are very complex. Hence, there is a constant research effort to better understand the relationship between these components and the microstructure of the asphalt binder. SARA analysis of five PG grade binders showed that aromatic is the predominating component in asphalt binder. However, higher PG grade binder has lower aromatic contents, which results in an increase in both asphaltenes and resins. Thus, with the increase of PG grade, asphaltenes and resins increases resulting in a hard and more viscous asphalt binder. Saturates and aromatics have similar bonds or functional groups. However, automatics contains less saturated hydrocarbons than the saturates. Also, resins and asphaltenes show many similar peaks in the FTIR spectra. But asphaltenes shows strong sulfoxide (S=O) and C=C bonds peak at 1030 and 1600 cm^{-1} wavenumbers.
- FTIR analysis reveals the functional groups in the asphalt binder. All five PG grade binders show different absorbance intensity for different functional groups. Different indices representing different functional groups are calculated to quantify the difference between the functional groups in the asphalt binders. Then this

functional groups are correlated with the SARA fractions. This was done to determine the relationship between the functional groups and SARA fractions. Results show that the sulfoxide group is highly correlated with the asphaltenes. Thus, if a binder shows high sulfoxide peak in FTIR analysis, then the binder has high percentage of asphaltenes. Similarly, carbonyl and aromatic indices represent the resins and aromatics respectively. None of the functional groups show strong correlation with saturates. However, the aliphatic chain length or methylene to methyl ratio shows negative correlation with the branched and aromatic structure, meaning binders with higher aliphatic chain length have less aromatic and branched structures.

- FTIR analysis of the damaged and healed PG asphalt binders showed that during damage the methylene groups decreases and after healing the methylene increases compared to the undamaged binder. From this it can be concluded that the fatigue damage breaks the long chains in the asphalt molecules and healing reconstructs the broken long chains in the asphalt molecules.

Data presented in this chapter contribute to the art knowledge of the asphalt binder's chemical compositions and structures and improve the understanding of the relationship between the chemical and physical properties of the asphalt binder. These results are used in the next chapter to link the healing mechanism and chemical properties of the asphalt binder.

CHAPTER 5

MECHANISM OF HEALING IN ASPHALT

5.1 General

In this chapter a physico-chemical healing model is developed for five different PG asphalt binders. The healing model is then related to the chemical properties of the binders. The first part of the chapter discusses the background and theory of the phenomenological healing model. The second part of the chapter discusses the experimental results and analysis to validate the healing mechanism for the asphalt binder.

5.2 Background

Healing depends on the cohesive strength, inter-diffusion and entanglement of the molecular chains of the material (Boiko and Prud'Homme 1998; Zhang and Rong 2012). All these properties are related to the chemical nature and the molecular length of the material (Zhang and Rong 2012). Therefore, a physico-chemical model, which is a conceptual model to explain the healing phenomenon using physical-chemical theories is employed to better understand the healing.

Healing of the asphalt binder has been studied by different research groups, however healing is mostly defined by the difference between the fatigue life predicted in the laboratory (mechanical) and the fatigue life observed in the field. Most of these studies used a shift factor to predict the fatigue life from laboratory test (Lytton et al. 1993). In Belgium, healing shift factor was used to estimate the pavement service life (Ullidtz 1999). The procedure of calculating shift factor has been already discussed in chapter 3.

A general evolution of damage-healing in self-healing material is depicted in Figure 5.1. As shown, at the micro or molecular scale, the micro-damage can be defined as the softening of the material due to the external loads. This softening is due to the rearrangement or breaking of the molecular chains within the material (Jahangir et al. 2015; Schmets et al. 2009). Therefore, the micro-damage initiates from a molecular rearrangement, resulting in loss of stiffness and then formulation of micro-cracks which also results in loss of stiffness. As healing is the reversal of the micro-damage, the backward process can be used to describe the healing mechanism. Thus, the healing would start by the closing of micro-cracks (or crack wetting), followed by strength gain across the wetted crack interface by molecular rearrangement. The mobility of lower molecular weights at the micro-damage trigger the wetting and then later leads to diffusion and molecular rearrangement. Wool and O’Connor (1981) proposed a multi-step healing model for polymer. This model mathematically relates the mechanically determined healing parameters to the wetting and inter-diffusion or molecular rearrangement. This model combines the mechanical response and molecular structure of the material to describe the healing mechanism.

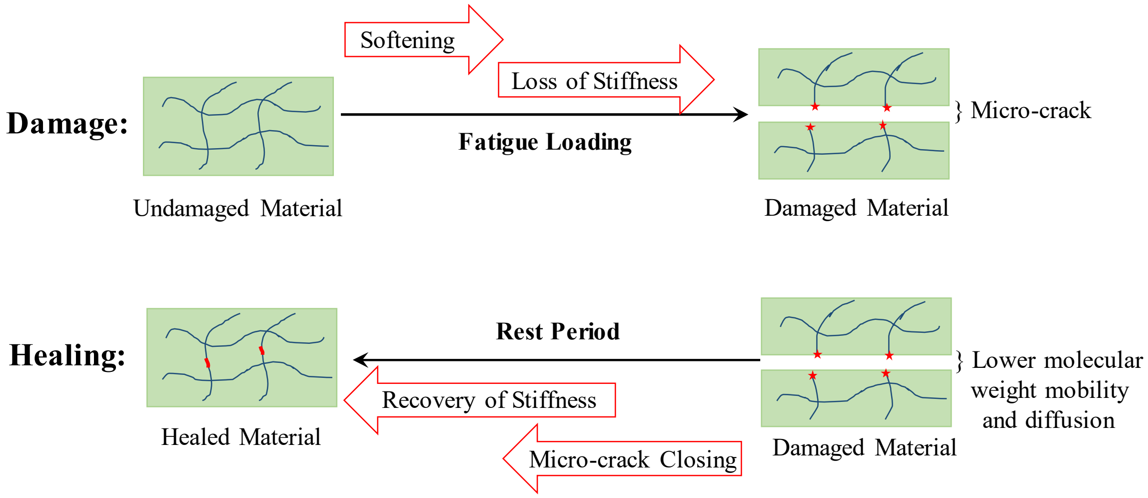

Figure 5.1: A schematic diagram of the evolution of ideal damage-healing in the asphalt binder

5.3 Healing Model

In this study, the model proposed by Wool and O'Connor (1981) is used to understand the asphalt binder healing from the mechanical and chemical point of view. This model describes five stages of healing: surface rearrangement, surface approach, wetting, diffusion and randomization. Figure 5.2 shows all five steps of healing and the random walk of the molecular chains on the surface of a micro-crack. The relations for the strength recovery (R) across the micro-crack interface for these steps are as follows:

Step (a) and (b): $R = 0$, no strength due to the micro-crack

Step (c): $R = R_0$, where R_0 is the strength recovery due to wetting or surface attraction

Step (d): $R = R_0 + R_d$, where R_d is the strength recovery due to random chains diffusing to an interpenetration distance (χ).

Step (e): $R = 1$, complete strength recovery due to healing of the micro-crack

Thus, the strength recovery due to healing starts with the micro-crack closing due to the wetting and is followed by diffusion. The wetting and diffusion can be determined using the mechanical properties of the material.

Wool and O'Connor mathematically modeled the overall healing ($R(t)$) as a convolution integral of the intrinsic healing ($R_h(t)$) and wetting distribution ($\phi(t)$) function. Eq. (5.1) shows the proposed healing model for the dimensionless healing ratio $R(t)$, where both wetting and intrinsic healing are simultaneous and time-dependent.

$$R(t) = \int_{-\infty}^{t} R_h(t-\tau)\frac{d\phi(\tau)}{d\tau}d\tau \tag{5.1}$$

$R_h(t)$ in Eq. (5.1) can be explained by the strength recovery during wetting and diffusion ($R_h(t) \approx R_0 + R_d$). The wetting component (R_0) is obtained by contacting the chains at the interface. Thus, the time dependent part in the healing model is controlled by the self-diffusion of interpenetrating chains. Wool and O'Connor used the reptation model of a polymer chain to explain the diffusion (de Gennes 1971). If the distance (l) travel by the chain over time t is given by the Einstein relation for a one-dimensional random walk in the tube as:

$$\left\langle l^2 \right\rangle = 2D_c t \tag{5.2}$$

where D_c is the diffusion coefficient and depends on the molecular weight. This random walk of the chain is related with the interpenetration distance (χ), as the chain diffuses via a double random walk process. Thus, χ can be defined as:

$$\left\langle \chi^2 \right\rangle \approx \left\langle l^2 \right\rangle^{1/2} = (2D_c t)^{1/4}$$

or

$$\left\langle \chi^2 \right\rangle \sim t^{1/4} \tag{5.3}$$

Eq. (5.3) implies that the diffusion of a chain is proportional to the one fourth of the time to travel. The strength recovery due diffusion (R_d) depends on the extent to which the chains are interpenetrated in each other, and thus the time depended strength recovery due to diffusion can be written as:

$$R_d = Kt^{1/4} \tag{5.4}$$

And the intrinsic healing function becomes

$$R_h(t) = R_0 + \left(Kt^{1/4} \otimes \dot{\psi}(t) \right) \tag{5.5}$$

Thus the Eq. (5.1) can be written as follows:

$$R(t) = \left[R_0 + \left(Kt^{1/4} \otimes \dot{\psi}(t) \right) \right] \otimes \dot{\phi}(t) \tag{5.6}$$

where $\dot{\psi}(t)$ is the diffusion initiation function and $\dot{\phi}(t)$ is the wetting rate. R_0 is the instant healing that defines the instantaneous strength gain due to wetting and the second part of the equation is the time dependent strength by the inter-molecular diffusion of micro-crack interface (K is the constant diffusion parameter).

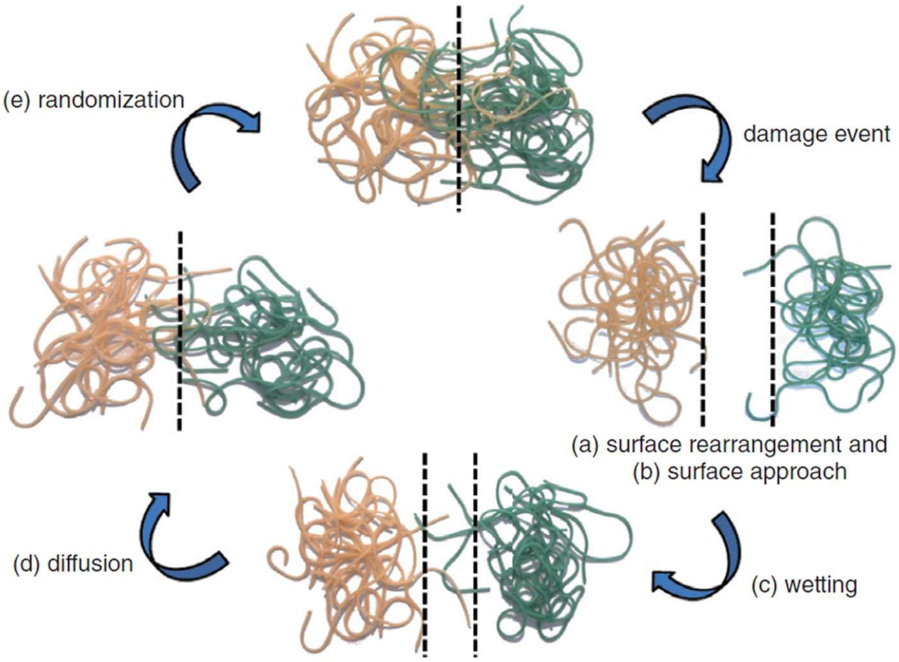

Figure 5.2: Proposed healing model by Wool and O'Connor (Braun et al. 2009)

Based on Eq. (5.6), healing processes can be divided into two parts: instantaneous strength gained due to interfacial cohesion and time dependent strength gained due to diffusion and randomization of molecules. Therefore, overall healing is divided into two parts instant healing (short-term healing) and long-term healing. As asphalt binder samples are prepared by pouring liquid binder and gradually cooling it down at room temperature, this ensures that the asphalt binder surfaces are in contact and free from any irregularities. This results in instantaneous wetting for the asphalt binder, which means instantaneous disappearance of micro-crack interface and complete molecular contact. For instant wetting Wool and O'Connor assumed $\dot{\phi}(t) = \delta(t)$ where $\delta(t)$ is the Dirac delta function. And if the end of molecular chain at the micro-crack interface do not need any rearrangement and they are available at the interface then the diffusion parameter can be assumed as $\dot{\psi}(t) = \delta(t)$. Then Eq. (5.6) can be rewritten as:

$$R(t) = R_0 + Kt^{1/4} \approx H(t) \tag{5.7}$$

Eq. (5.7) describes the overall healing process of the asphalt binder, where the total healing $R(t) \approx H(t)$ can be calculated from the healing test data as a function of the rest period. Here, R_0 represents the instant healing due to the crack surface wetting and depends on the cohesive property of material. K represents the inter-molecular diffusion rate between the crack surfaces at certain temperature. The second part is the long-term healing, which is dependent on the molecular diffusion at the crack surfaces and depends on the molecular chain length (Kausch 1991; Kausch and Dettenmaier 1982).

5.4 Healing in Asphalt Binders

5.4.1 Experimental Plan for Healing

Time sweep test with rest period (loading–rest–loading) was conducted on five different PG grade binders (PG52-22, PG 58-22, PG 64-22, PG 70-22, PG 76-22) using DSR to investigate healing of the asphalt binder. Cylindrical samples of 8 mm diameter and 2 mm thickness were used and tested under strain control cyclic loading mode. During the cyclic loading, a strain of 5% amplitude was applied, and during the rest period the temperature-gap control setting was used. This strain level for the loading period was chosen based on the linear viscoelastic (LVE) limit from the strain sweep test. For all the binders, the LVE range was 2.5% strain. To prompt the damage during loading period in the sample, the 5% strain was chosen. These tests were conducted at 20 °C temperature and at 10 Hz loading frequency. Three replicate samples were tested for all binders. All samples were loaded till the sample modulus (G^*) was reduced to 60% of the initial G^* value (G_i^*), then the loading was stopped and the samples were allowed to heal over different length of times (rest periods) ranging from 5 secs to 2 hours. After the rest period, the samples were again loaded until the failure. A schematic of the healing test configuration is shown in the Figure 5.3. Thus, the healing was estimated as a function of the rest period. The healing index (*H*) is calculated as follows:

$$H(t) = \frac{G_r^* - G_L^*}{G_i^* - G_L^*} \tag{5.8}$$

where G_r^* is the G^* after the rest period and G_L^* is the G^* after loading (Figure 5.3). $H(t)$ is calculated for different rest periods, then used in the healing model to quantify the instant healing and long-term healing.

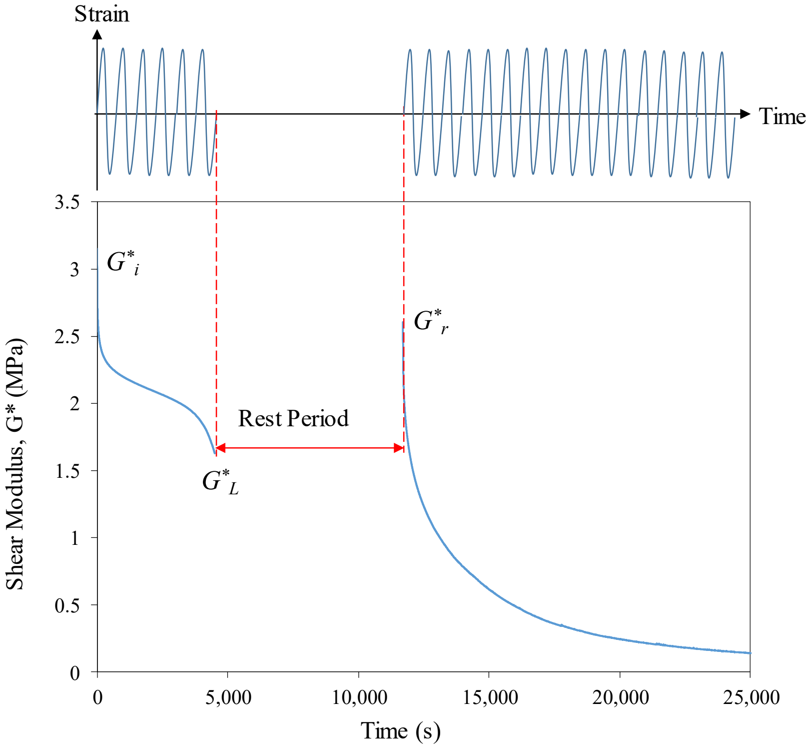

Figure 5.3: Healing test protocol and schematic of results

5.4.2 Healing Test Results

Figure 5.4 (a) show the healing index (H) calculated from Eq. (5.8) over various rest periods (t) for different binders at 20 °C. This figure shows that with the increase in rest period the healing increases which means that during the rest period some of the damage recovers and the modulus recovers close to the initial modulus. PG 58-22 has the highest H value over two hours of rest period and PG 76-22 has the lowest. Also, there is a rapid increase in the H value approximately in the first 40 secs, then the healing rate gradually decreases. Therefore, the overall healing in the binders can be divided into instant and long-term healing. As the binder shows these two distinct parts in healing therefore the model proposed by Wool and O'Connor can be used in the asphalt binder. The experimental data for the all five binders are plotted as H vs t and then Eq. (5.7) is fitted (Figure 5.4 (b)). The fitted curves and all the fitting parameters are listed in Table 5.1. For all the fitted curves, the coefficient of determination (R^2) value is above 0.89, which means the fitted model strongly agrees with the actual data. In Figure 5.4 (b) two distinct part can be seen in H, the initial part is constant and then the second part is time dependent.

Table 5.1 shows that, as the PG grade increases the R_0 value decreases. Which means that higher PG grade binders have less instant healing. Thus, the higher the binder grade the lower the instant strength recovery due to instant healing. Higher PG grade means higher stiffness than the lower PG grade binder at same temperature. Hence, it can be said that the harder binder has less instant healing than the softer binder. Also, long-term healing rate is predicted from the healing model using experimental data. Table 5.1 shows the value of all five binders' long-term healing rate (K). PG 76-22 has the lowest value of K and

PG 64-22 has the highest K value. This means that PG 76-22 has lower rate of long-term healing, resulting in slower strength recovery over the long rest period. In summary, it is possible to approximately measure the healing of asphalt binder using the physico-chemical model proposed by Wool and O'Connor.

Now the issue is to understand the relationship between these two parts of healing and the fundamental material properties. The instant and long-term healing depend on the wetting of micro-crack surfaces and the molecular diffusion at the wetted crack surfaces respectively. The instant healing is the part where material gains immediate strength due to interfacial cohesion at the micro-crack interface. The long-term healing is the part where material recovers due to the rearrangement of the molecules across the interface over time. Thus, to understand healing, these two parts needs to be explained from the chemical and microstructural point of view. The following subsections address one way of measuring the wetting parameter using binder cohesion, then relate that with the instant healing. Also, measure and relate the molecular chain length with long-term healing rate.

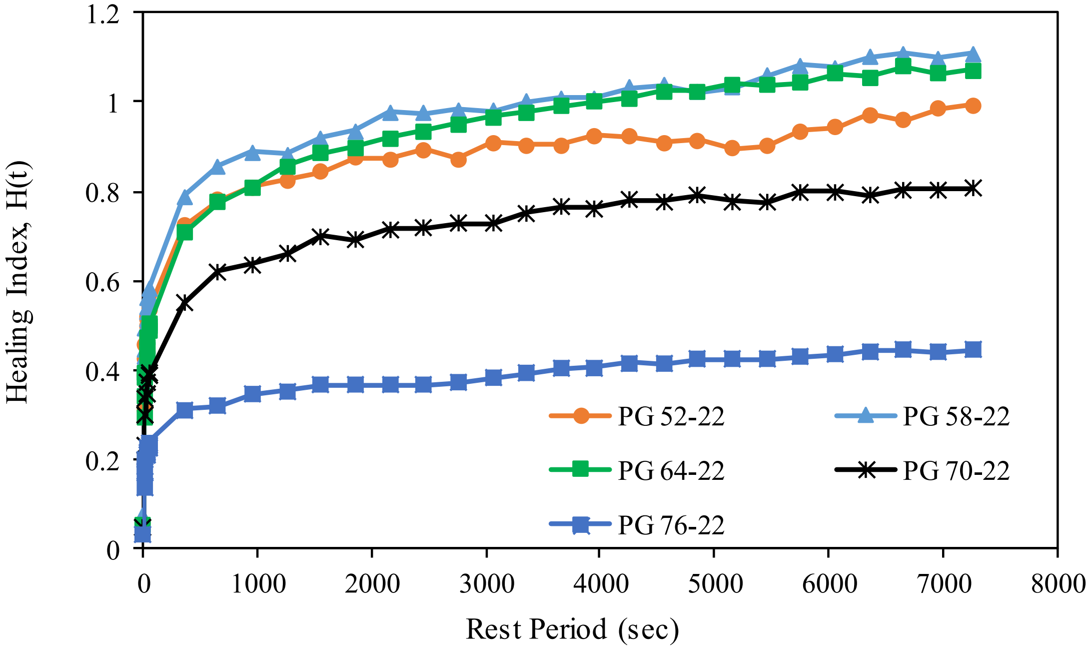

(a) Healing index over the rest period

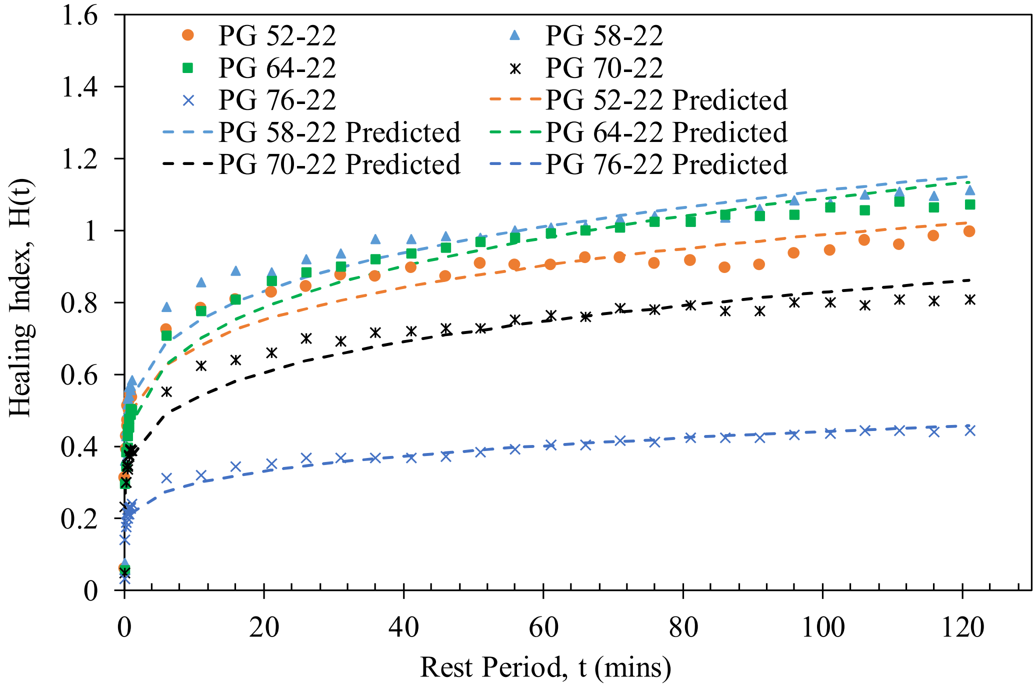

(b) Fitted curves of the healing model for all PG binders

Figure 5.4: Healing over different rest periods (healing time) and fitted healing model

Table 5.1: Healing model and the fitted parameters for all the binders

Binder type	Healing Model	R^2	R_0	K
PG 52-22	$H(t) = 0.2698 + 0.227\, t^{1/4}$	0.8973	0.2698	0.227
PG 58-22	$H(t) = 0.2677 + 0.2664\, t^{1/4}$	0.9304	0.2677	0.2664
PG 64-22	$H(t) = 0.173 + 0.2896\, t^{1/4}$	0.9566	0.173	0.2896
PG 70-22	$H(t) = 0.1579 + 0.2117\, t^{1/4}$	0.9423	0.1579	0.2117
PG 76-22	$H(t) = 0.1085 + 0.1054\, t^{1/4}$	0.9354	0.1085	0.105

5.4.2.1 Instant Healing

Instant healing depends on the interfacial cohesion between the micro-crack surfaces and is defined as wetting. Wetting of the crack surface can be explained by the fundamental material properties from the contact mechanics perspective. No external loading is applied during the rest period; thus, wetting is basically the intermolecular forces at the crack surface. Wetting ensures the contact of the crack surfaces and can be measured as the energy required to separate the interfacial surfaces. Schapery (1989) showed that the micro-crack wetting is a function of the fundamental material properties such as intermolecular surface forces and cohesion. A study by Wool (1991) showed that wetting is function of the tack strength. He showed that tack (force applied to the cross-sectional area) can determine the initial wetting and the time-dependent wetting. For the asphalt binder, immediate wetting is considered therefore, in this study the energy of separation (W_s) is used as a measure of the initial wetting. W_s is determined using tack test, which measures the energy required to separate the asphalt binder-binder surface (Kanitpong and Bahia 2005). W_s is an important parameter as it measures the ability of two material interfaces to resist the separation, when they bought into contact under high pressure and for a short period of time. The energy of separation (W_s) is proportional to the cohesive strength of the material but only influenced by the contact time (Hamed and Shieh 1983, 1985; Patrick 1981). Therefore, in this study the contact time of the tack test is kept the same for all the binders tested.

5.4.2.1.1 Tack Test

DSR was used to conduct the tack test to measure the cohesive strength or the energy of separation of the asphalt binder (Bahia et al. 2001). For this test, a sample with 25 mm diameter was used and three replicate samples were tested for each binder. DSR parallel plate geometry is used for the tack test. A schematic of the tack test is shown in Figure 5.5 (Creton and Fabre 2002). It can be seen in Figure 5.5 that the tack test consists of three intervals. Initially, the sample was compressed into 1.5 mm thickness and the normal force was kept to zero for 200 sec. Then an additional compressive normal force of 10N was applied to the sample to ensure that the DSR plate-binder contact. The upper plate of the DSR was moved upward at a speed of 0.1 mm/s. This upward tension causes debonding of the binder. DSR can measure the applied force and gap increase (vertical displacement) over time. The area under the force-time curve is referred to as the tack factor (T_c), which represents the stickiness of the binder (Kanitpong and Bahia 2005). This can also be represented by the energy of separation (W_s). W_s is calculated using the following equation:

$$W_s = \frac{1}{A}\int F \cdot v \cdot dt = d\int \sigma \cdot d\varepsilon \qquad (5.9)$$

where F is the applied force, v is the speed of separation, A is the contact area and d is the specimen thickness. W_s is an important parameter as it measures the energy required to separate the asphalt binder-binder surface (Kanitpong and Bahia 2005). As all the samples tested in this study showed cohesive failure (failure in the binder), W_s can be used as a measure of cohesive strength of the binder.

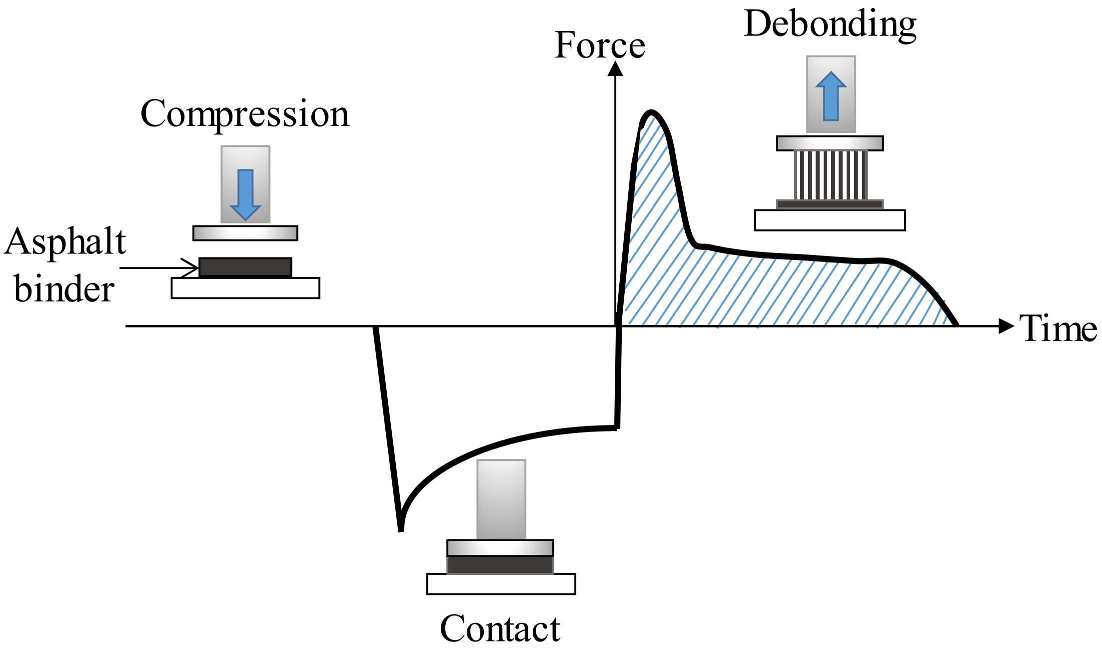

Figure 5.5: Schematic of the tack test by DSR (Creton and Fabre 2002)

5.4.2.1.2 Tack Test Results

Figure 5.6 shows the results from the tack test for all the binders. Figure 5.6 (a) shows the force vs. time curves for all the PG binders. Figure 5.6 (b) shows the stress-strain curves for all binders. The area under the stress-strain curve shows that PG 52-22 binder has the highest area and PG 76-22 has the lowest area. As PG 52-22 is a softer binder, it takes less force to pull out the binder compared to PG 76-22 binder. Figure 5.6 (c) shows the energy of separation (W_s) and the R_0 parameters from the healing model for all the binders. This figure shows that the higher the PG grade the lower the W_s value. This means that harder binder has less stickiness, which basically leads to a decrease in the cohesive strength. This reduction in cohesive strength can be due to the increase in asphaltenes and resins content in the asphalt binder. As showed in chapter 3, with the increase in the PG grade the sum of the asphaltenes and resins content (*As* + *R*) also increases, which results in a decrease in aromatics oil in the asphalt binder, which increases the hardness and decreases the cohesion. Therefore, the cohesion or the tackiness decreases with the increase in the hardness of the asphalt binder.

R_0 in the healing equation (Eq. 5.7) corresponds to the instant healing of the wetted surface, which can be related to the cohesive strength of the asphalt binder. The energy of separation has been previously used as the measure of cohesion property of the binder (Bahia et al. 2001). As asphalt binder has a very complex molecular structure, in this study the W_s from the tack test has been correlated with R_0 from the healing model as a measure of cohesion. Figure 5.6 (c) shows the comparison of the trends of R_0 values with that of W_s from the tack test for all binders. As predicted, the values of R_0 show the same trend as W_s. Figure 5.6 (d) shows the R_0 vs W_s plot, which shows that the relation between R_0 and W_s is strong, linear and positive. The Pearson correlation coefficient is +0.920. The fitted linear curve shows a coefficient of determination (R^2) value of 0.84. This means that R_0 can be reliably predicted using W_s. Also, the Pearson correlation coefficient between R_0 and (*As* + *R*) is -0. 874. Which means that with the increase of asphaltenes and resins instant healing decreases. As ($As + R$) represents the large molecules in the binder, this means that instant healing is negatively correlated with the large molecules in the binder. The fitted linear curve between R_0 and ($As + R$) shows a R^2 value of 0.76 (Figure 5.6 (e)). Thus, it can be concluded that as the binder hardens with the increase in asphaltenes and resins contents, the cohesive strength or the energy of separation decreases resulting in the reduction of the wetting capability of the binder. And the instant healing decreases with the increase in asphaltenes and resins components in binder molecule.

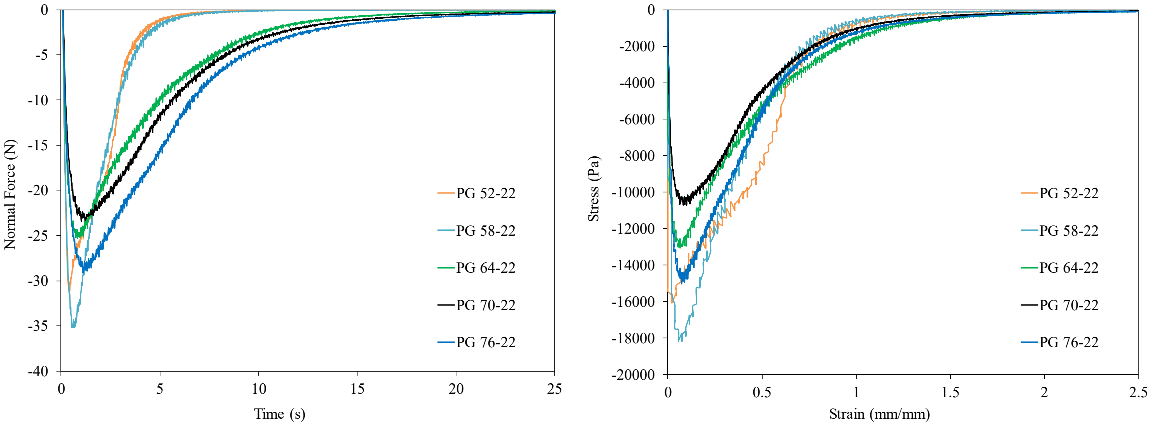

(a) Force vs. time plot (b) Stress vs. strain plot

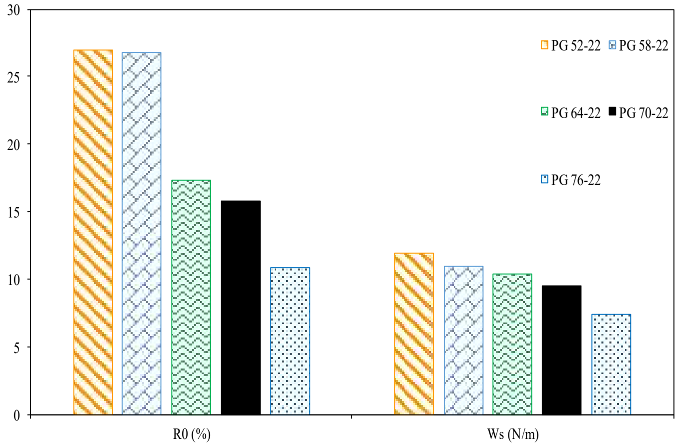

(c) R_0 and W_s

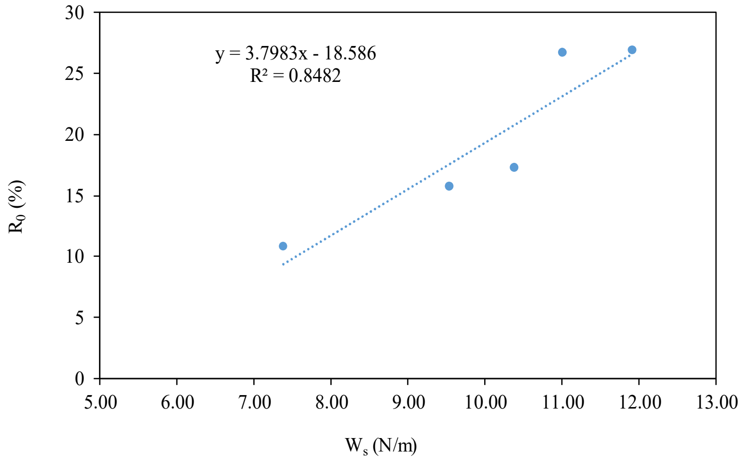

(d) Relation between R_0 and W_s

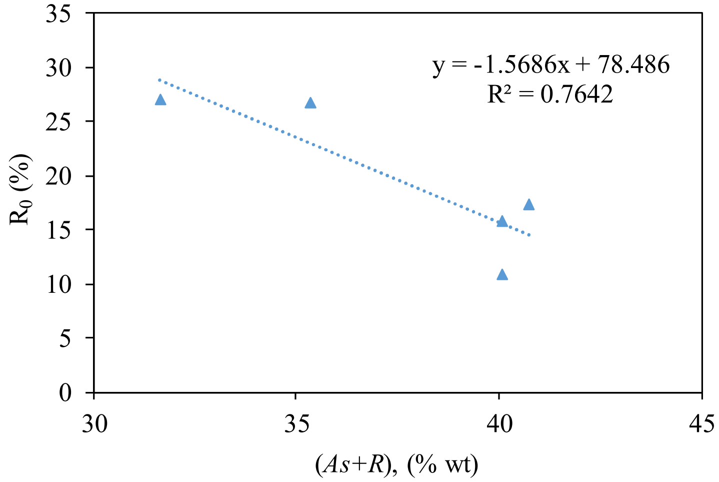

(e) Relation between R_0 and (asphaltenes + resins)

Figure 5.6: Tack test results and relation with the instant healing

5.4.2.2 Long-Term Healing

After the wetting of the micro-crack interface, the later part of healing is slow and depends on time. This time dependent healing is basically dependent on molecular chain and their motion. Thus, the long-term healing part is related to the mobility and self-diffusivity of the asphalt binder molecules. Based on the healing mechanism discussed above it can be concluded that the asphalt binder containing molecules with longer chains and few branches will show higher mobility and diffusivity to recover the damaged molecular structure. A study by de Gennes (1971) shows that the molecular mobility is very important for the movement of molecules across the crack interface and healing.

Figure 5.4(b) shows the long-term healing of different asphalt binders. PG 64-22 shows the highest rate of healing or rate of diffusion. The molecular diffusion rate of the PG asphalt binders increases with PG grade; however, for PG 76-22 it decreases. The order of the diffusion rate (K) for the PG binders are as follows: PG 64-22 > PG 58-22 > PG 52-22 > PG 70-22 > PG 76-22. Except for PG 64-22, the rest of the binders show a strong negative correlation of -0.816 between asphaltene content and diffusion rate (K). This means that as the percent of large molecules increases in the asphalt binder the movement of the molecules becomes difficult, resulting in a slow rate of diffusion. Thus, the increase in asphaltenes in the binder decreases the rate of long-term healing.

To further prove that longer chain and less branching in the binder results in high rate of diffusion FTIR analysis is conducted for all five binders. Then the diffusion rate is compared with the methylene to methyl ratio ($\frac{=CH_2}{-CH_3}$), which represents the length of the molecular chains in asphalt. The higher $\frac{=CH_2}{-CH_3}$ ratio means a lower content of branched-chain in asphalt, which results in a long chained molecular structure. Figure 5.7 (a) shows the comparison of the trends of K values with that of $\frac{=CH_2}{-CH_3}$ from the FTIR analysis for all binders. As expected, the values of K show the same trend as $\frac{=CH_2}{-CH_3}$. Figure 5.7 (b) shows the K vs. $\frac{=CH_2}{-CH_3}$ plot, which indicates that the relation between K and $\frac{=CH_2}{-CH_3}$ is strong, linear and positive with a Pearson correlation coefficient of +0.942. The fitted linear curve shows a R^2 value of 0.858. Thus, from the correlation coefficient it can be concluded that diffusion rate (K) is mostly dependent on the molecular chain length, rather than the asphaltene content in the binder.

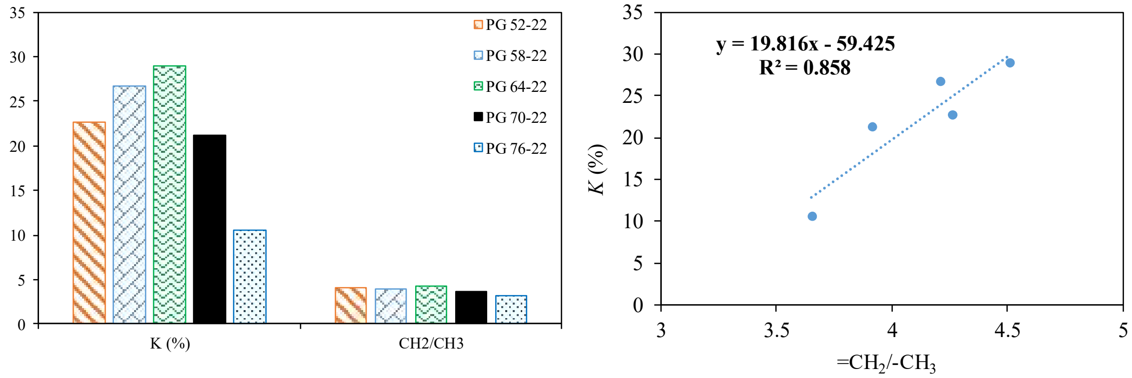

(a) K and $\frac{=CH_2}{-CH_3}$ (b) Relation between K and $\frac{=CH_2}{-CH_3}$

Figure 5.7: Long-term healing rate vs. methylene to methyl ratio from FTIR

5.4.2.3 Generalized Healing Model

The above discussion indicates that the instant healing and long-term healing have strong positive correlation with the energy of separation (W_S) and methylene to methyl ratio ($\frac{=CH_2}{-CH_3}$) respectively. Therefore, a generalized healing model for all asphalt binders is proposed using these two parameters. In this model, the healing index is assumed to be a function of the energy of separation, methylene to methyl ratio and rest period. This model follows the Wool and O'Connor model. It is assumed that in the overall healing there is an instant part which is linearly related to W_S and a time dependent part which is dependent on both $\frac{=CH_2}{-CH_3}$ and rest period. Therefore, the proposed equation for modeling the healing index (H) is as follows:

$$H(t) = a \times W_s + b \times \frac{=CH_2}{-CH_3} \times t^m \tag{5.10}$$

where a, b and m are the fitting parameters. Using nonlinear least square method in MATLAB, the experimental data for all five binders are fitted to this equation to calculate the fitting parameters. The value of a, b and m are found to be 0.0233, 0.0537 and 0.2566 respectively. The (R^2) value for this fit is 0.8659, which indicates that the fitted model strongly agrees with the actual data. Also, the sum of squares of the residuals (SSR) if this fit is found to be 3.2055, which is a measure of the deviation between the measured data and the fitted data. A small SSR indicates a good fit of the model to the measured data. After calculating the fitting parameters, the generalized healing model for all binders can be written as follows:

$$H(t) = 0.0233 \times W_s + 0.0537 \times \frac{=CH_2}{-CH_3} \times t^{0.2566} \tag{5.11}$$

Figure 5.8 shows the plot of the predicted vs. measured healing index of the five PG binders. This figure shows that all the points are near the line of equality (LOE) without any significant bias. It implies that the generalized healing model proposed in Eq. 5.11 provides a good prediction of the experimental healing index for the five PG binders.

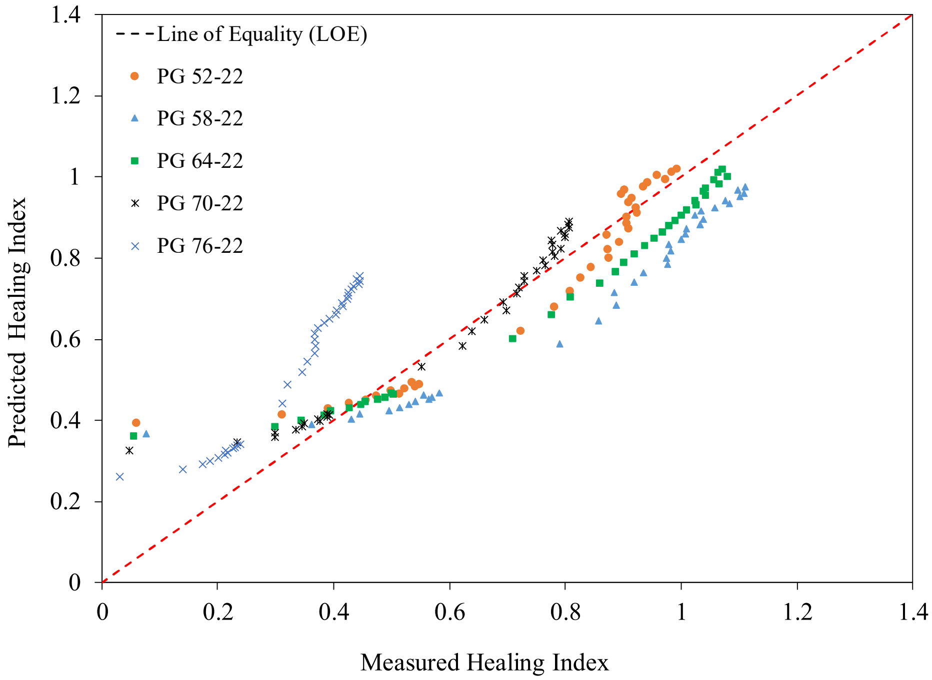

Figure 5.8: Comparison between the measured and predicted healing index using the generalized healing model

5.5 Remarks

The damage introduced by fatigue loading in the asphalt binder can heal over time. Asphalt binder healing can be explained by the physico-chemical healing model proposed by Wool and O'Connor. This model has been well accepted in polymer healing. Using this model the overall healing of the asphalt binder is divided into two parts: instant healing and long-term healing. Then these two parts of healing is explained from the molecular structural point of view. The main findings in this chapter are summarized as follows:

- Asphalt binder healing explained by the two-stage healing model, which distinguishes the wetting and the molecular diffusion at the crack interface during healing. As the asphalt binder shows instant wetting the healing due to the wetting is instantaneous and fast defined as instant healing. Whereas, molecular diffusion is a slow and time dependent process and defined as long-term healing.

- Instant healing of the asphalt binder depends on its cohesive properties. This study uses the energy of separation as the indicator of the cohesive property of the asphalt binder. Results show that as the PG grade of the binder increases the energy of separation decreases, which results in a reduction in instant healing. This decrease in energy of separation is due to the increase in large molecules such as asphaltenes and resins in the asphalt binder. The increase in large molecules in the asphalt binder reduces the mobility of binder resulting in a decrease in wettability.
- The long-term healing depends on the rate of molecular diffusion at the crack interface. This molecular diffusion mostly depends on the molecular structure. If a binder has long chained structure then it has high diffusion rate, but if the binder has more branched or ring type structure then the diffusion rate decrease. Results show that the asphalt binder with high methylene to methyl ratio has high diffusion rate. Thus, the binder with long chained structure will have higher long-term healing rate than the one with branched structure.
- The PG binders can be sorted according to the instant healing as: PG 52-22 > PG 58-22 > PG 64-22 > PG 70-22 > PG 76-22. Whereas, the order of long-term healing in the PG grade is as follows: PG 64-22 > PG 58-22 > PG 52-22 > PG 70-22 > PG 76-22.

From the above discussion, it can be concluded that healing of the asphalt binder depends on the its chemical composition and properties. Therefore, a generalized healing model for all binders is proposed by considering healing as a function of energy of separation, methylene to methyl ratio and rest period. All the binders studied in this chapter are unconditioned and unaged. However different types of conditioning (such as: moisture conditioning, aging and modification using different additives) can change the chemical composition and properties of asphalt of binder. Therefore, the influence of different conditioning on asphalt binder healing properties is studied in the next chapter.

CHAPTER 6

INFLUENCE OF DIFFERENT FACTORS ON HEALING

6.1 General

This chapter discusses the influence of aging and moisture conditioning on the asphalt binder healing. The chemical composition of the asphalt binder plays an important role in healing phenomenon of the asphalt binder. Different types of conditioning such as aging (or oxidation) and moisture conditioning can change or influence the chemical composition of the asphalt binder. Previous studies showed that aging changes the asphalt binder viscosity (Tarefder and Yousefi 2015; Traxler 1961). A study by García et al. showed that the viscosity of the asphalt binder plays an important role in asphalt binder healing (García 2012; García et al. 2015). From their study of healing they concluded that lower viscosity has higher healing. Moisture conditioning of the asphalt binder results in water diffusion into the binder. A study by Vasconcelos et al. (2012) shows that if asphalt binder is submerged under water for several days then the absorbed water in the binder is visible in the FTIR spectrum at 3100-3700 cm^{-1} wavenumber region. This change in asphalt composition can affect the asphalt binder healing. As aging and moisture conditioning changes the chemical composition of the asphalt binder, it is necessary to study the impact of these conditioning. Also, addition of fines/fillers in the binder to prepare mastic may interrupt the continuous molecular structure of the binder, which can also effect the healing ability of binder. Therefore, the effect of fine content on healing is also studied in this chapter.

6.2 Influence of Aging on Healing

To evaluate the effects of aging, PG 58-22 and PG 70-22 binders are aged in three different levels and then compared with the unaged binders. The changes in the functional groups due to aging are then evaluated using the Fourier Transform Infrared (FTIR) spectroscopy. The healing and cohesive properties of the binders are measured using healing test and tack test as discussed in chapter 5. Healing model developed in chapter 5 is used to calculate the instant and long-term healing of the aged binders. Then the chemical and mechanical changes due to aging is related with the instant healing and long-term healing.

6.2.1 Aging Procedure

Two Performance Grade binders, PG 58-22 and PG 70-22, were used and three types of aging were considered. Laboratory conditioning was performed using the Rolling Thin Film Oven (RTFO) and Pressure Aging Vessel (PAV). The RTFO simulates the short term aging and the PAV simulates the long-term aging (5 years) of the binder (Migliori and Corté 1998). To simulate more than 5 years of aging, a second PAV ($\approx$ 10 years) was done on the initially PAV aged binder. Short-term aging occurs during the production and construction process of the asphalt pavement and long-term aging occurs during the service life. The RTFO procedure took unaged asphalt binder in cylindrical glass bottles and placed them in a rotating carriage oven at 325 °F (163 °C) for 85 minutes at 15 RPM according to the AASHTO T 240-13 test protocol (AASHTO 2013). In PAV, RTFO aged asphalt binder was placed in stainless steel pans and then conditioned for 20 hours in a heated vessel pressurized to 305 psi according to the AASHTO R 28-12 test protocol (AASHTO 2012).

For the double PAV binder, the PAV aged binder was conditioned for 20 hours at 100°C and 305 psi according to the PAV procedure (a total of 40 hours PAV).

6.2.2 Healing Test Results

Figure 6.1 (a) and (b) show the healing index (H) over the rest periods (t) for different level of aging binders for PG 58-22 and PG 70-22 respectively. For all the aging levels, PG 58-22 binder shows more healing than PG 70-22. This figure shows that as the ageing of the asphalt binder increases the healing index decreases. The unaged binder shows highest healing index over time, which means that the recovery of damage in unaged binder is faster than in the aged binders. As the aging increases the healing index decreases. For the RTFO aged PG 70-22 binder the healing index decreases approximately 30% compared to the unaged binder, whereas for double PAV the reduction in healing index is about 80%. The PAV and double PAV aged binders show similar healing indices over the rest period. For aged binder, two distinct parts in the healing is observed: initially a sudden increase in the healing index in approximately the first 40 secs of the rest period and then a gradual increase over the rest period. Thus, aged binders also showed the similar healing pattern as the unaged binder. The fitted healing model curves and all the fitting parameters are listed in Table 6.1. For all the fitted curve R^2 value is above 0.91, which means that the fitted model strongly agrees with the actual data. In Figure 6.1 (a) and (b) two distinct parts can be seen in H, the initial part shows sudden increase in H and then the second part is time-dependent.

Table 6.1: Healing model and the fitted parameters for all aged binders

Binder	Aging condition	Healing Model	R^2	R_0	K
PG 58-22	Unaged	$H(t) = 0.2677 + 0.2664t^{1/4}$	0.9304	0.2677	0.2664
	RTFO	$H(t) = 0.376 + 0.1124t^{1/4}$	0.9238	0.3760	0.1124
	PAV	$H(t) = 0.1147 + 0.1922t^{1/4}$	0.9128	0.1147	0.1922
	Double PAV	$H(t) = 0.1371 + 0.1467t^{1/4}$	0.9225	0.1371	0.1467
PG 70-22	Unaged	$H(t) = 0.1579 + 0.2117t^{1/4}$	0.9423	0.1579	0.2117
	RTFO	$H(t) = 0.1014 + 0.1711t^{1/4}$	0.9551	0.1014	0.1711
	PAV	$H(t) = 0.0379 + 0.1539t^{1/4}$	0.9361	0.0379	0.1539
	Double PAV	$H(t) = 0.0228 + 0.1482t^{1/4}$	0.9634	0.0228	0.1482

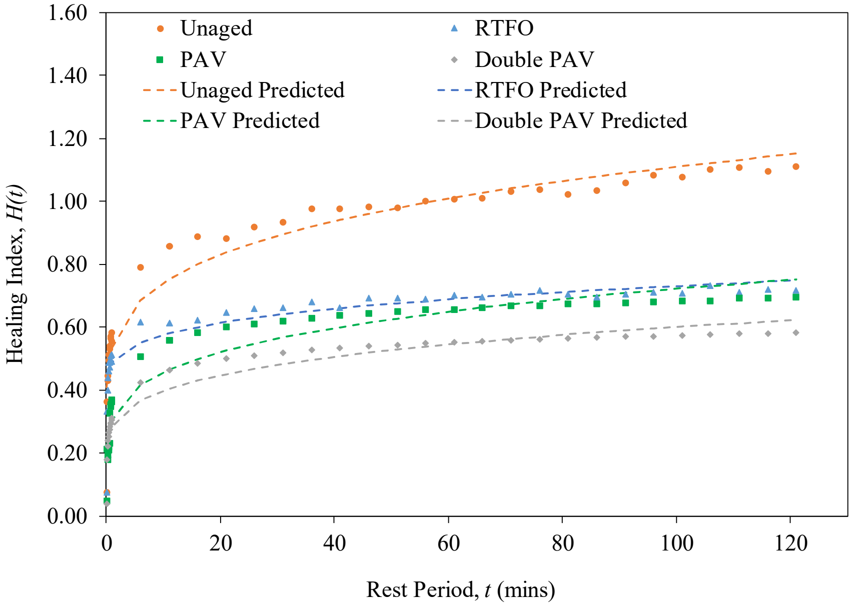

(a) Healing over time for PG 58-22 aged binders

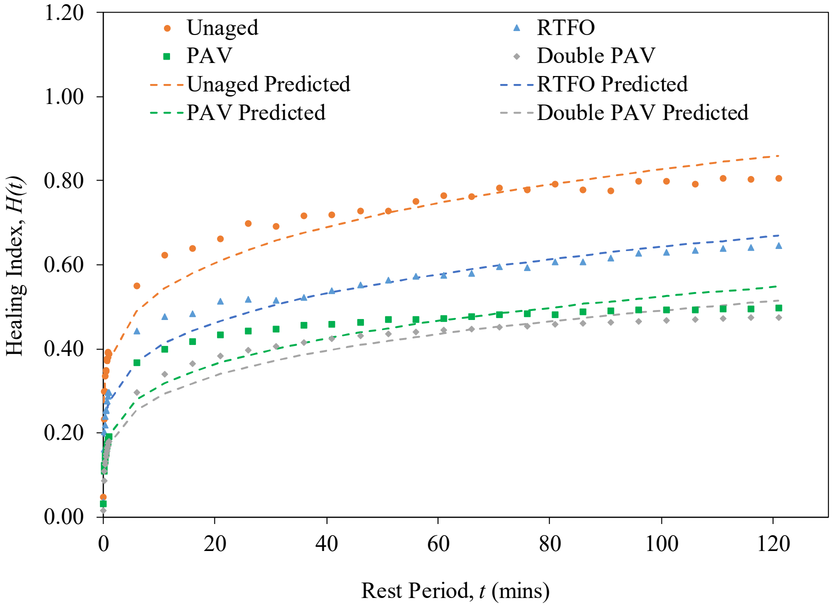

(b) Healing over time for PG 70-22 aged binders

Figure 6.1: Healing model for different levels of aged binder

Table 6.1 shows that, for PG 70-22 with aging R_0 value decreases dramatically. The R_0 value decreases by 75% and 85% for PAV and double PAV aged binders compared to the unaged binder respectively. It means that the aged binders have less instant healing. Thus, higher the level of aging the lower the instant strength recovery due to instant healing. Since with aging the hardness of the binder increases, it can be said that the harder binder has less instant healing than the softer binder. Also, the long-term healing rate of the aged binder is lower than the unaged binder. However, the decrease in the long-term healing rate is not as extreme as the instant healing. For the double PAV aged binder, the long-term healing rate decreases by about 29% with compare to the unaged binder.

6.2.2.1 Instant Healing

Figure 6.2 shows the relationship between R_0 with the energy of separation of PG 58-22 and PG 70-22 for all aging conditions. The energy of separation is calculated from the tack test as a measure of cohesion. The R_0 value decreases with the increase in aging. The energy of separation (W_s) does not show any particular pattern for aged binders. for all four aging conditions also show decreasing pattern except for RTFO aged binder. Thus, by using W_s from the tack test method the effects of aging on the instant healing cannot be explained. Therefore, W_s cannot be related to the instant healing of short-term aged binder.

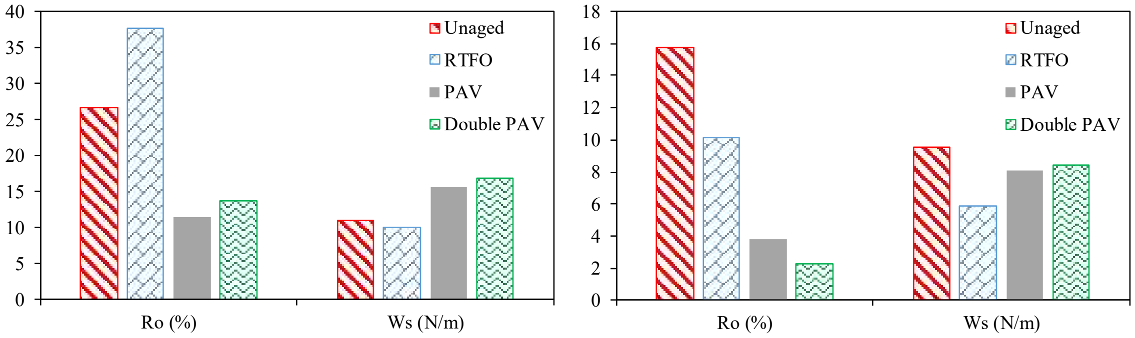

(a) PG 58-22 (b) PG 70-22

Figure 6.2: Relation between R_0 and W_s for aged binders

6.2.2.2 Long-Term Healing

FTIR analysis is conducted to observe the chemical changes in the binder due to aging and to relate that with the long-term healing. The functional groups in the material is assigned according to the FTIR spectra main bands. Figure 6.3 (a) and (b) shows the FTIR spectrum for PG 58-22 and PG 70-22 respectively. It shows that due to aging the only significant change is at 1030 cm^{-1} wavenumber. This is the sulfoxide peak and as discussed earlier, high sulfoxide represents high asphaltene contents. This means that with aging the asphaltene content increases in the binder. A study by Tarefder and Arisa (2011) showed the similar findings. It can be seen from Figure 6.3 that the % absorbance of some functional groups changes due to aging. To quantify these changes, different indices are calculated for all the functional groups in Table 6.2.

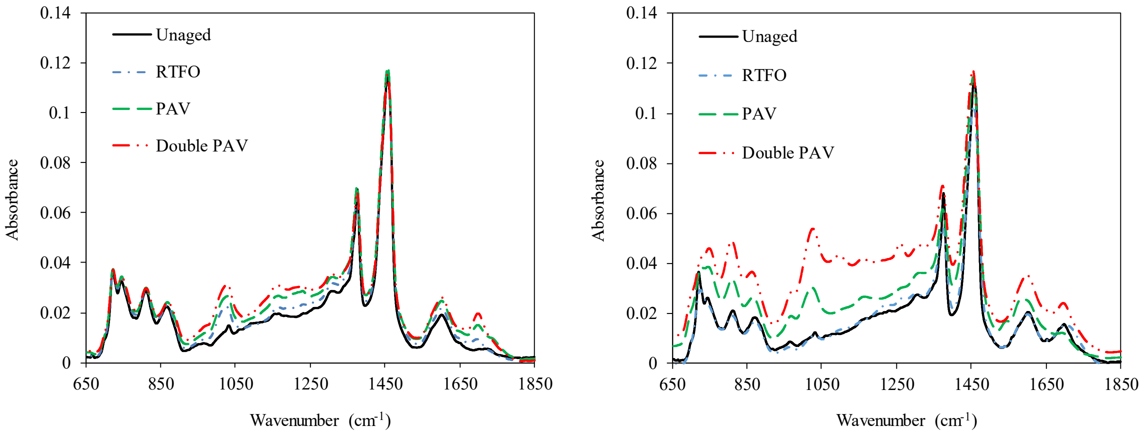

(a) PG 58-22

(b) PG 70-22

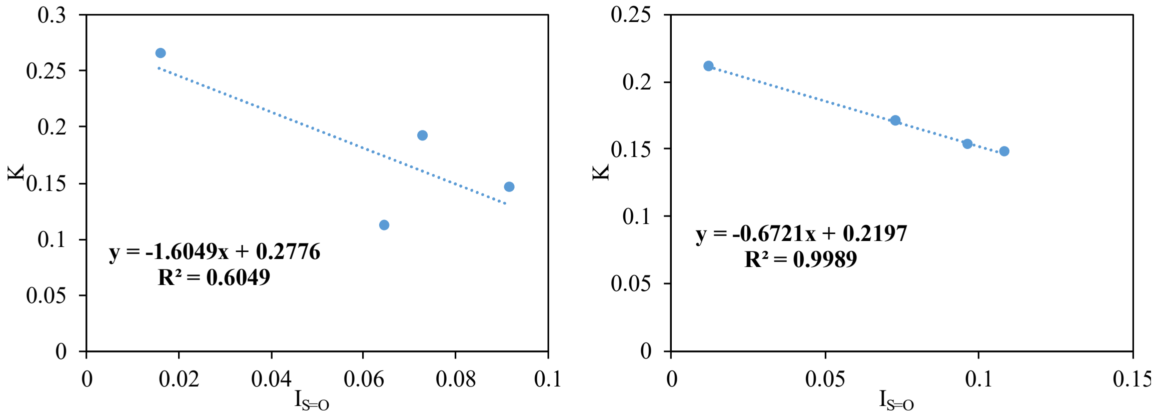

(c) K vs $I_{S=O}$ for PG 58-22

(d) K vs $I_{S=O}$ for PG 70-22

Figure 6.3. FTIR spectrum and relation with diffusion rate

Table 6.2: Functional group indices from FTIR spectrum for all aged binders

Binder	**Condition**	$\frac{=CH_2}{-CH_3}$	I_{al}	I_{ar}	$I_{C=O}$	$I_{S=O}$	I_{branch}	I_{long}
PG 58-22	**Unaged**	3.912	0.644	0.086	0.000	0.016	0.204	0.248
	RTFO	4.022	0.693	0.111	0.003	0.064	0.199	0.041
	PAV	3.700	0.657	0.108	0.042	0.073	0.213	0.043
	Double PAV	3.787	0.634	0.108	0.055	0.092	0.209	0.042
PG70-22	**Unaged**	3.632	0.659	0.091	0.049	0.012	0.216	0.241
	RTFO	4.330	0.630	0.077	0.016	0.073	0.188	0.183
	PAV	3.554	0.654	0.090	0.060	0.096	0.220	0.157
	Double PAV	3.946	0.545	0.103	0.038	0.108	0.202	0.180

Table 6.2 shows that I_{al} , $I_{C=O}$ and I_{ar} changes due to aging but none of these indices follow any trend (increasing or decreasing) with the increase in aging. However, $I_{S=O}$ increases and I_{long} decreases with aging. An increase in $I_{S=O}$ represents an increase in asphaltene contents. It basically means that with aging, as asphaltenes increases the long chained molecular structure of the asphalt binders becomes more breached and ring-like. Thus, the mobility of the molecule decreases due to aging resulting in the reduction in diffusion rate. Figure 6.3 (c) and (d) shows the K vs. $I_{S=O}$ plot, which show that the relationship between K and $I_{S=O}$ is strong, linear and negative. For the PG 58-22 binder, the Pearson correlation coefficient is -0.777 and linearly fitted curve shows an R^2 value of 0.6049. For the PG 70-22 binder, the Pearson correlation coefficient is -0.999 and the linearly fitted curve shows an R^2 value of 0.9989. Therefore, aging increases the asphaltene

content and thus decreases the diffusion rate (K), which can be related to the sulfoxide groups in the binder. Aging of the asphalt binder increases sulfoxide groups in the binder, which increases the stiffness of the binder resulting interconnected molecular structure. This decreases the long chained molecular structure in binder due to which the rate of diffusion decreases. Therefore, the rate of long-term healing also decreases for aged binder.

6.3 Influence of Moisture Conditioning on Healing

Two different PG binders are moisture conditioned in three different levels. The chemical changes that may have occurred due to the moisture conditioning are then evaluated using FTIR Spectroscopy. The healing and cohesive properties of the binders are measured using DSR. Healing models for all the moisture conditioned binders are developed using the Wool and O'Connor healing model (Wool and O'connor 1981). The study of chemical and mechanical changes and their effects on the asphalt binder healing due to moisture conditioning, may lead to a better understanding of the effects of moisture on asphalt healing.

6.3.1 Moisture Conditioning

Two unmodified performance grade (PG) asphalt binders were collected from a local plant in Albuquerque, NM. PG 70-22 and PG 58-22 were moisture conditioned using Moisture Induced Sensitivity Test (MIST). MIST conditioning was chosen for this study, because MIST does not apply freeze-thaw conditioning unlike the AASHTO T 283 method. MIST uses a cyclic pressure loading and high water temperatures to simulate a harsh moisture condition for the asphalt pavement, which affects the overall material strength (InstroTek

2012). In MIST, high temperature (60 °C) and pressurized (40 psi) water was forced into the asphalt binder and which accelerated the moisture conditioning of the binder. The schematic of the MIST conditioning is presented in Figure 6.4. The binders were placed in a small container inside the chamber and fully submerged in water. A thin layer (5mm) of binder was conditioned to ensure the proper conditioning of the binder from all the sides. Then the MIST lid was closed and a diaphragm at the bottom of the chamber was inflated and deflated by hydraulic pump and piston mechanism. Due to this the water pressure inside the chamber increased and decreased. When the pressure increases, water is pushed into the binder sample (blue arrows in Figure 6.4) and during depressurizing some of the water is pushed off (green arrows in Figure 6.4). This leads to the absorption and diffusion of water in the asphalt binder. The recommended test conditions for MIST consists of 3500 cycles under 40 psi pressure at 60 °C, which was considered as the equivalent of one cycle under AASHTO T 283 conditioning (Ahmad et al. 2017; AASHTO T 283-14 2014). The samples were conditioned by three repeated cycles in the MIST chamber to moisture condition the samples in three different degrees. These conditioned samples were labeled as MIST-cycle 1 (3500 cycles), MIST-cycle 2 (7000 cycles) and MIST-cycle 3 (10500 cycles).

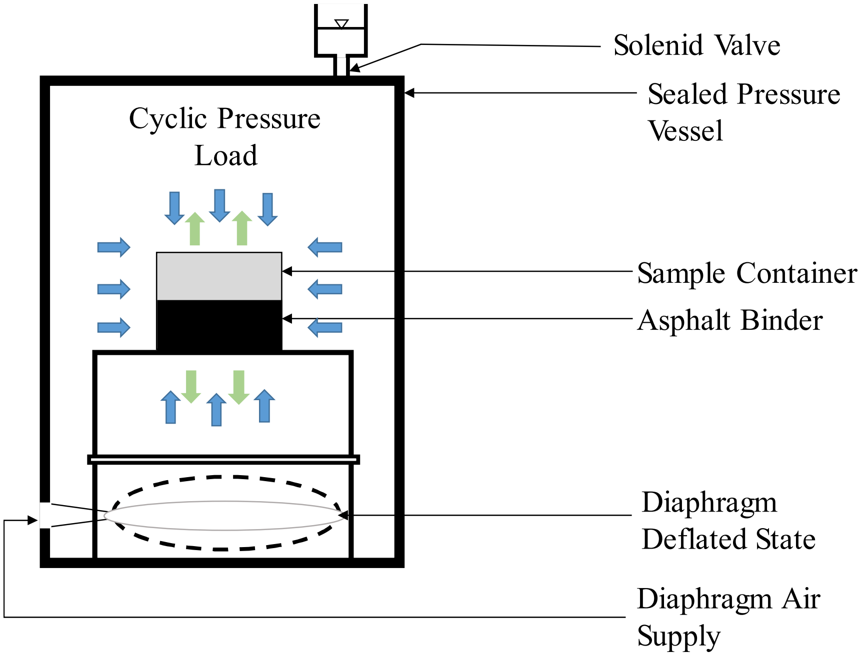

Figure 6.4: MIST moisture conditioning setup

6.3.2 Healing Test Results

Healing tests were conducted at three different temperatures (10, 15 and 20 °C) and at 10Hz loading frequency for different rest periods. Three different temperature was used to calculate the activation energy, since moisture conditioning may affect the long-term healing of the binder. This activation energy is calculated from the diffusion rate at different temperatures. Figure 6.5 (a) and (b) show the G_r^* values over various rest periods for different conditioned binders at 10 °C. Note that, PG 58-22 has faster and higher G^* recovery in the rest period than PG 70-22. The shear modulus of the control binder recovers faster over the rest period, thus has higher values than the moisture conditioned binders for both PG 70-22 and PG 58-22. However, moisture conditioning has more influence on the softer binder (PG 58-22) than the harder binder (PG 70-22). Due to moisture conditioning, the G^* recovery after the rest period is lower than the control binder for PG 58-22. Whereas, for PG 70-22, the effects of moisture conditioning on the G^* recovery after the rest period is not noticeable at 10 °C. However, at 15 °C and 20 °C, both binders show that moisture conditioning has a substantial effect on G^* recovery after the rest period. Also, with increase in temperature, the healing after the rest period increases for both binders. It is observed from Figure 6.5 (a) and (b) that there is a rapid recovery of the G^* in approximately the first 20 secs, then the recovery rate gradually decreases. Therefore, the overall healing in the binders can be divided into two parts: instant and long-term healing.

Figure 6.5 (c) presents the healing index (H) calculated from Eq. (5.8) vs. the fourth root of the rest period for the control PG 70-22 binder. At low temperature, H shows better linear relationship with the rest period than at higher temperature. Also, the healing increases with the increase in temperature, which can be due to the increase in the molecular movement at high temperature. Table 6.3 shows the healing equation for all moisture conditioned binders at three different temperatures. For all the binders, H shows a strong correlation with the rest period and the R^2 for all fitted curves are above 0.81. PG 70-22 has smaller R_0 values than PG 58-22. Hence, the harder binder has less instant healing than the softer binder. Also, the R_0 value initially decreases and then increases for a higher degree of moisture conditioning, although the control binder shows R_0 value than the moisture conditioned binders. Therefore, it can be concluded that moisture conditioning decreases the instant healing of the binders.

The fitted parameters R_0 and K are calculated by using linear regression (Table 6.3). The diffusion rate (K) in the healing model is a function of temperature. It can be expressed using the Arrhenius diffusion law as $K = K_0 e^{-E_a/RT}$, in which, K_0, E_a, R and T are fitting constant, activation energy, the universal gas constant (8.314 J/mol/K) and temperature in Kelvin respectively. Then from the $\ln(K)$ vs. $\frac{1}{T}$ plot (Figure 6.5 (d)) the activation energy, E_a is calculated using the following linear equation:

$$\ln(K) = \ln(K_0) - \left(\frac{E_a}{R}\right)\frac{1}{T} \tag{6.1}$$

Table 6.3 shows E_a for all moisture conditioned binders. E_a is the energy required for the inter-molecular diffusion between the micro-crack surfaces. Hence, if a binder has a higher activation energy then the rate of diffusion reduces resulting in a slower long-term healing. Results show that moisture conditioned binders have higher activation energy, which indicates that moisture conditioning reduces the rate of long-term healing.

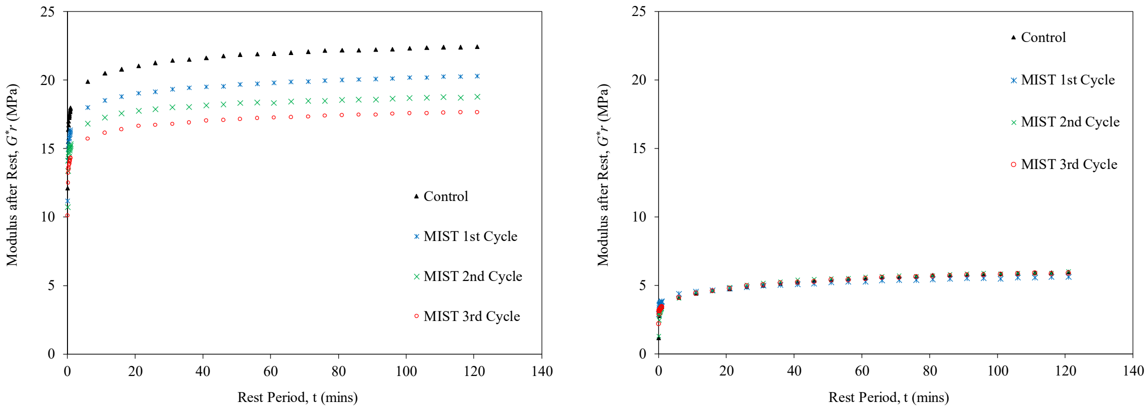

(a) G_r^* for PG 58-22

(b) G_r^* for PG 70-22

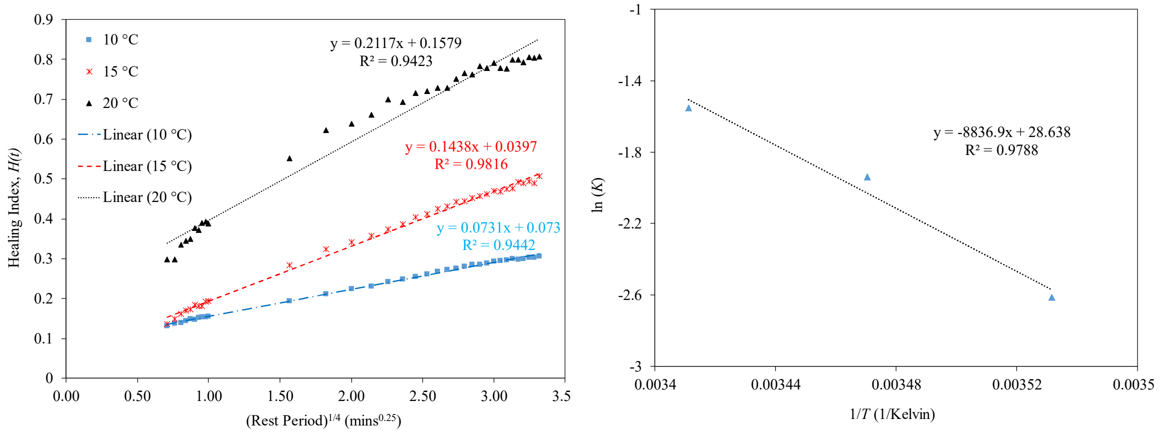

(c) H vs.$t^{1/4}$ for PG 70-22 (control)

(d) Calculation of E_a from K

Figure 6.5: Results and analysis of healing test data from DSR

Table 6.3: Different parameters of the healing equation for all moisture conditioned binders

Binder type	Conditioning	Temperature (°C)	Healing equation parameters $H(t) \approx R_0 + Kt^{1/4}$		R²	E_a (kJ/mole)
			R_0 (95% CI bounds)	K (95% CI bounds)		
PG 70-22	Control	10	0.073034 (0.0588, 0.0873)	0.073115 (0.0669, 0.0793)	0.944	73.45
		15	0.039698 (0.0239, 0.0555)	0.14381 (0.1370, 0.1507)	0.982	
		20	0.15791 (0.1159, 0.1999)	0.21168 (0.1159, 0.1999)	0.942	
	MIST 1st Cycle	10	0.010942 (0.0031, 0.0188)	0.085688 (0.0823, 0.0891)	0.987	77.03
		15	0.092599 (0.0669, 0.1183)	0.16503 (0.1538, 0.1762)	0.964	
		20	0.18675 (0.1405, 0.2330)	0.26136 (0.2412, 0.2815)	0.953	
	MIST 2nd Cycle	10	0.063822 (0.0470, 0.0806)	0.1033 (0.0960, 0.1106)	0.96	100.78
		15	0.16806 (0.1245, 0.2116)	0.21713 (0.1982, 0.2360)	0.941	
	MIST 3rd Cycle	10	0.020438 (0.0110, 0.0298)	0.099973 (0.0959, 0.1041)	0.986	103.10
		15	0.15686 (0.1184, 0.1953)	0.21376 (0.1971, 0.2305)	0.952	
PG 58-22	Control	10	0.32041 (0.2596, 0.3813)	0.21159 (0.1851, 0.2380)	0.886	16.22
		15	0.41395 (0.3248, 0.5031)	0.35977 (0.3210, 0.3985)	0.913	
		20	0.26775 (0.2093, 0.3262)	0.26636 (0.2410, 0.2917)	0.95	
	MIST 1st Cycle	10	0.31147 (0.2531, 0.3698)	0.20578 (0.1804, 0.2311)	0.889	16.49
		20	0.18675 (0.1405, 0.2330)	0.26136 (0.2412, 0.2815)	0.953	
	MIST 2nd Cycle	10	0.31927 (0.2593, 0.3792)	0.20519 (0.1791, 0.2312)	0.883	24.48
		20	0.23336 (0.1790, 0.2877)	0.29259 (0.2690, 0.3162)	0.949	
	MIST 3rd Cycle	10	0.29485 (0.2397, 0.3500)	0.19863 (0.1746, 0.2226)	0.893	27.29
		15	0.49268 (0.4020, 0.5833)	0.2386 (0.1992, 0.2780)	0.817	
		20	0.12955 (0.0901, 0.1690)	0.29505 (0.2779, 0.3122)	0.973	

6.3.2.1 Instant Healing

Figure 6.6 shows the results from the tack test for all the binders. Figure 6.6 (a) and (b) shows the load-displacement curves for PG 58-22 and PG 70-22 binders respectively. As PG 58-22 is a softer binder, it takes less force to pull out the binder compared to PG 70-22. Also, the control binder requires the highest force to pull-off. Figure 6.6 (c) shows the energy of separation (W_s) for all the binders. This figure shows that for PG 58-22, W_s decreases with an increase in moisture conditioning, except for MIST 2nd cycle sample. PG 70-22 shows a decreasing trend with an increase in moisture conditioning. Figure 6.6 (c) shows that the stickiness decreases with moisture conditioning, which basically leads to a decrease in the cohesion. Therefore, the cohesion or the tackiness of the asphalt binder decreases with moisture conditioning.

R_0 for different moisture conditioned binders are related to the binder energy of separation. Figure 6.6 (d) shows the comparison of the trends of R_0 values with that of W_s from the tack test for PG 58-22 binder. As expected, the values of R_0 show the same trend as W_s. With moisture conditioning, the energy of separation or cohesion decreases for MIST 1st cycle then it increases for the 2nd cycle and again decreases for the 3rd cycle and so does the R_0 from the healing equation. Thus, by using W_s from the tack test method, the effects of moisture on the instant healing can be explained. So, it can be concluded that moisture conditioning decreases the instant healing by decreasing the cohesion or W_s.

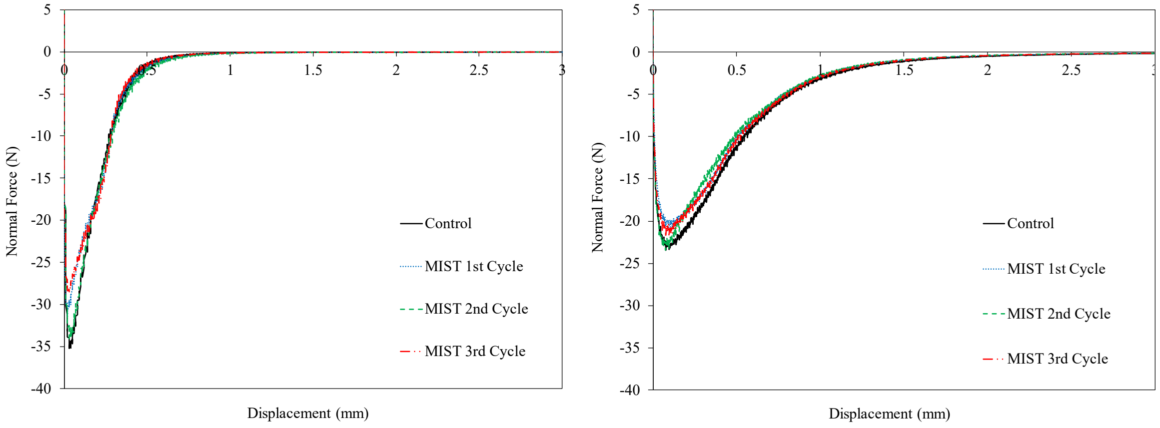

(a) PG 58-22

(b) PG 70-22

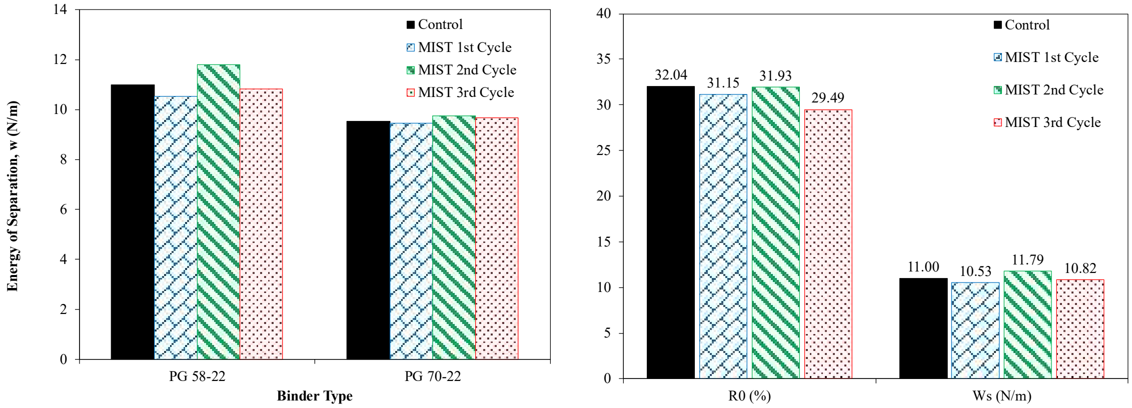

(c) Energy of separation (W_s)

(d) R_0 from healing test vs. energy of separation (W_s) from tack test.

Figure 6.6: Tack test results for moisture conditioned binders

6.3.2.2 Long-Term Healing

FTIR analysis is conducted to observe the chemical changes in the binder due to moisture conditioning and to relate that with the long-term healing. The functional group in the material is assigned according to the FTIR spectra main bands. Figure 6.7 (a) and (b) shows the FTIR spectrum for PG 58-22 and PG 70-22 respectively. It shows that due to moisture conditioning there is no change except at 1030 and 1700 cm^{-1} wavenumbers. However, the water absorption due to moisture conditioning is seen at the wavenumbers from 3100 to

4000 cm^{-1}, which are shown in Figure 6.7 (c) and (d) for PG 58-22 and PG 70-22 respectively. A study by Vasconcelos et al. (2012) showed that if the asphalt binder is submerged under water for several days then the absorbed water in binder is visible in the FTIR spectrum at 3100-3700 cm^{-1} wavenumber region. In this study the moisture conditioned samples showed a peak at 3400cm^{-1}, which represents the liquid water region. PG 70-22 has lower water absorbance than PG 58-22 binder, which means that water diffuses into softer binder faster than harder binder. As the hard binder has higher molecular weight than the soft binder, therefore the molecules in hard binder form a packed structure (Read and Whiteoak 2003). Due to this packed structure, hard binders absorb less water. This figure shows that the water absorbance percentage is very low compared to the overall spectrum however, the absorbance increases with moisture conditioning. For PG 58-22 (soft binder), with the increase in MIST cycle the water absorption increases. The 3rd MIST cycle shows the highest water absorption peak. Whereas for PG 70-22 (hard binder), with the increase in moisture conditioning the water absorption peak increases initially, but it starts to decrease at 3rd MIST cycle. Therefore, due to the MIST conditioning, asphalt binder absorbs water and it can be detected using the FTIR spectrum.

It can be seen from Figure 6.7, that the % absorbance of some functional groups change due to the moisture conditioning. To quantify these changes, different indices are calculated for all the functional groups in Table 4.1. Along with these, another index called hydroxyl index (I_{O-H}) is calculated using Eq. (6.2). All the calculated indices are shown in Table 6.4.

$$I_{O-H} = \frac{A_{3400}}{\sum A} \tag{6.2}$$

where

$$\sum A = Area\ under\ 2000\ and\ 600\ cm^{-1} = A_{1700} + A_{1600} + A_{1460} + A_{1376} + A_{1030} + A_{866} + A_{812} + A_{723}$$

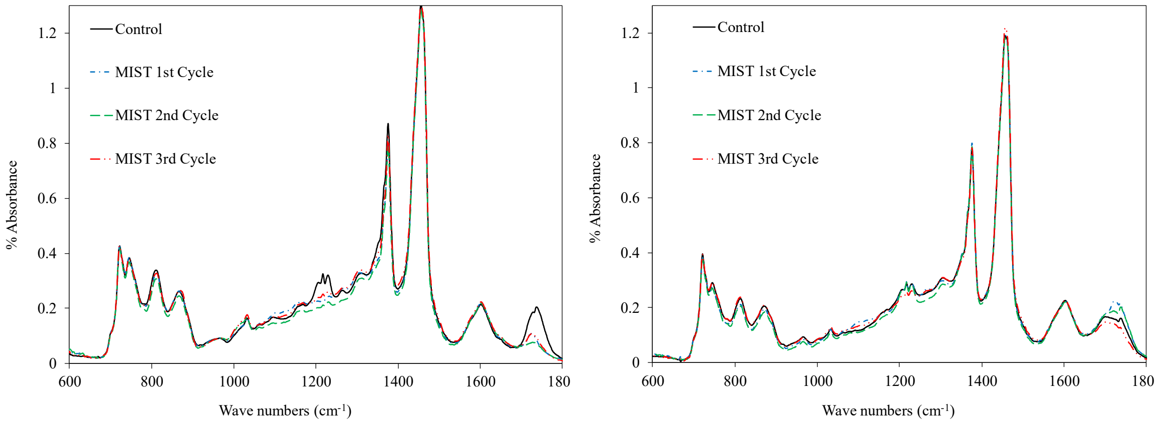

(a) PG 58-22 (b) PG 70-22

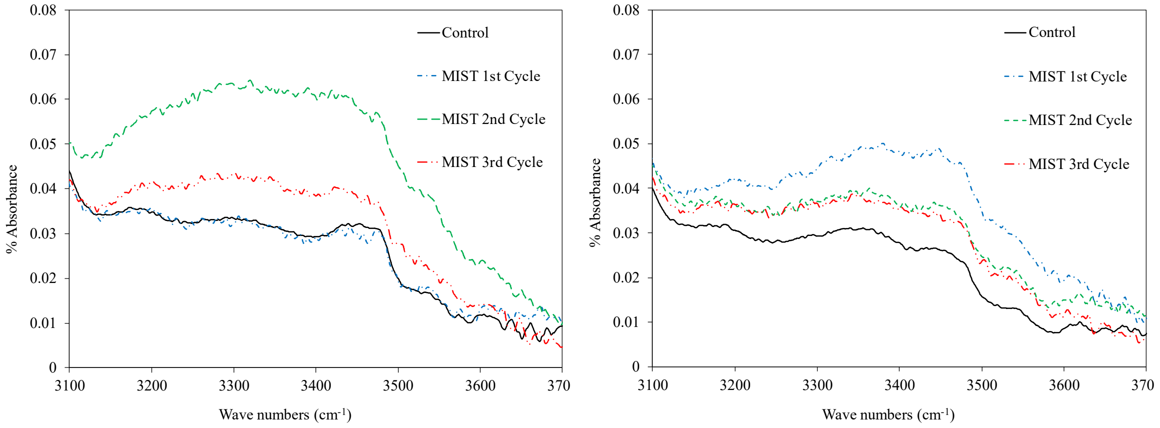

(c) *O-H* peak for PG 58-22 (d) *O-H* peak for PG 70-22

Figure 6.7: FTIR spectrum for different moisture conditioned binders

Table 6.4 shows that both control binders have the same aliphatic index. However, they change after moisture conditioning. I_{al} and I_{ar} do not change with moisture conditioning. Results show that $I_{C=O}$ does not follow any trend (increasing or decreasing) with the increase of moisture conditioning and the change in $I_{C=O}$ is not significant. However, $I_{S=O}$ increases with the increase in moisture conditioning. A study by Ouyang et al. (2006) showed that S=O increases due to the short-term aging and then decreases with the long-term aging in the asphalt binder. It implies that moisture conditioning only causes short-term aging in the binder; it does not affect the long-term aging. Similar results were found in a study by Ahmad et al. (2016). The I_{O-H} increases due to the moisture conditioning. One explanation may that be due to the moisture conditioning, water is absorbed into the binder showing a higher area under the *O-H* peak of the FTIR spectrum. This absorption of water into the binder may result in the deterioration of the asphalt binder cohesion which can affect the binder healing property. Also, the absorption of water into the binder can reduce the asphalt molecule mobility, thus the rate of diffusion decreases.

Table 6.4: Functional group indices from FTIR spectrum for all moisture conditioned binders

	Condition	**Aliphatic** I_{al}	**Aromatic** I_{ar}	**Carbonyl** $I_{C=O}$	**Sulfoxide** $I_{S=O}$	**Hydroxyl** I_{O-H}
PG58-22	**Control**	0.644	0.086	0.000	0.016	0.023
	MIST 1st Cycle	0.735	0.108	0.0193	0.015	0.026
	MIST 2nd Cycle	0.744	0.108	0.003	0.023	0.058
	MIST 3rd Cycle	0.726	0.103	0.022	0.022	0.127
PG70-22	**Control**	0.659	0.091	0.049	0.012	0.059
	MIST 1st Cycle	0.653	0.091	0.144	0.006	0.082
	MIST 2nd Cycle	0.662	0.092	0.135	0.006	0.016
	MIST 3rd Cycle	0.695	0.098	0.079	0.008	0.080

This change in the activation energy can be due to water diffusion into the binder. Figure 6.8 shows the comparison of the trends of E_a values with that of the I_{O-H} values for PG 58-22. As expected the value of E_a increases as the value of I_{O-H} increases. Therefore, as moisture is absorbed in the binder, the diffusion of micro-crack surfaces requires higher energy, thus the long-term healing of the binder diminishes.

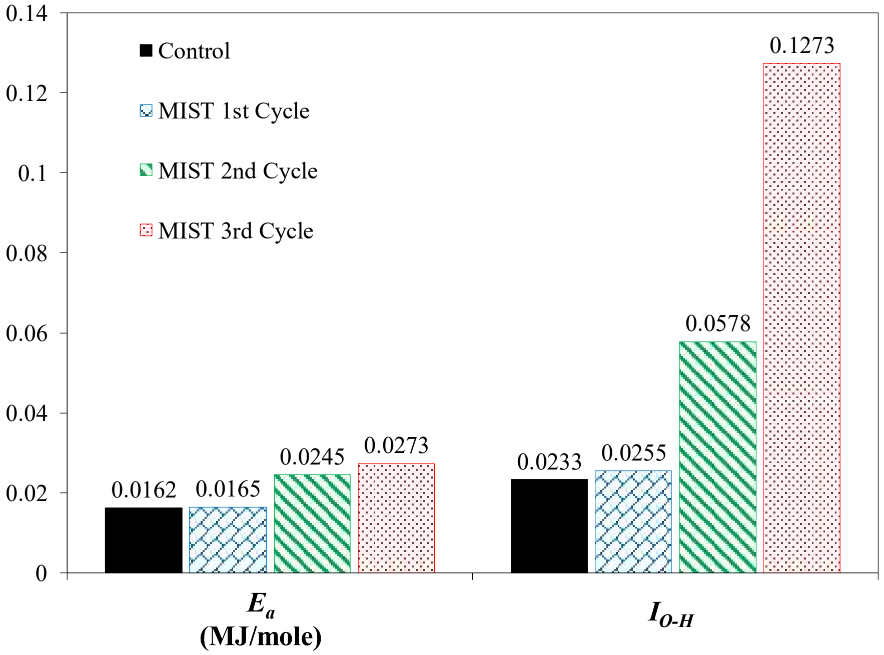

Figure 6.8: Activation energy from healing test vs. hydroxyl index (I_{O-H}) from FTIR

6.4 Effects of Filler Contents on Mastic Healing

Asphalt concrete is composite of graded aggregates blended with binder and mastic. Mastic is a mixture of asphalt binder and fine aggregates which essentially works as a binding agent among the aggregates. The mastic itself consists of fine aggregates which can pass through the #200 sieve, with a size less than 0.075mm (also called fillers) embedded in a medium of asphalt binder. The performance of asphalt concrete is a combination of the performance of the asphalt binder, mastic and aggregates. As healing can only occur in the cohesive part of the asphalt concrete, it is necessary to study the healing property of mastic along with asphalt binder to fully understand healing in the asphalt concrete (Cheng et al. 2002; Little et al. 1997).

Mastic healing differs from that in the pure asphalt binder because of the discontinuity created by the fines in the asphalt binder network. Previous study showed that the addition of fillers in the asphalt binder changes the rheological properties of binder by volume filling and physico-chemical interaction among the binder and fillers (Delaporte et al. 2007; Frigio et al. 2016). Furthermore, the presence of fillers in the asphalt binder disrupts the continuous binder medium, which reduces the cohesive potential of the binder (Mazzoni et al. 2016). In previous studies, healing of asphalt mastic has been measured using three-point bending test under fatigue loading with or without rest period (García 2012; Mazzoni et al. 2016; Underwood 2016). However, most of these studies failed to explain the reason behind the change in healing due to the addition of fillers in the binder. Given this background, there is a lack of the analytical approach to determine and relate the healing of the mastic with that of the binder. Therefore, it is fundamental to study the effects of filler content and binder type in the healing of mastic. The main objective of this chapter is to assess the effects of different filler contents and PG binders on mastic healing capability. To this aim, the physico-chemical healing model previously implemented for the asphalt binder in chapter 5 is used for mastics.

6.4.1 Materials

Two PG binders: PG 64-22 and PG 70-22 were used to prepare the mastic specimen. The fillers used was crushed stone the filler content in mastic was controlled by weight ratio between the binder and fillers. Mastic was prepared with 20%, 40% and 60% filler content of its weight. In total six mastic with three filler contents and two binders were prepared. Mastics were prepared using a protocol developed by Mannan et al. (2015b). The procedure is as follows: fillers and binder were heated at 150 °C for less than an hour. Then, fines were slowly added to the binder while mixing at 150 °C using a radial flow impeller at a speed of 700 rpm, and the mixture was blended for a period of 15 minutes to achieve homogeneous mastic. After mixing, mastic was cooled down to room temperature and stored in air-tight containers for further testing.

6.4.2 Experimental Plan

For mastic testing, rectangular sample (30mm ×12.5 mm × 6.25 mm) was prepared and then torsional loading was applied using DSR. Three types of strain controlled tests (strain sweep test, time sweep test and healing test) and relaxation test were conducted on the mastic sample. Initially, the LVE limit was determine using the strain sweep test. Then, relaxation test was conducted at lower strain level to determine the relaxation properties of asphalt mastic. Finally using strain levels larger than LVE, time sweep tests with and without rest period was conducted to evaluate the fatigue damage and healing in the asphalt mastic. Fatigue and healing testing for mastic was the same as the binder fatigue and healing tests.

6.4.3 Strain Sweep Test Results

The strain sweep tests result for both PG 70-22 and PG 64-22 are illustrated in Figure 6.9. As the figure shows the mastic with PG 70-22 has higher yield stress than the mastic with PG 64-22 binder. It means that binder hardness plays a significant role in the mastic yield stress. For PG 64-22 binder the addition of fines increases the yield stress, however for PG 70-22 binder the yield stress increases for 40% fines mastic and then for 60% fines mastic it decreases. The results of LVE range shows that for PG 70-22, up to 40% fines mastic the LVE region is at 0.1%, but for 60% fines mastic it is 0.05%. With the addition of fines the yield stress increase. Similar trend is found for PG 64-22 binder.

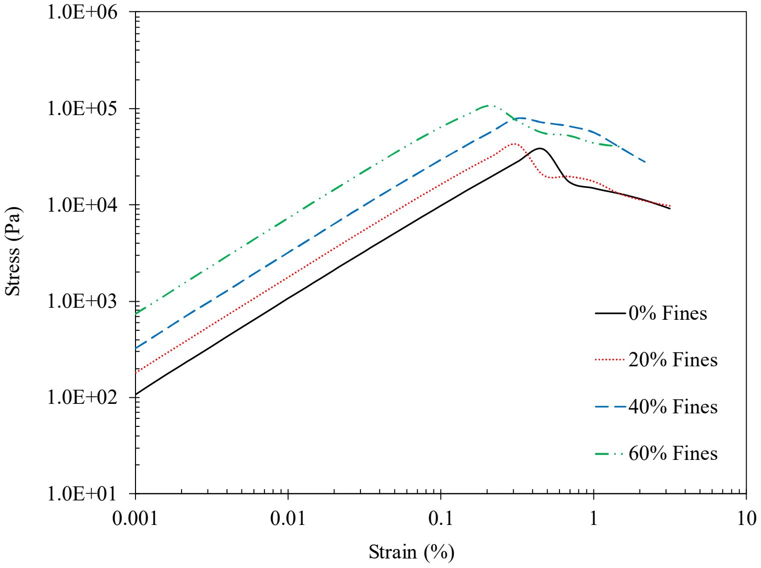

(a) PG 64-22

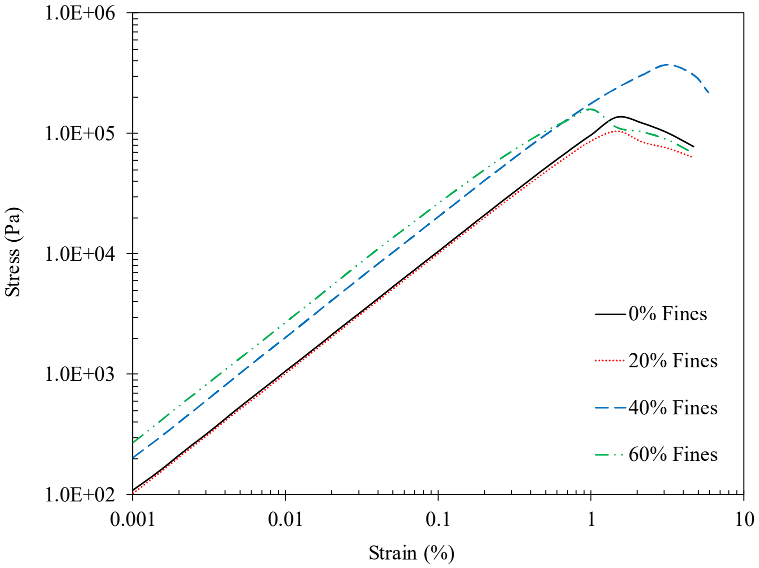

(b) PG 70-22

Figure 6.9: Torsional strain sweep test results for mastics with different fine contents and PG binders

6.4.4 Relaxation Test Results

Static relaxation tests are conducted to investigate the mastic capability to relieve stress under constant strain. All the mastics were tested at 20 ˚C and the loading time was 100 s. All the tests were carried out at 0.05% strain level. Figure 6.10 shows the stress vs. time plot for all the mastics. It shows that with the addition of fillers the relaxation property of mastic decreases for both PG 64-22 and PG 70-22. In the relaxation test the softer material will show more relaxation and harder material will show less relaxation of stress. From the mastic testing it can be concluded that the addition of fillers increases the stiffness of the mastic, thus resulting in a decrease in the relaxation behavior. Also, PG 64-22 mastics show more stress relaxation than that of PG 70-22. PG 64-22 binder is softer than PG 70-22, which allows the mastics prepared with PG 64-22 binder to relax more than PG 70-22 mastics. Thus, it can be concluded that the relaxation property of mastics is mainly controlled by the asphalt binder grade.

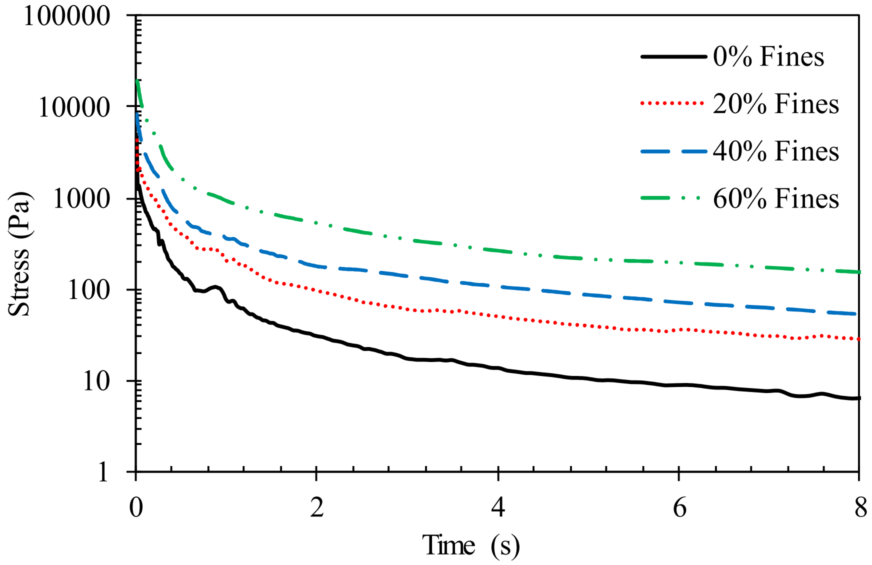

(a) PG 64-22

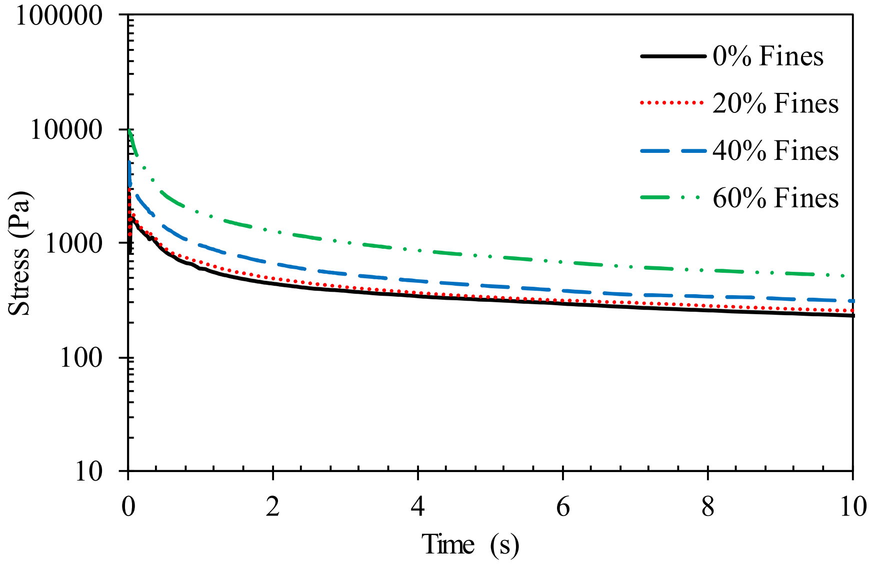

(b) PG 70-22

Figure 6.10: Relaxation test results for mastics with different fine contents and PG binders

6.4.5 Fatigue Test (Loading Without Rest Period) Results

For each mastic two specimens were prepared and tested for fatigue loading without rest period. All the samples were tested under strain controlled loading at 20˚C and 10Hz frequency. The number of loading cycles before the specimen fails were recorded. The stiffness reduction failure criterion (N_{f50}) was used for all the mastics. The results are listed below in Table 6.5. Their relationship with mastic filler content is plotted in Figure 6.11.

Table 6.5 Fatigue test results of different mastics

Binder type	Filler content	Strain level (%)	Number of cycles to failure (N_{f50})
PG 64-22	0%	0.25	288590
	0%	0.5	9960
	0%	0.65	13720
	20%	0.25	94180
	20%	0.5	51050
	20%	0.65	45000
	40%	0.25	582410
	40%	0.5	258440
	40%	0.65	19200
	60%	0.5	141660
	60%	0.65	9120
PG 70-22	0%	0.5	N/A
	0%	0.65	1243300
	0%	0.8	519440
	20%	0.65	1889200
	20%	0.8	1373000
	40%	0.65	250530
	40%	0.8	17590
	60%	0.65	10120
	60%	0.7	9420
	60%	0.8	9300

The N_{f50} values of different asphalt mastic show that the introduction of the fillers changes the fatigue property of the asphalt binder significantly. The number of cycles to fail increases with the addition of 20% fillers. However, the increase in fatigue resistance of mastics does not linearly increase as the filler content increase. Figure 6.11 shows that the number of cycles to fail reaches the maximum value for mastic with 20% fillers and then for 40% and 60% filler content the N_{f50} decreases drastically. Therefore, for fatigue resistance of mastic it can be said that 20% filler content is the optimum filler content for both the PG binders. As it can be seen from the figure, for PG 64-22 binder 20% fillers increases the mastic fatigue resistant by almost 300% compared to the binder (0% fillers). However, for PG 70-22 binder fatigue resistance increases about 51% in the 20% filler mastic than the binder itself. Therefore, it can be said that the addition of fillers up to 20% improves the fatigue resistance of the mastic and further addition of filler results in a decrease in the fatigue resistance of asphalt mastic.

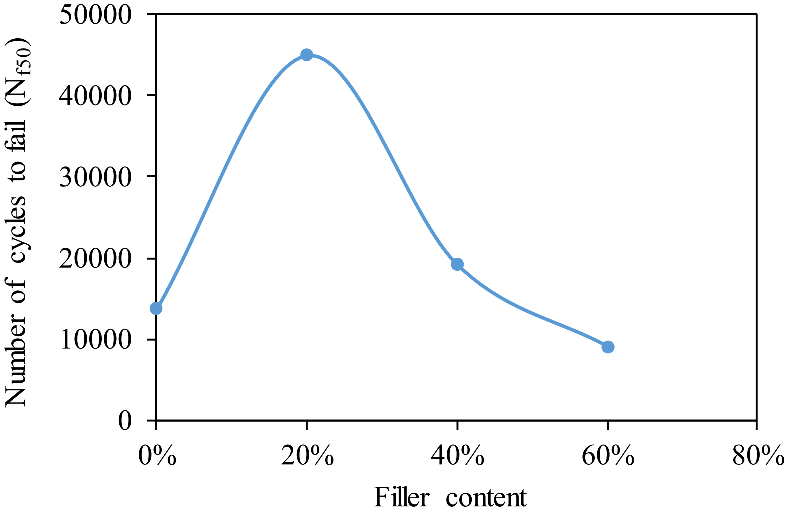

(a) PG 64-22

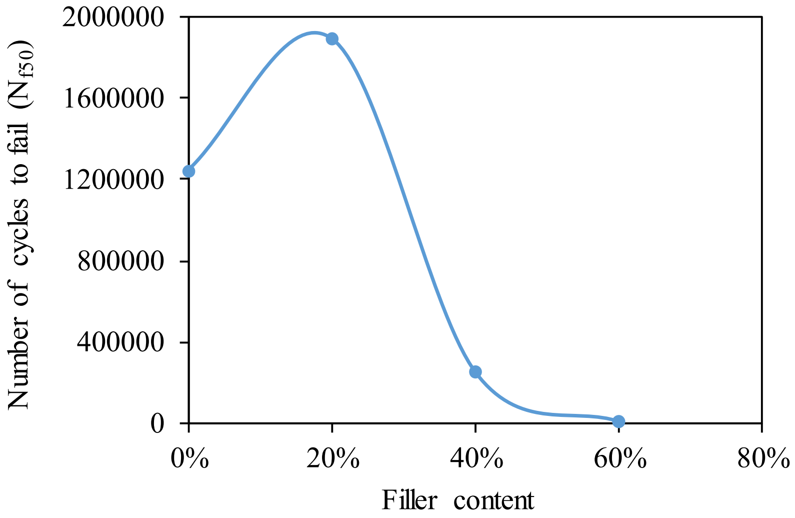

(b) PG 70-22

Figure 6.11: Number of loading cycles to fail for mastics with different fine contents at 0.65% strain

6.4.6 Healing Test (Loading with Rest Period) Results

All the mastic samples were tested under time sweep test with rest period (loading–rest–loading) similar to the healing testing conducted for the binders in chapter 5. The only difference is that here rectangular samples (30mm × 12.5 mm × 6.25 mm) of mastic were tested. During the cyclic loading, a strain of 0.65% amplitude was applied, this strain level in the loading period was chosen based on the LVE limit from the strain sweep test. To prompt the damage during loading period in the sample, a strain higher than LVE was chosen. Different length of rest periods from 5 secs to 2 hours was applied.

Figure 6.12 (a) and (b) show the healing index (H) calculated from Eq. (5.8) over various rest periods (t) for different mastics. This figure shows that with the increase in rest period the healing increases which means that during the rest period some of the damage recovers and the modulus recovers close to the initial modulus. The asphalt binder shows highest healing and with the addition of fillers the healing index decreases. For PG

64-22 binder, the 20% fines mastic healing index decreases considerably, however the decrease in healing index for 40% and 60% mastic is almost similar to the 20% fines mastic. For PG 70-22 binder, the healing index gradually decreases with the addition of fines. Also, unlike binders the instant healing in the mastic occurs within 20s of rest period, after this instant healing the healing gradually increases over time. Thus, similar to the binder, the instant and long-term healing is also found in mastic.

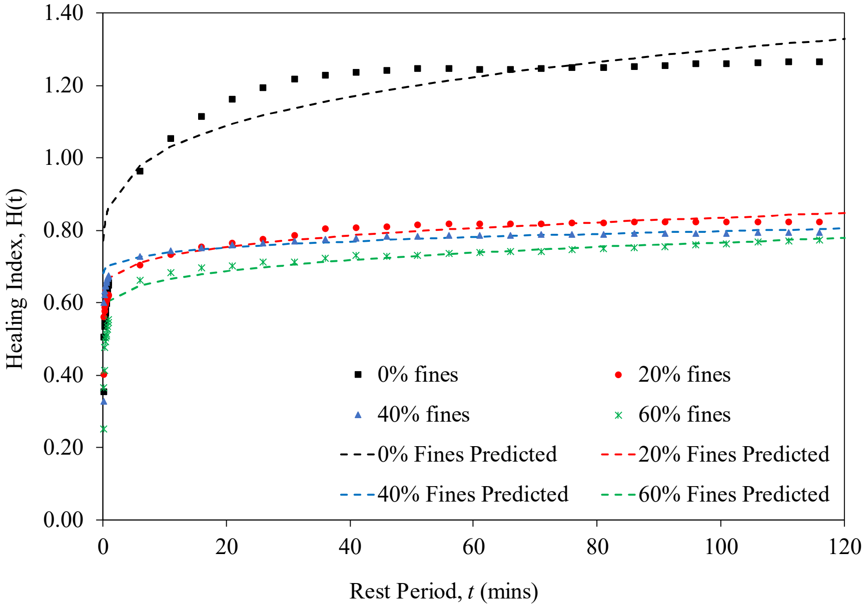

(a) Healing over rest period for PG 64-22 mastics

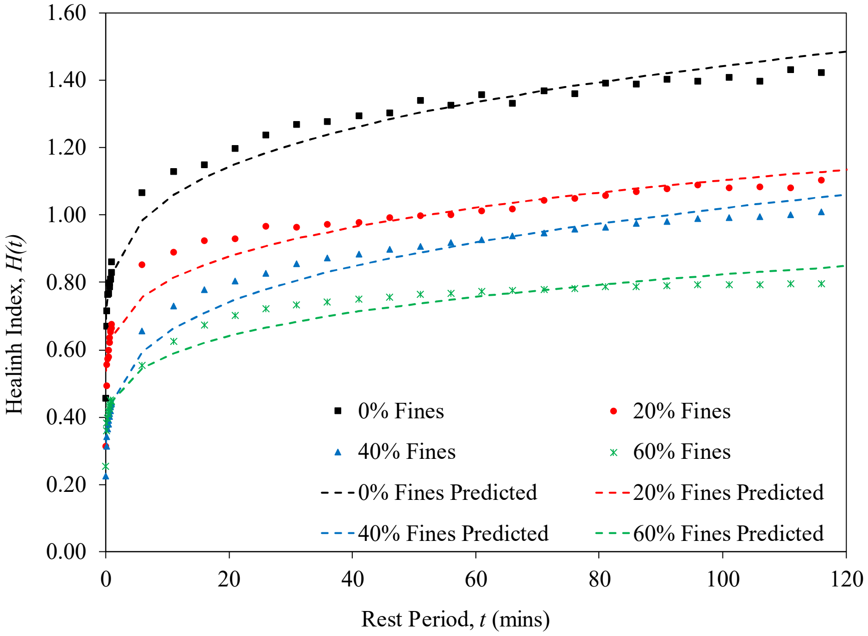

(b) Healing over rest period for PG 70-22 mastics

Figure 6.12: Healing over rest period and fitted healing model for mastics with different fine contents

The fitted healing model and all the fitting parameters are listed in Table 6.6. For all the fitted curves, the coefficient of determination (R^2) value is above 0.77, which means the fitted model strongly agrees with the actual data. The mastics with PG 64-22 binder shows a higher R_0 value than that of the PG 70-22 mastics. As shown in chapter 5, PG 64-22 binder has more instant healing ability than that of the PG 70-22, therefore, it can be concluded that the instant healing of mastic is primarily dependent on the binder type rather than the percentage of fillers in the mastic. This is because the R_0 mainly depends on the binder cohesive properties and PG 64-22 has more cohesive strength than PG 70-22. Figure 6.13 (a) shows that the addition of fillers in the mastic decreases its instant healing. PG 70-22 mastics show more deterioration in the instant healing than PG 64-22 mastics. Table 6.6 shows the long-term healing rate (K) for all the mastics. The PG 70-22 mastics show higher value of K than PG 64-22. This is the opposite to the trend found in the binder healing testing. Thus, it can be concluded that the long-term healing of the mastic is controlled by the percent fillers rather than the binder grade. The rate of long-term healing (K) shows a decreasing trend with the increase in % fillers in the mastic (Figure 6.13 (b)). This is because the fillers disturb the continuous asphalt binder medium and make the molecular diffusion difficult and slow. As the molecular diffusion rate decreases so does the rate of long-term healing.

Table 6.6: Healing model and the fitted parameters for all mastics

Binder type	Filler content	Healing Model	R^2	R_0	K
PG 64-22	0%	$H(t) = 0.6636 + 0.201 t^{1/4}$	0.7761	0.6636	0.201
	20%	$H(t) = 0.5893 + 0.077 t^{1/4}$	0.8846	0.5893	0.077
	40%	$H(t) = 0.6579 + 0.044 t^{1/4}$	0.9021	0.6579	0.044
	60%	$H(t) = 0.5285 + 0.0752 t^{1/4}$	0.9191	0.5285	0.0752
PG 70-22	0%	$H(t) = 0.5348 + 0.2861 t^{1/4}$	0.9647	0.5348	0.2861
	20%	$H(t) = 0.4207 + 0.2158 t^{1/4}$	0.9434	0.4207	0.2158
	40%	$H(t) = 0.1754 + 0.2672 t^{1/4}$	0.9814	0.1754	0.2672
	60%	$H(t) = 0.2725 + 0.1741 t^{1/4}$	0.9607	0.2725	0.1741

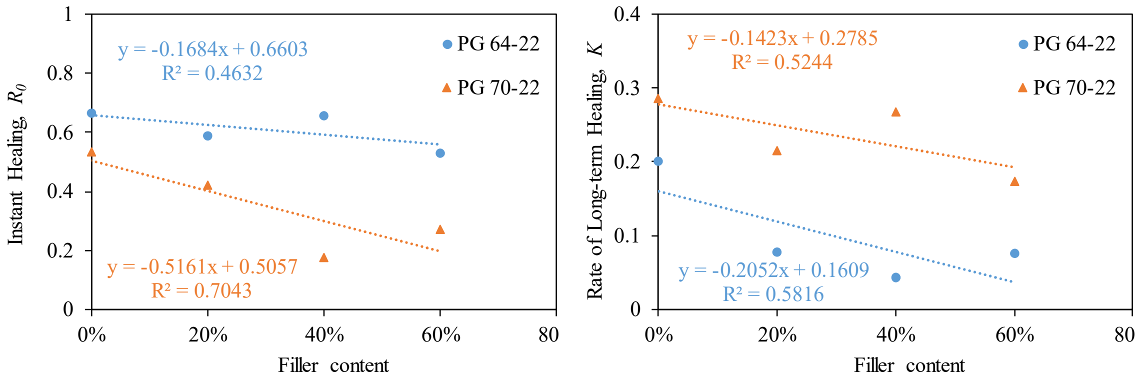

(a) Instant heading of mastic (b) Long-term healing of mastic

Figure 6.13: Instant healing and long-term healing rate for different mastics

One explanation of this reduction in healing can be explained by the effects of fillers on the constituents of the binder. Addition of fillers in the asphalt binder changes the chemical interaction between asphalt molecules. This can be determined using the IR spectrum of different mastics (Figure 6.14). Figure 6.14 shows the FTIR spectra of all the mastics. For all the mastics, there is a new and strong peak from 805 to 1200 cm^{-1} wavenumber. This range of wavenumber range represents the silicon-oxygen (Si-O) functional groups. Some of the functional groups within these wavenumbers are: Si-O-Si asymmetric stretch (1200-1000 cm^{-1}), Silanol Si-O stretch (1000-940 cm^{-1}) and Si-O-Si symmetric stretch (940-805 cm^{-1}). With the addition of fillers, the height of this peak increases, which means the Si-O-Si functional groups increases in the mastics. This increase in the Si-O-Si functional groups decreases the molecular mobility of the asphalt binder. As the molecular mobility decrease the likelihood of inter-molecular diffusion decreases, which results in a slower rate of diffusion and reduction in the long-term healing rate.

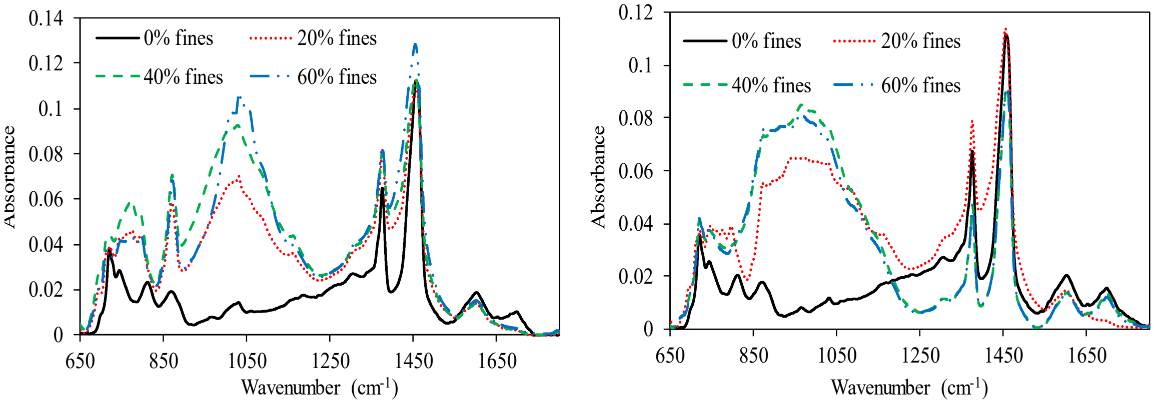

(a) PG 64-22 mastics (b) PG 70-22 mastics

Figure 6.14: FTIR spectra for all mastics

The above discussion indicates that the instant healing and long-term healing of asphalt mastic depends on asphalt binder type and filler contents respectively. Therefore, a generalized healing model for all asphalt mastic is proposed using these two parameters. In this model, the healing index is assumed to be a function of the mastic modulus to binder modulus ratio ($\frac{G_m}{G_b}$), filler content (f) and rest period (t). This model follows the Wool and O'Connor model. It is assumed that in the overall healing there is an instant part which is linearly related to $\frac{G_m}{G_b}$ and a time dependent part which is dependent on both filler content and rest period. Therefore, the proposed equation for modeling the healing index is as follows:

$$H(t) = a \times \frac{G_m}{G_b} + b \times e^{-mf} \times t^n \qquad (6.3)$$

where a , b , m and n are the fitting parameters. In Eq 6.3, f is in decimal, t is in mins. Also G_m and G_b are mastic and binder modulus respectively. Using nonlinear least square method in MATLAB, the experimental data for all six mastics are fitted to this equation to calculate the fitting parameters. The value of a , b , m and n are found to be 0.0180, 0.7520, 1.0832 and 0.1179 respectively. The (R^2) value for this fit is 0.701, which indicates that the fitted model agrees with the actual data. Also, the sum of squares of the residuals (SSR) if this fit is found to be 2.5287, which is a measure of the deviation between the measured data and the fitted data. A small SSR indicates a good fit of the model to the measured data. After calculating the fitting parameters, the generalized healing model for all mastics can be written as follows:

$$H(t) = 0.018\frac{G_f}{G_b} + 0.752 \times e^{-1.083f} \times t^{0.12} \tag{6.4}$$

Figure 6.15 shows the plot of the predicted vs. measured healing index of the six mastics. This figure shows that all the points are near the line of equality (LOE) without any significant bias. It implies that the generalized healing model proposed in Eq. 6.4 provides a good prediction of the experimental healing index for the asphalt mastic.

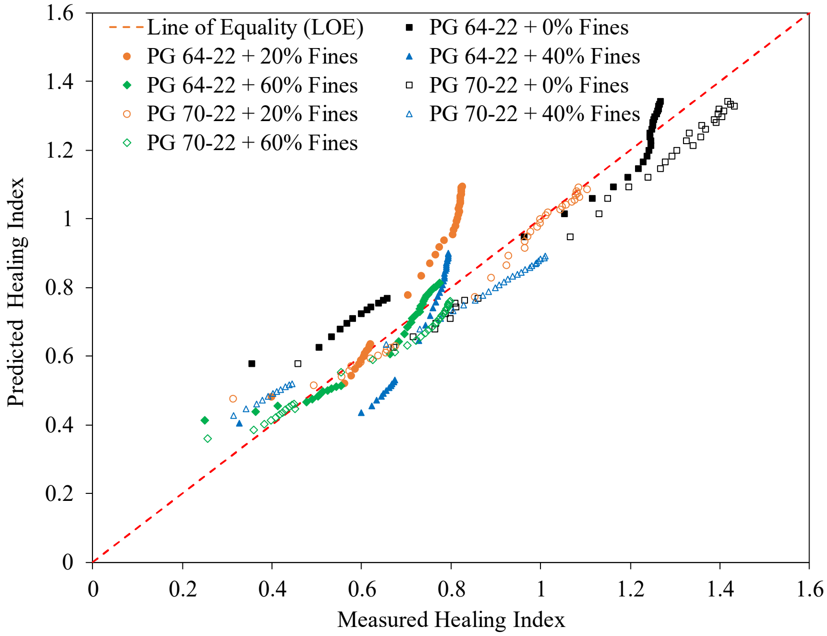

Figure 6.15: Comparison between the measured and predicted healing index of mastics

6.5 Remarks

The effects of aging and moisture conditioning on the healing of the asphalt binder is discussed in this chapter. Also, the effects of filler content in asphalt mastic fatigue and healing is studied. Two PG asphalt binders are aged in three different levels and moisture conditioned in three different levels. Six different mastics are prepared using three different filler content and two PG binders. The healing models and all the healing parameters are estimated from the healing test for binders and mastics. In addition, the effects of aging and moisture on the chemical and cohesive properties of the binder are determined and their effects on asphalt healing is examined. Based on the findings from the test results, the following conclusions can be drawn:

- FTIR spectrum captures the changes in the chemical functional groups due to aging. The FTIR spectrum shows an increase in the sulfoxide groups due to aging. Also, increase in the sulfoxide group index indicates an increase in asphaltenes content in the binder, which results in a more branched structure with less molecular mobility.

- Results show that long-term healing rate is inversely proportional to sulfoxide groups of the aged binder. The instant healing (R_0) did not show similar pattern as the energy of separation of the tack test. Thus, the energy of separation cannot be related to the instant healing of aged binder.
- Aging has a negative impact on the healing property of the asphalt binder. As aging decreases the molecular mobility and increases the sulfoxide, which results in a decrease in the instant and long-term healing respectively.
- FTIR spectrum captures the changes in the chemical functional groups due to moisture conditioning. The FTIR spectrum shows an increase in the hydroxyl group due to moisture conditioning. Also, from the sulfoxide group index it can be concluded that moisture conditioning results in short-term aging of the asphalt binder.
- The healing of moisture conditioned binder is divided in to two parts: instant and long-term healing. Results show that long-term healing rate is inversely proportional to percent water absorbed in the binder due to moisture conditioning. And the instant healing (R_0) is proportional to the energy of separation calculated from the tack test. Moisture conditioning has a negative impact on the healing property of the asphalt binder. The absorption of water into the binder reduces the asphalt molecule mobility, which results in a decrease in healing for the moisture

conditioned binders. However, moisture conditioning has greater effect on the healing of the softer binder (PG 58-22) than that of the harder binder (PG 70-22).

- The fatigue and healing behavior of mastics mostly dominated by the binder type. The mastics prepared with PG 70-22 show higher fatigue resistances, whereas mastics with PG 64-22 binder show higher healing index over the rest period. Also, the relaxation test results show that the mastics with PG 64-22 experience more stress relaxation than the PG 70-22 mastics. Thus, the asphalt binder plays a crucial role in the overall fatigue and healing properties of the asphalt mastic.
- The fatigue test results showed that fatigue resistance of the asphalt mastic increases with the addition of 20% fines and then with further addition of the fillers the fatigue resistance of mastic decreases. Therefore, in terms of fatigue resistance of the mastic it can be concluded that 20% filler content is the optimum filler content for the asphalt mastic.
- The healing test results show that the mastics show less healing than the binder. The addition of fillers in the asphalt mastic decreases the instant healing and the mastic with higher PG binder show higher reduction in instant healing. The presence of fillers makes the inter-molecular diffusion in the mastic more difficult as it interrupts the continuous binder medium. This results in a slower molecular diffusion, which leads to a slower rate of long-term healing for mastics containing higher percent of fillers. In summary, the healing in mastic is mostly controlled by the asphalt binder type. The instant healing of the mastic solely depends on the cohesive properties of the binder. On the other hand, the long-term healing rate of

the mastic depends on the binder-filler interaction and the concentration of the filler in the binder network.

CHAPTER 7

INCORPORATION OF HEALING IN A VISCOELASTIC-VISCOPLASTIC-DAMAGE CONSTITUTIVE MODEL

7.1 General

This chapter presents a novel general constitutive framework to model the fatigue damage and healing of the asphalt material under cyclic shear loading with and without rest periods. This model divides the overall damage into recoverable and permanent parts. Simultaneously, viscoelastic and viscoplastic aspects are included to simulate the non-linear behavior of the asphalt binder.

7.2 Background

Asphalt pavement is constructed using asphalt concrete, which mainly consists of asphalt binder with fine and coarse aggregates. The aggregates are considered elastic materials as their stiffness is higher than the binder and independent of time and temperature. Asphalt binder is used as a binding agent in the asphalt concrete for its superior cohesion and adhesion properties (Abbas et al. 2007; Bandyopadhyaya et al. 2008). It is a mixture of different hydrocarbons of varying molecular weights and assumed to be a viscoelastic material. However, asphalt binder behaves nonlinearly under heavy traffic loading and intermediate service temperature. Repetitive traffic loading causes micro-damage in the pavement, which later accumulates and leads to fatigue damage. Healing of this micro-damage occurs during the rest period between traffic loading, which results in the recovery of strength. Also as a viscoelastic material, asphalt binder shows viscoelastic recovery, which occurs at any loading level with or without damage. Thus, the overall recovery of strength in the asphalt binder is the sum of the viscoelastic recovery and micro-damage healing. During initial loading cycles (early life of the pavement), asphalt binder will only experience viscoelastic recovery and once micro-damage has occurred, the binder will experience both viscoelastic recovery and micro-damage healing. Therefore, to properly model the fatigue damage in the asphalt under cyclic loading, the strength of recovery due to both micro-damage healing and viscoelastic recovery should be considered.

The continuum damage model proposed by Kachanov (1986) has been used by many researchers to model irreversible damage processes in engineering materials (Kachanov 1986; Lemaitre and Chaboche 1994; Rabotnov et al. 1970; Voyiadjis 2012). However, as the experimental observations in this study and many other studies clearly show that asphalt has the potential to heal and recover part of its damage under rest period and unloading (Bhasin et al. 2008, 2010; Kim et al. 2001; Little and Bhasin 2007; Mannan et al. 2017). Several studies attempted to model the healing into the damage model, however most of them are phenomenological (Ando et al. 2002; Little and Bhasin 2007; Simpson et al. 2000). Only the models proposed by Miao et al. (1995) and Alfredsson and Stigh (2004) are applicable for materials which heals during rest period and unloading. The limitation of these two models is that they are only suitable for simple materials such as elastic solids. Along with the viscoelasticity asphalt binder shows loading rate dependency and plasticity characteristics at intermediate temperature under dynamic loading. Several studies have coupled viscoelastic-viscoplastic models with a damage model by Schapery (1975) to predict damage in the asphalt concrete (Bai et al. 2014; Darabi et al. 2012; Gibson 2006; Kim and Little 1990; Lee et al. 2000; Levenberg 2009; Park et al. 1996; Park and

Schapery 1999). However in all these damage models asphalt binder is assumed to be a viscoelastic material and the viscoplastic strain in the asphalt binder has always been neglected (Lu 2013). Also, these damage models did not consider healing of damage in their constitutive damage equation. Another drawback of all these models is that these are developed for tensile and static loading conditions, whereas in realistic loading case, fatigue damage occurs due to the development of shear stress in the asphalt caused by repetitive traffic loading.

There appears to be little or no work done to combine the intrinsic phenomena of fatigue damage and healing of the asphalt material under cyclic loading. In this chapter, a damage model is developed with the incorporation of healing to investigate the effect of mechanical response of materials under cyclic fatigue loading. Moreover, the current model also couples the damage and healing model with the viscoelasticity and viscoplasticity model to capture the overall behavior of the material. The details of such a model is presented in this chapter which provides the unique feature of damage evolution into recoverable (to capture healing) and permanent (to capture failure) parts. Furthermore, with increased loading the recoverable part may decrease and the permanent part may increase. Failure is associated with a critical value of the permanent damage. The results from the experimental data for cyclic loading paths obtained as part of this study, indicate complex features that are reflected by this model. The model has been constructed in a manner that allows for a straightforward generalization to a truly three-dimensional constitutive equation.

7.3 Laboratory Procedure

One of the most common test procedures to measure the fatigue damage of the asphalt binder is the time sweep testing at ambient temperature because the data obtained from such procedure show a good correlation with the asphalt mixture fatigue performance (Bahia et al. 2001; Mannan et al. 2015a). In this study, the experimental setup consisted of a thin cylindrical specimen placed between two parallel plates with the bottom plate fixed and the upper plate rotated to provide a loading path to the specimen, which can be considered pure shear in the plane of the specimen. It was assumed that there was no slippage between the specimen and the loading plates, and that the normal component of traction imposed axially by the loading plates was insignificant. The torque and angle of rotation (or deflection angle) were the parameters recorded during the test. The series of tests conducted for this study consisted of continuous cyclic loading, with and without rest periods for various number of cycles. All specimens were 8mm in diameter and 2mm thick. Under continuous cyclic loading, micro-damage occurred, with a corresponding reduction in the load-bearing capacity of the material. Experimental observations suggested that this reduction in the load-bearing capacity was related to the reduction in shear modulus. Therefore, the focus of the experimental phase of the investigation was to obtain values of the shear modulus from a shear test.

For example, a PG 70-22 asphalt binder was tested under deformation controlled cyclic loading to understand the fatigue damage of the material. The sample was loaded until it could not take any more load due to the accumulation of damage. Figure 7.1 (a) shows that the shear modulus ($G*$) decreases over the loading time. The reduction G^* is caused by the damage accumulation of the material under cyclic loading. The overall damage accumulation can be divided into three phases: at the first phase, the reduction in modulus has a faster rate (steep slope), then the reduction rate becomes almost constant over some loading time (second phase) and then in the third phase the modulus reduction rate again increases. This behavior implies that initially the damage accumulates slowly over the loading cycles. However, with the increase in loading time the damage accumulation rate increases which eventually causes failure of the specimen.

In the laboratory, the fatigue damage performance of the asphalt binder is evaluated via continuous cyclic loading in the shear direction, which is designed to simulate the traffic loading patterns. However, in real field there will be rest periods between traffic loading. This rest period allows the binder to heal some of the micro-damages. To illustrate the point that the rest period heals the damage and the binder recovers the strength, a test was conducted on the same binder with rest periods between cyclic loading as shown in Figure 7.1 (b). The results from the test without rest period are included in the figure for comparison. The sample was loaded for 500 secs and then allowed to rest for 1200 secs. Results show that the shear modulus recovers during the rest period. Initially, the shear modulus recovers almost fully over the rest period, later the amount of recovery during the rest period decreases with the increase in loading cycle. This is an indication that permanent damage has occurred. As the loading scenario continues, the amount of recovery decreases and the rate of permanent damage increases. If the results of the test with rest and without rest are compared, then it can be said that the transition from the second phase to the third phase shifts to the right, which means if rest period is applied then the accumulation of damage is slower. Also, the recovery of modulus due to the rest period is high until the second phase and then at rest it decreases. After the second phase, the recovery of modulus decreases for similar rest period, which causes faster accumulation of damage resulting in failure.

As the experimental data showed, overall damage under cyclic loading of the asphalt binder has two components, a recoverable part (healing) and a permanent part. The recoverable part of the damage recovers completely during the rest period but the amount of recoverable part decreases as loading progresses. The permanent damage accumulates faster with continued loading cycles with the eventual failure of the sample. With the increase of loading cycle, the amount of recoverable damage decreases and the amount of permanent damage increases.

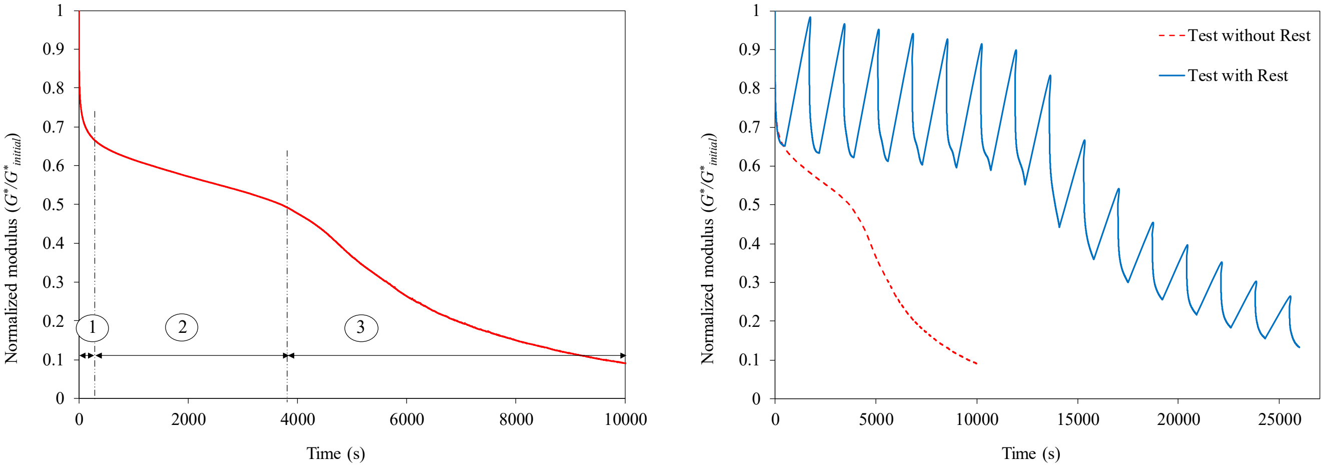

(a) Cyclic loading without rest period

(b) Cyclic loading with and without rest period

Figure 7.1: Experimental results for fatigue loading with and without rest periods

7.4 Modeling Scope

The experimental data presented above is conducted on a cylindrical asphalt binder sample assuming no slippage between the specimen and the loading plates, and that the normal component of traction imposed axially by the loading plates is insignificant. However, the problem with the thin cylindrical specimen used in these tests is that direct measurements of the shear stress and strain cannot be made but must be inferred indirectly from the torque and deflection angle. Because of the close proximity of the loading heads, and with no slip, it is reasonable to assume that the shear strain is given by $e = \phi r / h$, where ϕ is the deflection angle, r is the radial position of a material point from the center of the disc, and h is the thickness of the specimen. The outer material point is defined by $r = R$, the radius of the specimen and the point at which the maximum shear strain (e) occurs. In the following development, the term "shear strain" denotes this variable which is related to the angle of twist by

$$e = \frac{\phi R}{h} \tag{7.1}$$

If a linear elastic constitutive equation is used, then the shear stress is simply the shear modulus (G) times the shear strain, with which the shear stress varies linearly with r. It is then possible to derive the classical relationship between the shear stress (σ) at the outer fiber, and the torque (T) as follows:

$$\sigma = \frac{R}{h}\frac{T}{J} \tag{7.2}$$

where $J = \frac{\pi R^4}{2}$. For nonzero strain, the shear modulus is $G^* = \sigma / e$ and the constitutive equation is formulated in terms of σ, e and G^*. Where the shear modulus changes (damage) from the initial elastic modulus of G_0 and the shear stress varies linearly along the radius.

Since, the constitutive equation developed in this study is considered nonlinear, the shear stress will not vary linearly with r even if the reasonable assumption is made that the shear strain is proportional to r. For any loading path as prescribed by the deflection angle as a function of time, the amplitude of the strain will vary with r, and consequently a nonlinear constitutive equation will yield a stress which will not be linear in r. The torque can be determined from appropriate integration as follows:

$$T = 2\pi \int_0^R r^2 \cdot \sigma \cdot dr \tag{7.3}$$

This study assumes a linear variation of strain over the radius of the sample and the sample is divided into several elements along the radius. Then using the constitutive equations, the stress is calculated considering damage and healing coupled viscoelastic-viscoplastic models. Then using this calculated stress, the torque of each element is determined and then integrated to obtain the torque at the outer radius. Then, the predicted torque is compared with the experimental torque to see if the model can capture the key feature of the experimental data. This will provide the response of the overall system. If this model can capture the experimental response, then this can be used to understand the pavement response in the field. This will be a fair comparison rather than just comparing the modulus predicted by the model with experimental modulus. Also, this elemental analysis along the radius will provide the stress distribution and damage evolution in the sample along the radius, which cannot be achieved from the experimental data. This will help to understand how the binder behaves under pure shear.

The objective of this study is to develop a constitutive model for the shear modulus considering damage, healing, viscoelasticity and viscoplasticity, that can capture the nonlinear behavior of the material and capture the key features to match the experimental data. Also, the constitutive equation is developed in a form so that it can be easily used in the three-dimensional constitutive equation.

7.5 Constitutive Model Formulation

7.5.1 Damage Model

The experimental results showed that the modulus decreases due to damage with loading. Therefore, a constitutive equation is required which relates the stress, strain and modulus, where the modulus is a function of strain, strain rate and damage. This study uses the damage model based on the concept of actual stress introduced by L. Kachanov (1986). The main assumption of this approach is that due to the micro-cracks during fatigue loading, the load transfer capacity of the material decreases (Lemaitre and Chaboche 1994). This results in degradation of the material properties such as shear modulus G over the loading time or loading cycle. Now the damage (D) in the material due to loading can be expressed as:

$$\frac{G}{G_0} = (1 - D)$$

or,

$$G = G_0(1 - D) \tag{7.4}$$

$$\sigma = 2\,G\,e^e \tag{7.5}$$

where G_0 is the initial shear modulus, G is the shear modulus over the time, e^e the elastic strain and σ is shear stress. G_0 is the shear modulus of the undamaged material. Initially, for the undamaged material $D = 0$. If D evolves to the value unity ($D = 1$), then the material cannot sustain any more stress and fracture (when a macroscopic crack is initiated) occurs. Here in this model the criterion for fracture is assumed to be simply $D = 1$.

Typically, when loading occurs in a continuous manner, the parameter D increases monotonically. However, if loading is interrupted and the specimen is allowed to sit at zero stress, it is noted that a certain amount of recovery (reduction in the value of D) occurs, which is defined as healing. This suggests that there are two mechanisms at work. For example, if a material consists of several different bonds and is connected by links with each other, then one mechanism may be the breaking of bonds, which would be permanent, while another mechanism may be the breaking of links that can reattach or heal over time, which would be a recoverable. It is assumed that with continuous loading first the links separate before the bonds begin to break. Based on this argument, the total damage consists of two parts; a recoverable part (D^r) and a permanent part (D^p), or

$$D = D^r + D^p \tag{7.6}$$

The recoverable part (D^r) essentially represents the healing as the viscoelastic recovery will be taken care of with the consideration of viscoelastic model. This D^r represents the repairable portion of the damage. The accumulation of the permanent part (D^p) causes the failure.

7.5.2 Strain Decomposition

The material is modeled assuming that the viscoelastic and viscoplastic strain decomposition is possible (Guedes 2010). Essentially, it is proposed that viscoplasticity is associated with the permanent part of the damage. Therefore, the influence of viscoelastic recovery can be separated from the damage and healing. Considering viscoelasticity and viscoelasticity, the total strain is following:

$$e = e^{e} + e^{ve} + e^{vp} \tag{7.7}$$

where e is the total strain, e^{e} the elastic strain, e^{ve} the viscoelastic strain and e^{ve} the viscoplastic strain. Here, the elastic strain (e^{e}) and the viscoelastic strain (e^{ve}) are the reversible strains, as they vanish with time when the stress vanishes.

7.5.3 Viscoelasticity

The viscoelastic strain rate equation used in this study is shown in Eq. 7.8. This proposed constitutive equation is similar to the equation proposed by Simo and Hughes (2006) .

$$\dot{e}^{ve} = \frac{1}{\tau^{e}} e - \frac{1}{\tau^{ve}} e^{ve} \tag{7.8}$$

where $\dot{e}^{ve}$ is the viscoelastic strain rate, e is the total strain τ^{e} and τ^{ve}, are the material constants with the time dimension. In Eq. (7.8), the first term on the right is the forcing term, therefore a large value of τ^{e} indicates that the forcing effect is small. On the other hand, the second term causes the viscoelastic strain (e^{ve}) to reduce, or relax, and τ^{ve} can be considered as a characteristic relaxation time. Therefore, if the shear strain becomes zero after a loading phase, the viscoelastic strain relaxes to zero at a rate governed by τ^{ve}.

7.5.4 Viscoplasticity

The purpose of incorporating viscoplasticity is to address the damage due to the irreversible strain. The viscoplastic strain is irreversible because if the stresses vanish, this strain does not go to zero. Therefore, this strain can be associated with both permanent deformation and damage. It is assumed that the viscoplastic strain is developed due to loading past a critical value of strain or stress. Viscoplastic strain occurs only when the stress reaches the actual yield stress, which corresponds to a yield function. A yield function (F) is defined such that if F < 0, there is no contribution to the viscoplastic strain. The state F = 0 denotes the transition stage, and the plastic strain evolves if F > 0.

$$\dot{e}^{vp} = 0 \;\; if \begin{cases} F < 0 \\ \dot{F} < 0 \end{cases}, \;\; \dot{e}^{vp} \neq 0 \;\; if \begin{cases} F \geq 0 \\ \dot{F} \geq 0 \end{cases} \tag{7.9}$$

The yield function can be either strain-based or stress-based. The proposed model uses a stress-based yield function. This is similar to the constitutive equation of the Perzyna type (Perzyna 1966; Simo and Hughes 2006). The proposed evolution equation for the viscoplastic strain rate is the following:

$$\dot{e}^{vp} = \frac{1}{\tau^{vp}} sign\{\sigma\} f(F) \qquad Where, f(F) = F^{\gamma} \tag{7.10}$$

where

$$F = \begin{cases} 0 & \text{if } \left(|\sigma| - \sigma_Y\right) \leq 0 \\ \dfrac{1}{\sigma_Y}\left(\sigma^2 - \sigma_Y^2\right)^{1/2} & otherwise \end{cases}$$

and,

$$\sigma_Y = \sigma_{Y0}\left(1 - D_P\right)$$

where σ_{Y0} is the value of the total stress at which "yielding" or plasticity occurs and F is the yield function. The material constant (τ^{vp}) is a reference time and renders the equation dimensionally consistent. $f(F)$ is a prescribed positive function of F with the exponent $\gamma \leq 1$.

7.5.5 Damage-Healing Evolution Model

7.5.5.1 Evolution of Recoverable Damage

From the experimental data (Figure 7.1) it is seen that the maximum value of the damage recovery at the rest periods varies approximately from 0.35 to 0.15 over the loading cycles. Therefore, the initial maximum value is chosen to be $D^r_{\max} = 0.35$. This The evolution equation for the recoverable damage rate is chosen as

$$\dot{D}^r = C^r\left(\dot{\bar{e}}\right)\left(D^r_{\max} - D^r\right) - \frac{1}{\tau^r}\sqrt{D^r} \tag{7.11}$$

where the effective strain rate ($\dot{\bar{e}}$) is always positive and defined as,

$$\dot{\bar{e}} = \left|\dot{e}\right| \tag{7.12}$$

In Eq. (7.11), D^r is not allowed to exceed $D^r_{\max}$. The parameters C^r and τ^r are the material constants. The first term is a forcing part which causes D^r to increase up to a maximum value of $D^r_{\max}$ while the second term provides possible healing and may decrease it back to the value 0. At the loading phase, the first term dominates and the last term is negligible. However, at the rest period the second term becomes dominant as $\dot{\bar{e}} = 0$. Initially, the second term is negligible, which results in an increase in the damage. If $D^r = D^r_{\max}$, the second term becomes dominant, which results in the healing of the recoverable damage. Thus, once the material reaches $D^r_{\max}$, the healing starts, which results in a decrease in the recoverable damage. Thus, this second part of the equation incorporates the recovery due to the healing in the damage.

7.5.5.2 Evolution of Permanent Damage

For the evolution of the permanent part (D^p) of the damage variable, the maximum value of D^p will be $D^p = 1$. Analogous to the recoverable damage evolution equation, the proposed equation for the permanent damage rate is as follows:

$$\begin{aligned} \dot{D}^p &= C^p \left(\dot{e}^{vp}\right)^m \left(1 - D^p\right) \\ C^P &= C_0^P + C_1^P H\left[D - 0.5\right] \end{aligned} \qquad (7.13)$$

where C^p and m are the material constants. C^p has two parts: initially when D is small, only ${C_0}^p$ governs and once D is equal or greater than 0.5 then both ${C_0}^p$ and ${C_1}^p$ governs. This 0.5 value of D is chosen from the experimental data where the rate of reduction of modulus increases from a constant rate to a faster rate (shift from the second phase to the third phase in Figure 7.1). This is the transition point or the critical point for the material after which the micro-cracks in the material start to accumulate. C^p in the permanent damage represents the change in the rate of the permanent damage before and after the transition point. Note that for the permanent damage there is no recovery part. The exponent m is always less than or equal to 1. As the $\dot{e}^{vp}$ increases the rate of D^p also increases. However, as the D^p accumulates close to 1, the rate of D^p slows down and in the end, it becomes zero.

7.5.5.3 Coupling of Permanent Damage and Recoverable Damage

As indicated previously, the maximum amount of the recoverable damage appears to decrease with permanent damage. This feature can be exhibited by allowing the maximum recoverable damage to explicitly depend on the permanent damage, i.e. ($D^r_{\max} = f(D^p)$). A simple relation would be

$$D^r_{\max} = D^{r,0}_{\max}(1 - D^p) \tag{7.14}$$

This equation shows that the maximum allowable permanent damage increases over the loading time. So, at failure, all damage is permanent and $D^P = 1$. Thus, both the damage evolution equations become

$$\begin{aligned} \dot{D}^r &= C^r \dot{e}^{ve}\left(D^r_{\max} - D^r\right) - \frac{1}{\tau^r}\sqrt{D^r} \\ \dot{D}^p &= C^p \left(\dot{e}^{vp}\right)^m \left(1 - D^p\right) \end{aligned} \tag{7.15}$$

where $D^r_{\max}$ is calculated using Eq. (7.14). The deformation resulting from a given load will depend on the properties of the material. It may be reversible (elastic or recoverable deformation), or irreversible (viscoplastic, plastic or permanent deformation, or flow), or it may comprise of both a recoverable and a permanent part. This model intends to express the behavior of a material in the form of a constitutive equation, i.e. an equation which specifies the properties of the material in a manner which is independent of the geometry (i.e. the size or shape) of the body and depends only on its material nature. Constitutive equations are also referred to as rheological equations of state.

7.6 Parameter Determination

7.6.1 Material Parameters

The proposed model has the following set of material parameters relating all the key constituents: τ^{e} and τ^{ve} for the viscoelastic strain and τ^{vp} for the viscoplastic strain. Following subsections describe the procedures to determine all the parameters, which are also are listed in Table 7.1.

7.6.2 Parameters Related to Viscoelasticity

The viscoelastic parameters τ^{e} and τ^{ve} are determined from a relaxation test performed under a constant shear deformation (shear strain) at 20°C. The relaxation test at 1% strain for a small time is used for determining the model parameters. Small strain over a small amount of time is applied to the sample to ensure that there is no damage in the material and no permanent deformation will occur in the sample. Using Eq. (7.8), τ^{e} and τ^{ve} parameters are determined using the nonlinear least squares method. The determined values of the parameters are: $\tau^{e} = 0.4537$ and $\tau^{ve} = 0.4341$, with a sum of squared error of 3.56. Then using these parameters, stress is predicted over time for different strain levels: 0.05% and 0.1%. The experimental and the predicted stress values are shown in Figure 7.2. Note that the determined parameters can predict the relaxation behavior at different strain levels which is close to the experimental values.

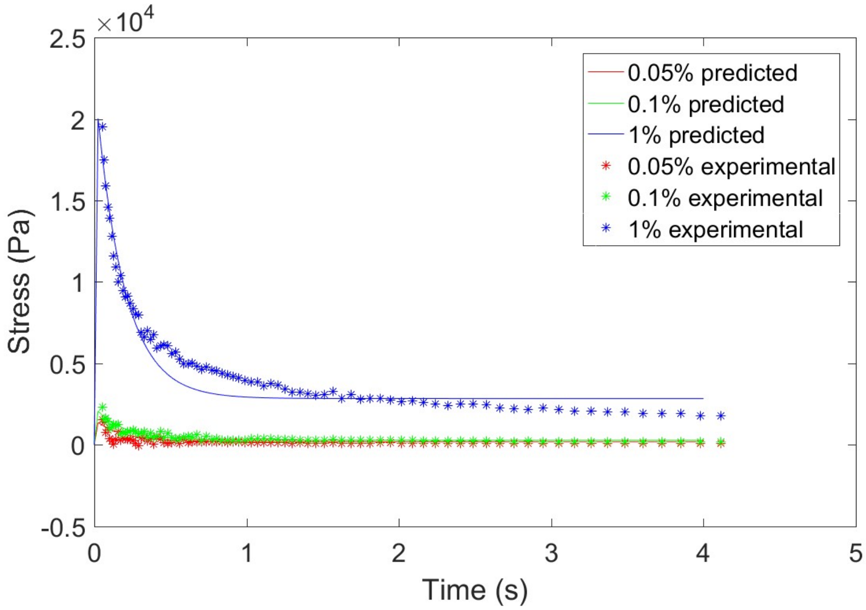

Figure 7.2: Determination of the viscoelastic parameters (comparison between predicted and experimental data from relaxation test)

7.6.3 Parameters Related to Viscoplasticity

The stress-strain curve from the constant strain rate test is used to determine the viscoplastic model parameters (τ^{vp} and γ). A constant strain rate of 0.05 sec^{-1} is applied to the sample for a very small time so that no damage occurs in the sample. The yielding stress (σ_{Y0}) of the asphalt binder calculated from the strain sweep test. Eq. (7.10) is used to determine the viscoplastic strain once the total stress is greater than the yield strain. Thus, both viscoelastic and viscoplastic (if present) strain rates are calculated for the chosen time increment, dt . Once both strain increments are calculated, the strain is updated for the time ($t + dt$). Using this updated strain, new stress is obtained for ($t + dt$) time. The model is run until the stress over entire loading time of the experimental data is predicted. Then the error between the predicted and the experimental data is calculated. The optimized sets of final viscoplastic parameters (τ^{vp} and γ) are obtained by minimizing the error using least squares methods. The experimental and predicted stress values are shown in the Figure 7.3. Figure 7.3 (a) shows the experimental and predicted curves for $0.05s^{-1}$ strain rate and figure 7.3(b) shows the curves for a strain rate of $0.03s^{-1}$. Both plots show that the determined viscoplastic parameters can predict the viscoplasticity for different strain rates.

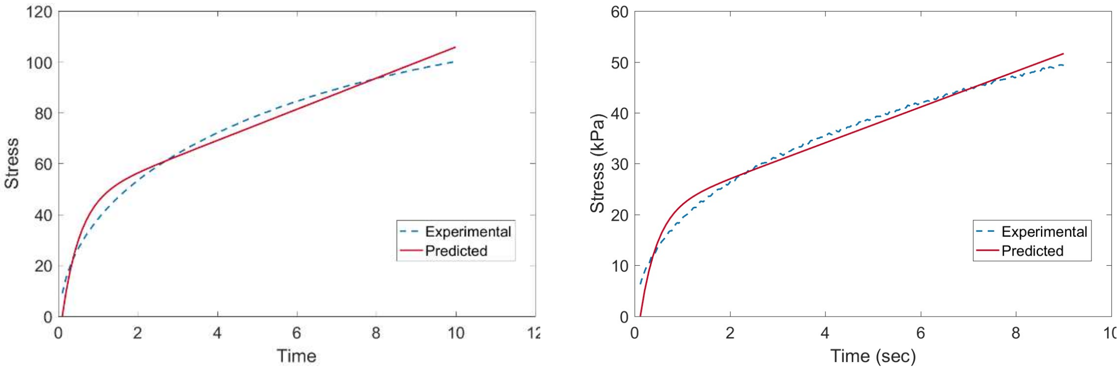

(a) strain rate $0.05s^{-1}$ (b) strain rate $0.03s^{-1}$

Figure 7.3: Determination of the viscoplastic parameters (comparison between predicted and experimental data from constant strain rate test)

Table 7.1: Determined model parameters for the proposed model at 20°C

Viscoelastic model parameters	
τ^{e}	0. 4537
τ^{ve}	0. 4341
Viscoplastic model parameters	
τ^{vp}	50
γ	0.5
σ_{Yo}	100 kPa

7.7 Simulation of Experiments

7.7.1 General

In this section, the damage-healing model coupled with viscoelastic–viscoplastic model is used to simulate the laboratory fatigue testing with and without rest period under strain-controlled loading conditions. In the fatigue loading without rest period, the samples are loaded until more than 90% of the damage is accumulated. In the fatigue loading with rest period, samples are loaded for 500 seconds and then a rest period of 1200 seconds is applied. This sequence of loading and rest period is continued until the total accumulated damage is more than 90%. The following subsections use the identified material parameters of the viscoelastic–viscoplastic model and predict the change in the modulus due to fatigue loading by considering both recoverable and permanent damage as well as damage coupling.

This study assumes a nonlinear variation of stress along the radius. Thus, the sample is divided into several elements along the radius to compute the stress. Then strain and stress is calculated using the proposed constitutive equations at the radius of each element. Figure 7.4 shows a schematic of the elemental distribution. For this model, a linear distribution of strain along the radius is assumed. Thus, the strain for each element is calculated as $e_{el} = \frac{r_e}{R}\gamma$, where, r_e is the distance between the centroid of the element to the center of the sample. Then using the constitutive equations, the stress is calculated for each element. The total torque is calculated from the sum of the elemental torque from the stress. This elemental analysis is conducted for different number of elements (e.g. 2, 4, 8, 16, 32 ,64 and 128) along the radius. Increasing the number of the elements above 32 does not show any noticeable difference in the predicted values. Therefore, 32 elements are used for all the analysis. Initially the model is used for continuous cyclic loading and then it is run for cyclic loading with rest period.

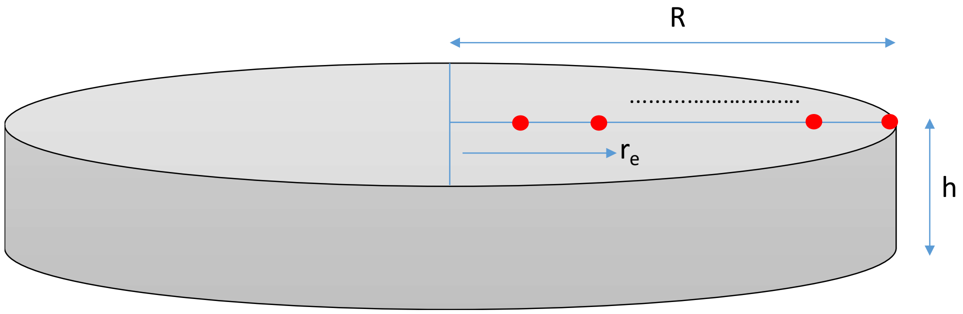

Figure 7.4: Schematic distribution of the elements along the radius

7.7.2 Fatigue Loading Without Rest (Continuous Cyclic Loading)

In this subsection, the model is validated against the continuous cyclic loading under strain controlled condition. Asphalt binder is loaded at a large amplitude cyclic loading (5% strain), so that both recoverable and permanent damages occur. The damage model parameters used for the examples presented in this section are as follows: $C^r = 0.35$, $\tau^r = 1050$, $m = 0.65$, $C_1^P = 1\times10^{-3}$ and $C_1^P = 3.5\times10^{-3}$. Comparisons of the experimental results and model predictions are shown in Figure 7.5(a). The model predicted values are very close to the experimental data. The model is used to simulate a strain-controlled shear fatigue loading test in MATLAB software. The strain rate and damage rate for time increment dt is calculated and the updated strain and damage for the time ($t + dt$) is used to update the modulus and stress. The model is run until the stress over the entire loading time of the experimental data is predicted. For this example, the total loading time is 10,102 secs (101,020 cycles). Figure 7.5 (b) shows the stress-strain curve for different loading cycles. It can be noted that as the loading cycles increases the maximum stress decreases. Also, the area under the curve decreases for higher number of loading cycles. At the 101,020 th cycle the stress is almost zero, this means that at this point the binder cannot bear anymore loading due to the accumulation of damage. Figure 7.5(c) shows the normalized modulus and damage over time for the outer element. As the figure shows, the proposed model captures all three phases in the modulus reduction seen in the fatigue testing discussed in Figure 7.1(a). Figure 7.5(c) shows that the accumulation of damage degrades the modulus. Figure 7.5(d) shows both permanent and recoverable damage accumulation over the loading time for the outer element. This figure shows that the recoverable damage rate is higher during the initial loading time. As it can be seen, due to the damage coupling the recoverable damage decreases over time whereas the permanent damage increases. Initially the rate of permanent damage is slower. However, once the modulus decreases to 50%, the rate of permanent damage increases. This increase is caused by the activation of both C_0^p and C_1^p parameters in the permanent damage evolution equation. Therefore, with the increase in loading over time, the damage recovery or healing capacity of the material decreases and the permanent damage starts to grow at a faster rate. This accumulation of the permanent damage leads to the failure of the material due to fatigue loading.

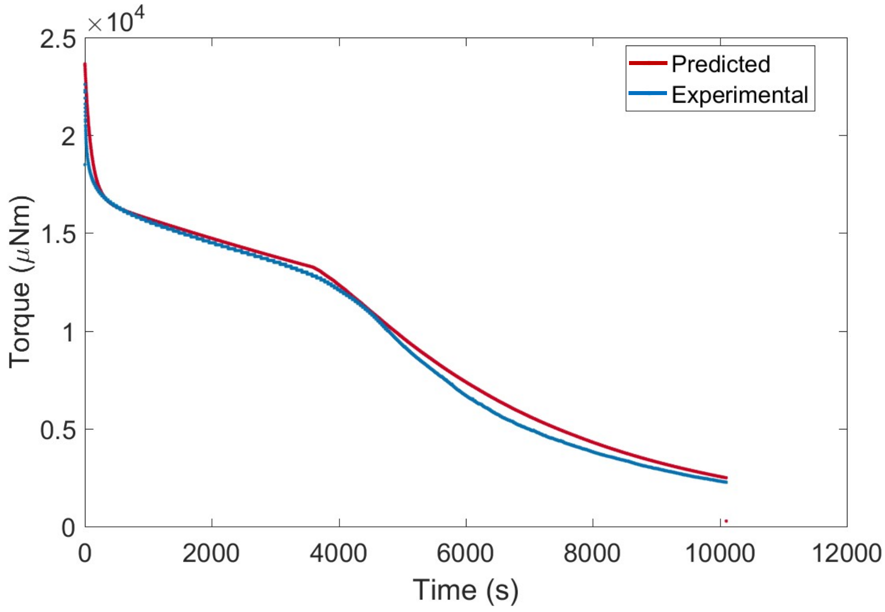

(a) Comparison of experimental and model predicted torque

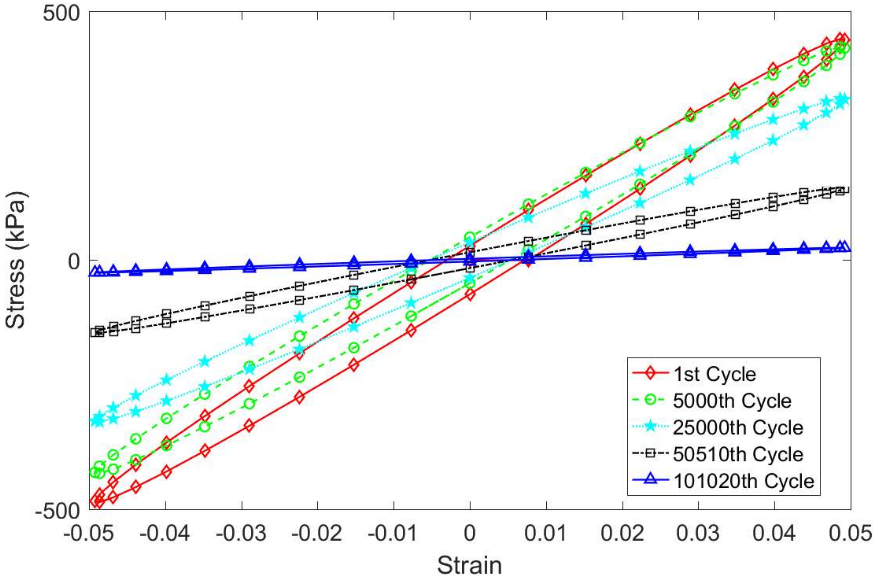

(b) Stress vs. strain for different cycles at the outer element

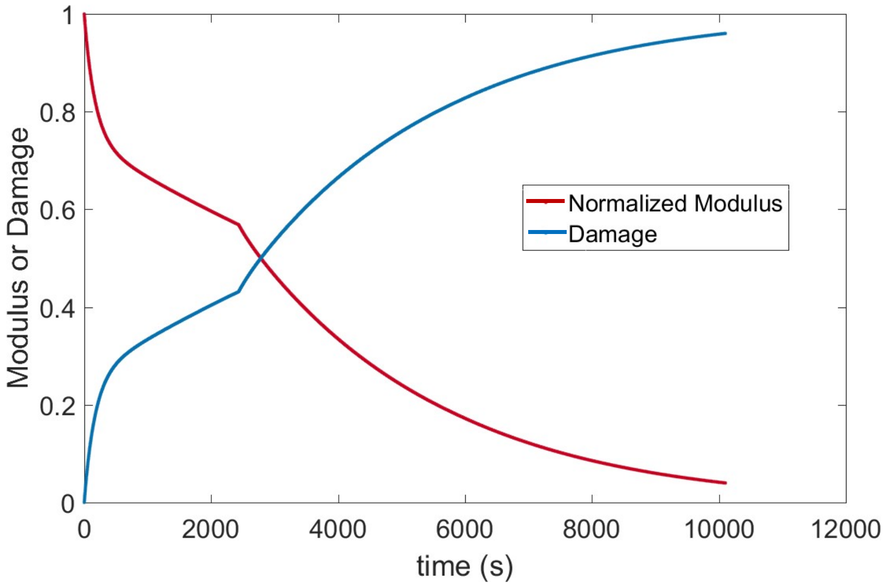

(c) Comparison of normalized modulus and damage at the outer element

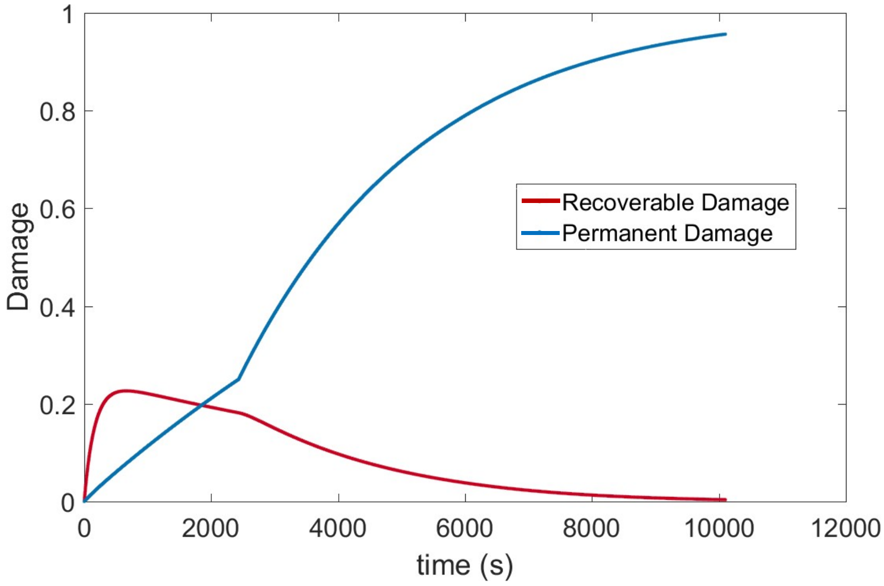

(d) The evolution of recoverable and permanent damage

Figure 7.5: Simulation of fatigue loading without rest period

Figure 7.5 shows that the total predicted values agree with the experimental values. Figure 7.6 shows the change in stress and damage along the radius of the cylindrical sample model. Figure 7.6 (a) and (b) shows that the stress distribution along the radius is nonlinear.

Figure 7.6 (a) and (c) shows the stress and damage evolution after 100 s of loading. Note that there is almost no permanent damage along the radius, as a result there is no decrease in the stress along the radius either. However, after 10102 s of loading the stress value decreases indicating the degradation of material strength (Figure 7.6 (c)). Figure 7.6 (d) shows that as the permanent damage increases along the radius, the stress of the material starts to decrease and becomes close to zero at the outer radius. Also at the initial stage of loading the recoverable damage governs along the radius, whereas after long continuous loading the recoverable damage at the outer radius decreases to zero. This decrease in recoverable damage results in an increase in permanent damage, accumulation of which results in failure of the material. Therefore, the developed model can predict the fatigue damage evolution of the asphalt binder due to continuous cyclic loading. Also, the elemental analysis shows the damage and stress development along the radius of the modeled cylindric asphalt binder sample.

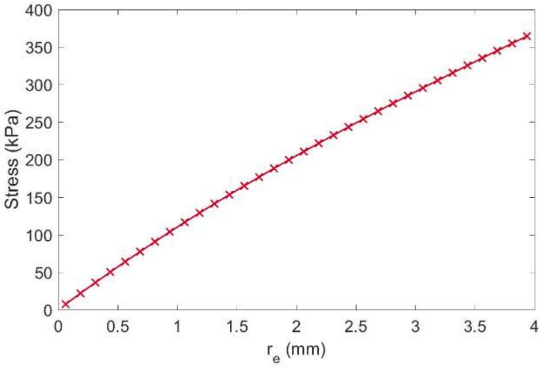

(a) Stress along the radius after 100 s of loading

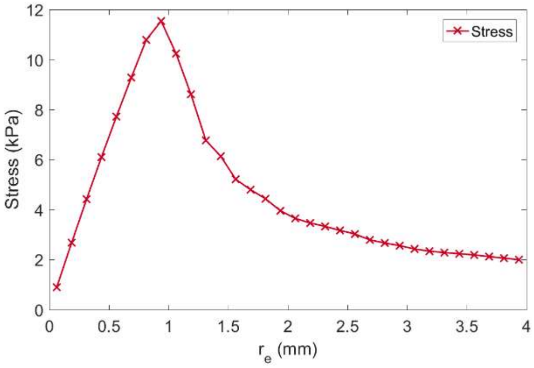

(b) Stress along the radius after 10102 s of loading

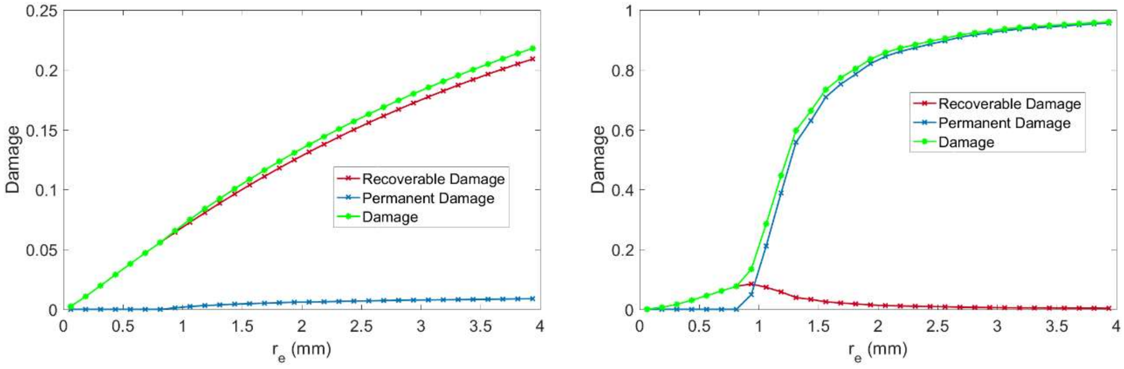

(c) Damage along the radius after 100 s of loading

(d) Damage along the radius after 10102 s of loading

Figure 7.6: Predicted strain, stress and damage evolution along the radius for continuous loading

In the next subsection, the damage evolution is predicted due to fatigue loading with rest period. Healing of the binder during this rest period will be considered. Also, it will be demonstrated that part of the recoverable damage recovers, resulting in a decrease in total damage.

7.7.3 Fatigue Loading with Rest Period (Interrupted Cyclic Loading)

In this subsection, the developed model is validated against the interrupted cyclic loading (series of loading and rest periods) under strain controlled condition. The asphalt binder is loaded at a large amplitude cyclic loading (5% strain) for 500 secs and then rested for 1200 secs. The damage accumulates during the loading period and recovers due to healing during the rest period. Comparisons of the experimental results and model predictions are shown in Figure 7.7(a). It can be seen from the experimental data that initially the recovery of torque is high due to rest period. However, with the repetition of loading and rest period the recovery of torque decreases. Using the proposed model, the strain rate and damage rate for the time increment, dt is computed and the updated strain and damage for the time ($t + dt$) are used to update the modulus and stress. The model successfully captures reduction and recovery of torque during loading and unloading respectively. The model prediction also agrees with the experimental values. Figure 7.7(b) shows the normalized modulus and total damage over time for the outer element. It shows that the damage increases during the loading time resulting in a decrease in modulus and heals during the rest period resulting in the recovery of modulus. Figure 7.7(c) shows both permanent and recoverable damage accumulation over the loading time for the outer element. Initially the permanent damage is very small and the recoverable damage dominates. Also, initially the recoverable damage is higher and during the rest period it recovers or heals completely. However, with more loading cycles the maximum recoverable damage decreases due to the damage coupling and the recovery during the rest period decreases. Whereas, initially the permanent damage increases during the loading time and remains almost constant over the rest period. However, after several loading and rest period sequences it accumulates faster which results in slower recovery in the rest period. Therefore, this proposed model can predict all the key features in fatigue testing such as damage and recovery due to healing.

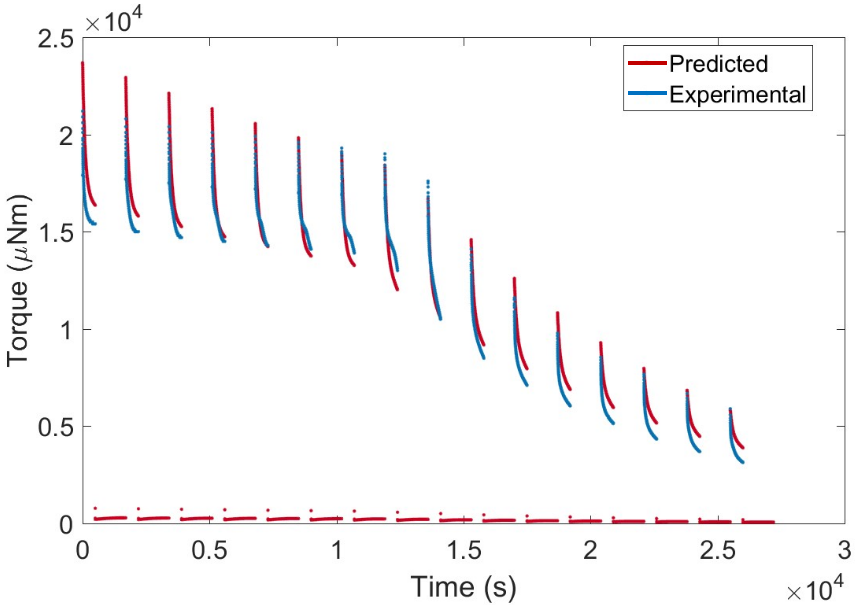

(a) Comparison of experimental and model predicted torque

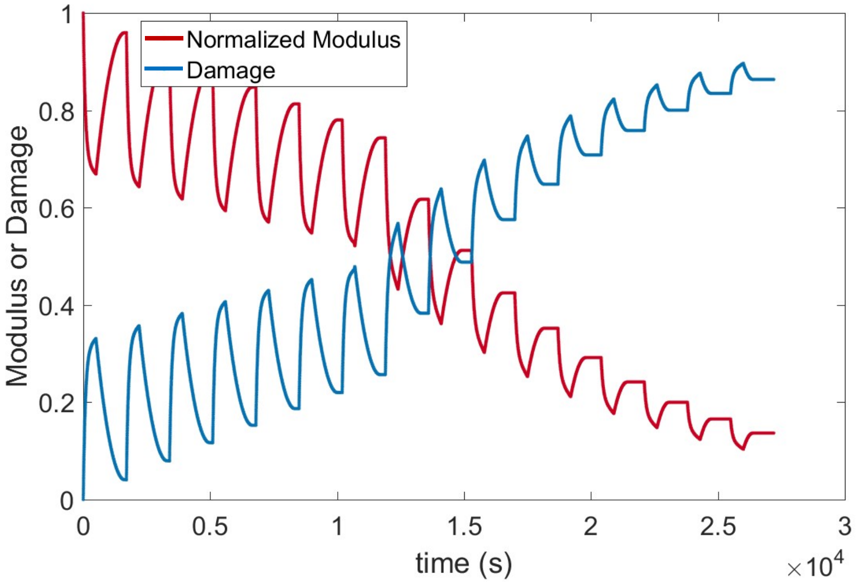

(b) Comparison of normalized modulus and damage at the outer element

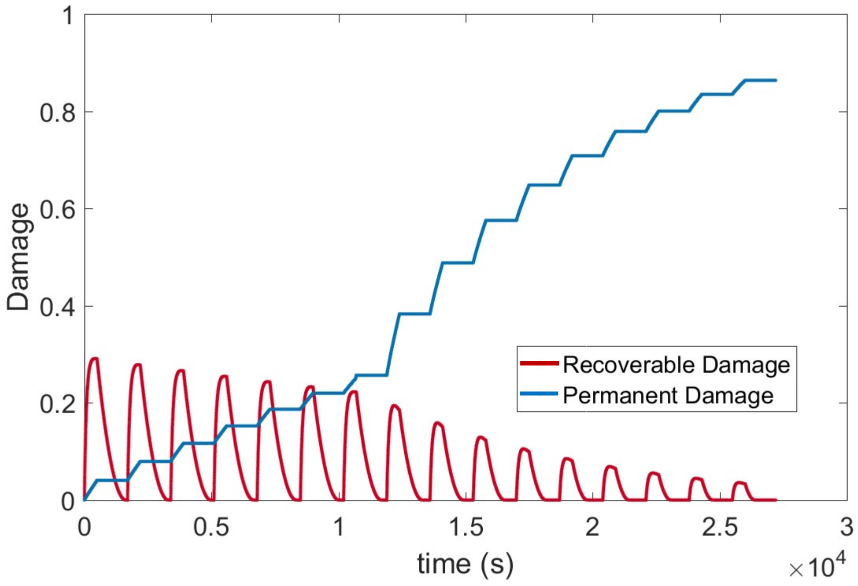

(c) The evolution of recoverable and permanent damage

Figure 7.7: Simulation of fatigue loading with rest period

Figure 7.7 shows that the developed model can also predict fatigue damage for interrupted loading (loading with rest period). Using the damage parameters determined in continuous loading this model can predict the fatigue damage for interrupted loading. Also, the outer element of the cylindrical sample model shows reduction in the modulus over time similar to the experimental values. Figure 7.8 shows the change in stress and damage along the radius of the cylindrical sample model for the interrupted loading scenario. Figure 7.8 (a) and (b) shows that the stress distribution along the radius is nonlinear. Figure 7.8 (a) and (c) shows the stress and damage evolution after 100 s of loading (no rest period). Note that there is almost no permanent damage along the radius, which is why there is no decrease in the stress along the radius. However, after 16 repetitions of 500 s of loading and 1200 s of rest period the stress value is almost zero along the radius (Figure 7.8(b)). Figure 7.8 (d) shows that the recoverable damage along the radius is almost zero, thus the total damage is equal to the permanent damage and close to 1. Therefore, the proposed model can predict the fatigue damage evolution of asphalt binder for cyclic loading with or without rest period.

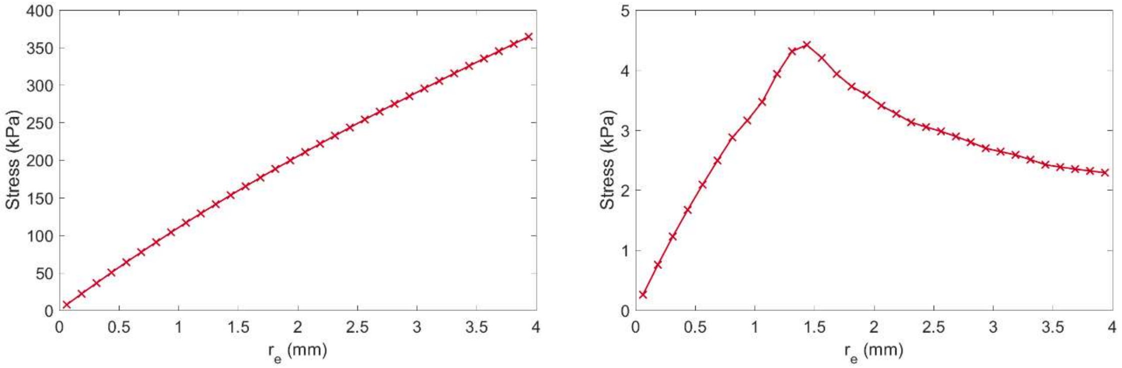

(a) Stress along the radius after 100 s of loading

(b) Stress along the radius after 16 load-rest repetitions

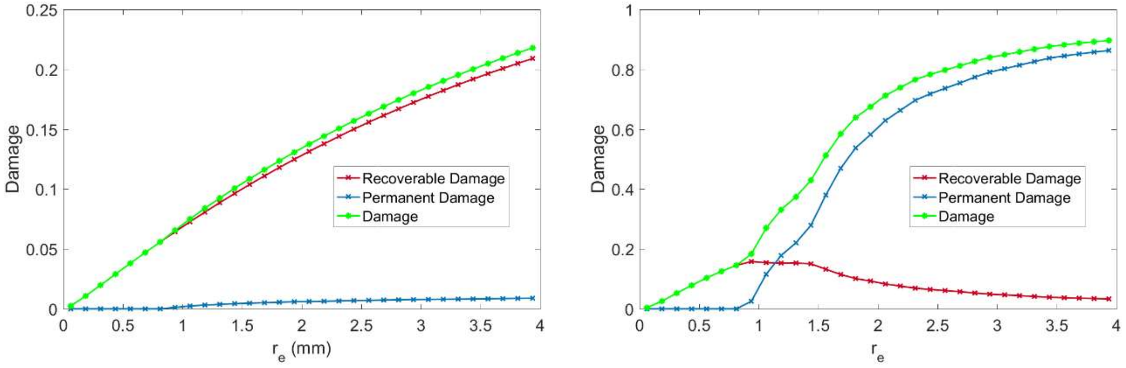

(c) Damage along the radius after 100 s of loading

(d) Damage along the radius after 16 load-rest repetitions

Figure 7.8: Predicted strain, stress and damage evolution along the radius for loading with rest period

The model is also run for different rest periods (300s and 600s) after 500s of loading. The above results are for a loading of 500s and rest period of 1200s. Figure 7.9 shows the comparison of the experimental and model predicted torque amplitudes for two different rest periods. As the figure shows, the model can capture the recovery during different rest periods. The values predicted by the model agree with the experimental data.

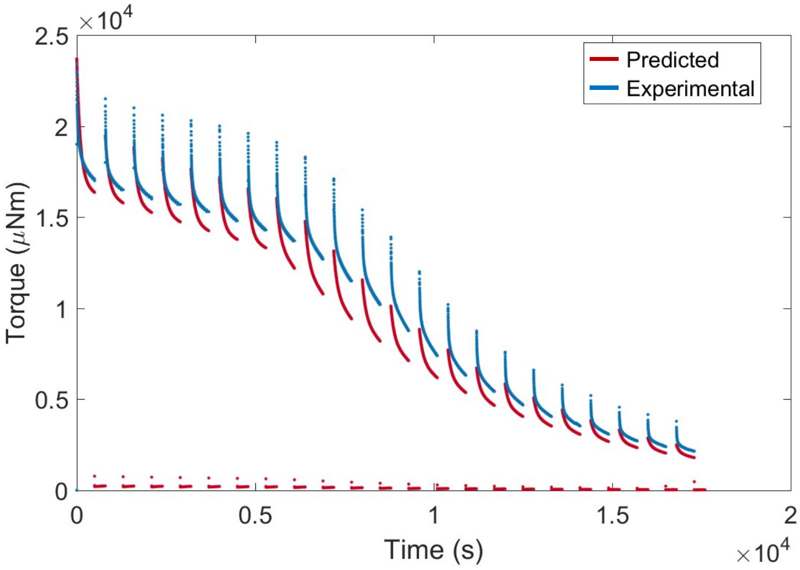

(a) 500s of loading and 300s of rest period

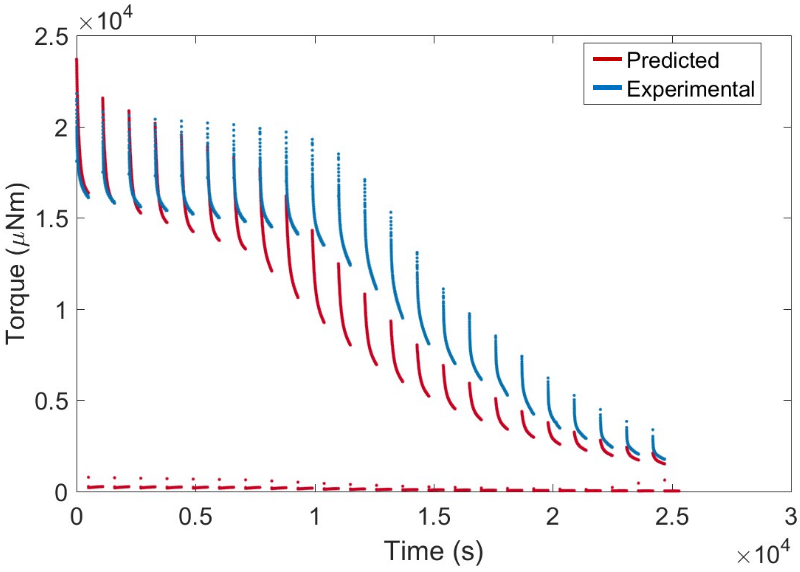

(b) 500s of loading and 600s of rest period

Figure 7.9: Model prediction for different rest periods

7.8 Findings

In this chapter, a damage model is formulated by coupling the permanent and recoverable damage to evaluate the change of modulus, stress and strain due to mechanical damage and healing under fatigue loading and rest period. A novel and more realistic damage model is proposed in this study by coupling strain and stress with viscoelasticity, viscoplasticity, recoverable damage and permanent damage. Previous studies also tried to explain some of these in their damage models, but in this study the fatigue damage is examined from shear cyclic loading stand point by incorporating nonlinearity in the analysis. The specific damage evolution equation is motivated by the experimental observations, which show two distinct types of damages due to the cyclic loading. Also, the experimental observations show that asphalt has micro-damage healing potential during the cyclic loading. Thus, the overall damage is divided into two parts: recoverable and permanent damage. With the increase in loading time, the recoverable damage decreases and permanent damage increases, which leads to the failure of the material. To capture this damage-healing phenomenon, a damage and healing model with viscoelastic–viscoplastic model has been developed which includes a viscoelastic part, a viscoplastic part and a continuum damage function, to predict the behavior of the asphalt material under cyclic shear loading with and without rest period.

The viscoelastic and viscoplastic parameters in the model can be determined using relaxation and constant strain rate tests in the shear direction. All the damage parameters can be identified from continuous fatigue loading. The developed model can correctly capture the overall response of the asphalt binder under fatigue loading with and without rest period. As a result of incorporating healing as a variable in the damage evolution equation, the model prediction agrees with the experimental measurements under cyclic loading with and without rest period. The comparison of the experimental and predicted results shows that this model can accurately capture the fatigue-healing behavior of the asphalt binder.

This viscoelastic-viscoplastic-damage constitutive model is expected to improve the fundamental understanding of fatigue damage-healing under cyclic loading and better predict the long-term behavior of the asphalt materials. The purpose of this model is to identify the key features which must be considered in developing a 3D constitutive equation. The current approach focuses on the material behavior in the shear direction, which can be used directly as the deviatoric aspect of the 3D constitutive equation.

CHAPTER 8

CONCLUSIONS AND RECOMMENDATIONS

8.1 Conclusions

This study attempts to characterize the healing of the asphalt binder in relation to its chemical composition and healing mechanism at the macroscopic level. In the first part prior to the study of healing, the chemical properties of the asphalt binders are characterized in relation to their composition. Next the healing of fatigue damage is investigated through experimental analysis. The chemical and mechanical properties of the asphalt binder are then correlated to the healing properties. Changes in the healing of the asphalt binder due to aging, moisture conditioning and addition of fillers are also examined. In the second part of the study, a constitutive equation combining damage and healing is developed to capture the key features of the asphalt binder fatigue damage.

The findings from this study are summarized below:

1. Investigation of the chemical properties of the asphalt binder reveals that among the four generic fractions in asphalt, aromatics is the predominating component. However, higher PG grade binder has lower aromatic contents and higher amounts of asphaltenes and resins. This increase in asphaltenes and resins results in more solid-like binder which is hard and more viscous. FTIR of these components shows that saturates and aromatics; and resins and asphaltenes show many similar peaks. The relationship between the functional groups and SARA fractions is determined

next. Results show that sulfoxide, carbonyl and aromatic indices represent the asphaltenes, resins and aromatics in the asphalt binder respectively. The aliphatic chain length or methylene to methyl ratio shows a negative correlation with the branched and aromatic structure, meaning that the binder with higher aliphatic chain length has less aromatic and branched structures. FTIR analysis of the damaged and healed PG asphalt binders showed that during damage the methylene groups decrease and after healing they increase. Therefore, the damage and healing of the binder is essentially the breaking and reconstruction of the long chains in the asphalt molecules respectively.

2. Healing mechanism and data analysis method are developed to evaluate the healing of the asphalt binder. The healing of the asphalt binder occurs in two stages: first an instantaneous recovery and then a time dependent recovery. All five binders show these two-distinct parts in the overall healing. These two stages in healing are termed as instant healing and long-term healing, which basically distinguishes between wetting and molecular diffusion at the crack interface during healing. A physico-chemical model developed by Wool and O'Connor for polymers is fitted to the experimental healing data for the binder to predict the instant healing and long-term healing. The fitted model for asphalt binder shows that the healing index of the asphalt binder is linearly correlated to the one fourth power of the rest period.
3. A parameter called energy of separation is used to measure cohesion in this study. This parameter was determined by analyzing the tack test data. The predicted instant healing from the fitted model is related to the energy of separation in order to relate binder cohesion with instant healing. Instant healing of the asphalt binder

shows a positive correlation with the energy of separation. Results show that as the PG grade of the binder increases the energy of separation decreases, which results in a reduction in instant healing. This decrease in the energy of separation is due to the increase in larger molecules such as asphaltenes and resins in the asphalt binder. The increase in larger molecules in the asphalt binder reduces the molecular mobility of the binder resulting in a decrease in its wettability. The ranking of the PG binders based on the instant healing found in this study is: PG 52-22 > PG 58-22 > PG 64-22 > PG 70-22 > PG 76-22.

4. The long-term healing depends on the rate of inter-molecular diffusion at the micro-crack interface, which depends on the random walk of the molecular chain. The binder with long chained structure has high diffusion rate, but the binder with more branched or ring-type structure has less diffusion rate. The methylene to methyl ratio from FTIR represents the length of the aliphatic chain; high value of this ratio means that the binder has long aliphatic chain without branching. Thus, the long-term healing rate or diffusion rate is found to be proportional to the methylene to methyl ratio. The order of the PG binders used in this study according to long-term healing is: PG 64-22 > PG 58-22 > PG 52-22 > PG 70-22 > PG 76-22.
5. Aged and moisture conditioned asphalt binders are also investigated using the same physico-chemical model. The FTIR spectrum shows an increase in the sulfoxide groups due to aging, which indicates an increase in asphaltenes in the binder. Therefore, aging of binder results in stiff binder and makes the molecular diffusion difficult. Thus, this increase in sulfoxide group decreases the long-term healing rate. The FTIR spectrum shows an increase in the absorbed water groups due to

moisture conditioning, which reduces the molecular mobility. Thus, moisture conditioning decreases the cohesion and increases the activation energy, resulting in a decrease in instant healing and long-term healing respectively. For moisture conditioned binders, results show that the long-term healing rate is inversely proportional to the percent water absorbed in the binder due to moisture conditioning. Thus, both aging and moisture conditioning decrease healing in the asphalt binder.

6. Healing of mastic is also studied to investigate the effects of percent filler (20%, 40% and 60%) on the fatigue damage and healing of mastic. Results show that the asphalt binder type plays a very important role in the overall fatigue and healing properties of mastic. Mastics prepared with PG 70-22 show higher fatigue resistance, whereas mastics with PG 64-22 binder show higher healing index over the rest period. Mastics with 20% filler show highest fatigue resistance. The presence of fillers in the binder disturbs the continuous binder medium, resulting in a slower wetting of micro-crack surface and less molecular diffusion in the mastic. As a result, the addition of fillers in the binder decreases both the instant and long-term healing of the mastics.
7. A constitutive damage model considering healing is developed. A general constitutive framework is utilized to model the fatigue damage and healing under cyclic shear loading. The damage is divided into recoverable and permanent parts to capture both damage and healing. Simultaneously, this damage model is coupled with the viscoelastic and viscoplastic mechanisms to simulate the non-linear behavior of the asphalt material. These material properties are calculated from the

relaxation and constant strain rate tests. Damage in this model is triggered by the yield stress condition. In the initial loading stage, the recoverable damage governs and permanent damage is almost zero. Eventually over continuous cyclic loading, permanent damage increases and the accumulation of permanent damage results in material failure. The healing of the asphalt binder is incorporated in the recoverable damage rate evolution equation. During loading both recoverable and permanent damage increases. However, in the rest period, a part of the recoverable damage heals. During initial loading, the recoverable damage heals completely, but over the loading time the healing ability decreases which results in more permanent damage. The model predictions were compared with the experimental measurements under cyclic loading with and without rest period and is found to be in good agreement.

8.2 Recommendations

The following recommendations are made for future study:

1. The healing mechanism of the asphalt binder studied in this dissertation focuses only on the wetting and molecular diffusion at the micro-crack surface. However, other healing mechanisms such as bond reformation and chain elongation may exist in the asphalt binder. Therefore, further study using molecular modeling is required for these mechanisms.
2. The constitutive damage model is developed and validated only for the experimental shear loading condition. The force interaction between the wheel and the pavement shows that the shear stress dominates and affects the fatigue damage simulations. As the model is developed for shear loading, validation of this model

using the loading sequence from the field will provide accurate prediction of the asphalt damage and healing. For this, a finite element (FE) analysis using the developed constitutive damage equations is recommended. However, before implementing the developed model in the FE analysis a 3D constitutive equation needs to develop. The currently developed equations can be used directly as the deviatoric aspect in the 3D constitutive equation.

3. The constitutive damage model is only developed for fatigue and healing of the virgin asphalt (unconditioned). Other factors (e.g. aging, moisture, etc.) affecting the damage and healing in the binder should also be incorporated in the model. By incorporating these, the constitutive model will be able to predict the response of the asphalt under realistic loading and environmental conditions.

REFERENCES

AASHTO, R. 28-12. (2012). “Standard practice for accelerated aging of asphalt binder using a Pressurized Aging Vessel (PAV).”

AASHTO, T. 240. (2013). “Standard Method of Test for Effect of Heat and Air on a Moving Film of Asphalt (Rolling Thin-Film Oven Test).” *American Association of State Highway and Transportation Officials*.

AASHTO T 283-14. (2014). “Standard Method of Test for Resistance of Compacted Asphalt Mixtures to Moisture-Induced Damage.”

Abbas, A., Masad, E., Papagiannakis, T., and Harman, T. (2007). “Micromechanical modeling of the viscoelastic behavior of asphalt mixtures using the discrete-element method.” *International Journal of Geomechanics*, 7(2), 131–139.

Abbas, A. R., Mannan, U. A., and Dessouky, S. (2013). “Effect of recycled asphalt shingles on physical and chemical properties of virgin asphalt binders.” *Construction and Building Materials*, 45, 162–172.

Ahmad, M., Mannan, U. A., Islam, M. R., and Tarefder, R. A. (2016). “Effects of Moisture Conditioning on Chemical and Mechanical Properties of Asphalt Concrete.” *Transportation Research Board 95th Annual Meeting*.

Ahmad, M., Mannan, U. A., Islam, M. R., and Tarefder, R. A. (2017). “Chemical and mechanical changes in asphalt binder due to moisture conditioning.” *Road Materials and Pavement Design*, 1–14.

Airey, G. D., and Brown, S. F. (1998). “Rheological performance of aged polymer modified bitumens.” *Journal of the Association of Asphalt Paving Technologists*, 67.

Ajam, H., Lastra-González, P., Gómez-Meijide, B., and García, Á. (2016). “Self-Healing of Dense Asphalt Concrete by Two Different Approaches: Electromagnetic Induction and Infrared Radiation.” Springer, 241–246.

Alfredsson, K., and Stigh, U. (2004). “Continuum damage mechanics revised: A principle for mechanical and thermal equivalence.” *International Journal of Solids and Structures*, 41(15), 4025–4045.

Al-Khateeb, G., Stuart, K., Mogawer, W., and Gibson, N. (2009). “Fatigue performance: asphalt binder versus mixture versus full-scale pavements.” *Canadian Journal of Transportation*, 2(1).

Al-Rub, R. K. A., Darabi, M. K., Little, D. N., and Masad, E. A. (2010). “A micro-damage healing model that improves prediction of fatigue life in asphalt mixes.” *International Journal of Engineering Science*, 48(11), 966–990.

Ando, K., Chu, M.-C., Tsuji, K., Hirasawa, T., Kobayashi, Y., and Sato, S. (2002). “Crack healing behaviour and high-temperature strength of mullite/SiC composite ceramics.” *Journal of the European Ceramic Society*, 22(8), 1313–1319.

ASTM, D. (1988). “Standard Test Method for separation of asphalt into four fractions.” *American Society for Testing and Material: Philadelphia*.

Bahia, H. U., Hanson, D., Zeng, M., Zhai, H., Khatri, M., and Anderson, R. (2001). *Characterization of modified asphalt binders in superpave mix design*. National Cooperative Highway Research Program, Washington, D.C.

Bahia, H. U., Zhai, H., Bonnetti, K., and Kose, S. (1999). “Non-linear viscoelastic and fatigue properties of asphalt binders.” *Journal of the Association of Asphalt Paving Technologists*, 68, 1–34.

Bai, F., Yang, X., and Zeng, G. (2014). “Creep and recovery behavior characterization of asphalt mixture in compression.” *Construction and Building Materials*, 54, 504–511.

Bandyopadhyaya, R., Das, A., and Basu, S. (2008). “Numerical simulation of mechanical behaviour of asphalt mix.” *Construction and Building Materials*, 22(6), 1051–1058.

Barth, E. J. (1962). *Asphalt; science and technology*. Gordon and Breach Science Publishers.

Bateman, D. (2012). “Laboratory investigation of fatigue endurance limits in asphalt concrete.” Doctoral Dissertation, University of New Mexico.

Bazin, P., and Saunier, J. (1967). “Deformability, fatigue and healing properties of asphalt mixes.” *Intl Conf Struct Design Asphalt Pvmts*.

Bhasin, A., Bommavaram, R., Greenfield, M. L., and Little, D. N. (2010). “Use of molecular dynamics to investigate self-healing mechanisms in asphalt binders.” *Journal of Materials in Civil Engineering*, 23(4), 485–492.

Bhasin, A., Little, D. N., Bommavaram, R., and Vasconcelos, K. (2008). “A framework to quantify the effect of healing in bituminous materials using material properties.” *Road Materials and Pavement Design*, 9(sup1), 219–242.

Bhasin, A., Palvadi, S., and Little, D. (2011). “Influence of aging and temperature on intrinsic healing of asphalt binders.” *Transportation Research Record: Journal of the Transportation Research Board*, (2207), 70–78.

Boiko, Y. M., and Prud’Homme, R. E. (1998). “Surface mobility and diffusion at interfaces of polystyrene in the vicinity of the glass transition.” *Journal of Polymer Science Part B: Polymer Physics*, 36(4), 567–572.

Bonnaure, F., Huibers, A., and Boonders, A. (1982). “A laboratory investigation of the influence of rest periods on the fatigue characteristics of bituminous mixes (with discussion).” *Association of Asphalt Paving Technologists Proceedings*.

Bonnetti, K., Nam, K., and Bahia, H. (2002). “Measuring and defining fatigue behavior of asphalt binders.” *Transportation Research Record: Journal of the Transportation Research Board*, (1810), 33–43.

Branthaver, J. F., Petersen, J., Robertson, R., Duvall, J., Kim, S., Harnsberger, P., Mill, T., Ensley, E., Barbour, F., and Scharbron, J. (1993a). *Binder characterization and evaluation. Volume 2: Chemistry*.

Branthaver, J., Petersen, J., Robertson, R., Duvall, J., Kim, S., Harnsberger, P., Mill, T., Ensley, E., Barbour, F., and Schabron, J. (1993b). “SHRP-A-368, binder characterization and evaluation, volume 2: Chemistry.” *Strategic Highway Research Program, National Research Council, Washington, DC*.

Braun, P. V., Cho, S. H., White, S. R., Sottos, N. R., and Andersson, H. M. (2009). “Self-healing polymers.” U.S. Patent and Trademark Office, Washington, DC.

Capron, I., Robert, P., Colonna, P., Brogly, M., and Planchot, V. (2007). “Starch in rubbery and glassy states by FTIR spectroscopy.” *Carbohydrate Polymers*, 68(2), 249–259.

Carpenter, S., Ghuzlan, K., and Shen, S. (2003). "Fatigue endurance limit for highway and airport pavements." *Transportation Research Record: Journal of the Transportation Research Board*, (1832), 131–138.

Carpenter, S. H., and Jansen, M. (1997). "Fatigue behavior under new aircraft loading conditions." *Aircraft/Pavement Technology In The Midst Of Change*.

Carpenter, S., and Shen, S. (2006). "Dissipated energy approach to study hot-mix asphalt healing in fatigue." *Transportation Research Record: Journal of the Transportation Research Board*, (1970), 178–185.

Castro, M., and Sánchez, J. A. (2006). "Fatigue and healing of asphalt mixtures: discriminate analysis of fatigue curves." *Journal of transportation engineering*, 132(2), 168–174.

Chen, Y., Furmann, A., Mastalerz, M., and Schimmelmann, A. (2014). "Quantitative analysis of shales by KBr-FTIR and micro-FTIR." *Fuel*, 116, 538–549.

Chen, Y., Mastalerz, M., and Schimmelmann, A. (2012). "Characterization of chemical functional groups in macerals across different coal ranks via micro-FTIR spectroscopy." *International Journal of Coal Geology*, 104, 22–33.

Cheng, D., Little, D. N., Lytton, R. L., and Holste, J. C. (2002). "Use of surface free energy properties of the asphalt-aggregate system to predict moisture damage potential (with discussion)." *Journal of the association of asphalt paving technologists*, 71.

Coates, J. (2000). "Interpretation of infrared spectra, a practical approach." *Encyclopedia of analytical chemistry*.

Corbett, L. W. (1969). "Composition of asphalt based on generic fractionation, using solvent deasphaltening, elution-adsorption chromatography, and densimetric characterization." *Analytical Chemistry*, 41(4), 576–579.

Creton, C., and Fabre, P. (2002). "Chapter 14 - Tack A2 - Chaudhury, M." *Adhesion Science and Engineering*, A. V. Pocius, ed., Elsevier Science B.V., Amsterdam, 535–575.

Daniel, J. S., and Kim, Y. R. (2001). "Laboratory evaluation of fatigue damage and healing of asphalt mixtures." *Journal of Materials in Civil Engineering*, 13(6), 434–440.

Daniel, J. S., and Kim, Y. R. (2002). "Development of a simplified fatigue test and analysis procedure using a viscoelastic, continuum damage model (with discussion)." *Journal of the Association of Asphalt Paving Technologists*, 71.

Darabi, M. K., Al-Rub, R. K. A., Masad, E. A., Huang, C.-W., and Little, D. N. (2012). "A modified viscoplastic model to predict the permanent deformation of asphaltic materials under cyclic-compression loading at high temperatures." *International Journal of Plasticity*, 35, 100–134.

Deacon, J. A. (1965). "Fatigue of Asphalt Concrete. Graduate Report, Institute of Transportation and Traffic Engineering." *University of California, Berkeley*.

Delaporte, B., Di Benedetto, H., Chaverot, P., and Gauthier, G. (2007). "Linear viscoelastic properties of bituminous materials: from binders to mastics (with discussion)." *Journal of the Association of Asphalt Paving Technologists*, 76.

Di Benedetto, H., Nguyen, Q. T., and Sauzéat, C. (2011). "Nonlinearity, heating, fatigue and thixotropy during cyclic loading of asphalt mixtures." *Road Materials and Pavement Design*, 12(1), 129–158.

Dickie, J. P., and Yen, T. F. (1967). "Macrostructures of the asphaltic fractions by various instrumental methods." *Analytical chemistry*, 39(14), 1847–1852.

Elber, W. (1971). “The significance of fatigue crack closure.” *Damage tolerance in aircraft structures*, ASTM International.

Frigio, F., Ferrotti, G., and Cardone, F. (2016). “Fatigue rheological characterization of polymer-modified bitumens and mastics.” Springer, 655–666.

García, Á. (2012). “Self-healing of open cracks in asphalt mastic.” *Fuel*, 93, 264–272.

García, A., Norambuena-Contreras, J., Bueno, M., and Partl, M. N. (2015). “Single and multiple healing of porous and dense asphalt concrete.” *Journal of Intelligent Material Systems and Structures*, 26(4), 425–433.

de Gennes, P.-G. (1971). “Reptation of a polymer chain in the presence of fixed obstacles.” *The journal of chemical physics*, 55(2), 572–579.

Gibson, N. H. (2006). “A viscoelastoplastic continuum damage model for the compressive behavior of asphalt concrete.” Doctoral dissertation, University of Maryland, MD.

Gong, M., Yang, J., Wei, J., Pauli, T., and Yu, H. (2017). “Quantitative characterisation of asphalt’s composition–microstructure relationship based on atomic force microscopy, differential scanning calorimetry, and Fourier transform infrared spectroscopy tests.” *Road Materials and Pavement Design*, 18(3), 507–532.

Grant, T. P. (2001). “Determination of asphalt mixture healing rate using the Superpave indirect tensile test.” Doctoral dissertation, University of Florida.

Groenzin, H., and Mullins, O. C. (2000). “Molecular size and structure of asphaltenes from various sources.” *Energy & Fuels*, 14(3), 677–684.

Guedes, R. M. (2010). *Creep and fatigue in polymer matrix composites*. Elsevier.

Hamed, G., and Shieh, C. (1983). “Relationship between the cohesive strength and the tack of elastomers.” *Journal of Polymer Science: Polymer Physics Edition*, 21(8), 1415–1425.

Hamed, G., and Shieh, C. (1985). “Relationship between the cohesive strength and the tack of elastomers: Part II, contact time effects.” *Rubber chemistry and technology*, 58(5), 1038–1044.

Hopman, P., Kunst, P., and Pronk, A. (1989). “A renewed interpretation method for fatigue measurements, verification of miner’s rule.” 557–561.

InstroTek. (2012). *Moisture induced sensitivity test (MIST).* Raleigh, NC.

Jahangir, R., Little, D., and Bhasin, A. (2015). “Evolution of asphalt binder microstructure due to tensile loading determined using AFM and image analysis techniques.” *International Journal of Pavement Engineering*, 16(4), 337–349.

Jennings, P., Desando, M., Raub, M., Moats, R., Mendez, T., Stewart, F., Hoberg, J., Pribanic, J., and Smith, J. (1992). “NMR spectroscopy in the characterization of eight selected asphalts.” *Fuel science & technology international*, 10(4–6), 887–907.

Jiang, Z., Liu, Z., Fei, B., Cai, Z., and Yu, Y. (2012). “The pyrolysis characteristics of moso bamboo.” *Journal of analytical and applied pyrolysis*, 94, 48–52.

Johnson, C., Wen, H., Martono, W., and Bahia, H. (2008). “Developments in Intermediate-Temperature Binder Specifications (Fatigue).” *Rocky Mountain Asphalt User Group Conference*.

Jones, A., and Dutta, H. (2010). “Fatigue life modeling of self-healing polymer systems.” *Mechanics of Materials*, 42(4), 481–490.

Jones, D. R. (1993). *SHRP materials reference library: Asphalt cements: A concise data compilation*. Strategic Highway Research Program, National Research Council Washington, DC.

Kachanov, L. (1986). *Introduction to continuum damage mechanics*. Springer Science & Business Media.

Kanitpong, K., and Bahia, H. (2005). “Relating adhesion and cohesion of asphalts to the effect of moisture on laboratory performance of asphalt mixtures.” *Transportation Research Record: Journal of the Transportation Research Board*, (1901), 33–43.

Kausch, H. H. (1991). “Mechanical aspects of polymer blending.” *Makromolekulare Chemie. Macromolecular Symposia*, Wiley Online Library, 155–163.

Kausch, H. H., and Dettenmaier, M. (1982). “On some mechanical effects in glassy polymers attributed to chain entanglements.” *Colloid & Polymer Science*, 260(2), 120–123.

Kebukawa, Y., Kilcoyne, A. D., and Cody, G. D. (2013). “Exploring the potential formation of organic solids in chondrites and comets through polymerization of interstellar formaldehyde.” *The Astrophysical Journal*, 771(1), 19.

Kessler, M., Sottos, N., and White, S. (2003). “Self-healing structural composite materials.” *Composites Part A: applied science and manufacturing*, 34(8), 743–753.

Kim, Y. H., and Wool, R. P. (1983). “A theory of healing at a polymer-polymer interface.” *Macromolecules*, 16(7), 1115–1120.

Kim, Y., Lee, H., Little, D., and Kim, Y. R. (2006). “A Simple Testing Method to Evaluate Fatigue Fracture and Damage Performance of Asphalt Mixtures (With Discussion).” *Journal of the Association of Asphalt Paving Technologists*, 75.

Kim, Y. R., Lee, H.-J., and Little, D. N. (1997). “Fatigue characterization of asphalt concrete using viscoelasticity and continuum damage theory (with discussion).” *Journal of the Association of Asphalt Paving Technologists*, 66.

Kim, Y. R., and Little, D. N. (1990). “One-dimensional constitutive modeling of asphalt concrete.” *Journal of engineering mechanics*, 116(4), 751–772.

Kim, Y. R., Little, D. N., and Benson, F. C. (1990). “Chemical and mechanical evaluation on healing mechanism of asphalt concrete (with discussion).” *Journal of the Association of Asphalt Paving Technologists*, 59.

Kim, Y.-R., Little, D., and Lytton, R. (2001). “Evaluation of microdamage, healing, and heat dissipation of asphalt mixtures, using a dynamic mechanical analyzer.” *Transportation Research Record: Journal of the Transportation Research Board*, (1767), 60–66.

Kim, Y.-R., Little, D., and Lytton, R. (2002). “Use of dynamic mechanical analysis (DMA) to evaluate the fatigue and healing potential of asphalt binders in sand asphalt mixtures (with discussion and closure).” *Journal of the Association of Asphalt Paving Technologists*, 71.

Kim, Y.-R., Little, D., and Lytton, R. (2003). “Fatigue and healing characterization of asphalt mixtures.” *Journal of Materials in Civil Engineering*, 15(1), 75–83.

Lee, H.-J., Daniel, J. S., and Kim, Y. R. (2000). “Continuum damage mechanics-based fatigue model of asphalt concrete.” *Journal of Materials in Civil Engineering*, 12(2), 105–112.

Lee, H.-J., and Kim, Y. R. (1998a). "Viscoelastic constitutive model for asphalt concrete under cyclic loading." *Journal of Engineering Mechanics*, 124(1), 32–40.

Lee, H.-J., and Kim, Y. R. (1998b). "Viscoelastic continuum damage model of asphalt concrete with healing." *Journal of Engineering Mechanics*, 124(11), 1224–1232.

Lee, J. S., Lee, S., and Kim, Y. R. (2011). "Evaluation of healing effect by rest periods on asphalt concrete slab using MMLS3 and NDE techniques." *KSCE Journal of Civil Engineering*, 15(3), 553–560.

Lee, N. K., Morrison, G. R., and Hesp, S. (1995). "Low temperature fracture of polyethylene-modified asphalt binders and asphalt concrete mixes (with discussion)." *Journal of the Association of Asphalt Paving Technologists*, 64.

Lemaitre, J., and Chaboche, J.-L. (1994). *Mechanics of solid materials*. Cambridge university press.

Lesueur, D. (2009). "The colloidal structure of bitumen: consequences on the rheology and on the mechanisms of bitumen modification." *Advances in colloid and interface science*, 145(1), 42–82.

Levenberg, E. (2009). "Viscoplastic response and modeling of asphalt-aggregate mixes." *Materials and structures*, 42(8), 1139–1151.

Little, D. N., and Bhasin, A. (2007). "Exploring Mechanism of Healing in Asphalt Mixtures and Quantifying its Impact." *Self healing materials*, 205–218.

Little, D. N., Lytton, R. L., Chairl, B., and Williams, D. (1999). "An analysis of the mechanism of microdamage healing based on the application of micromechanics first principles of fracture and healing." *Association of Asphalt Paving Technologists*.

Little, D. N., Lytton, R. L., Williams, D., and Kim, Y. R. (1997). *Propagation and healing of microcracks in asphalt concrete and their contributions to fatigue*. Marcel Dekker, New York.

Liu, Q., García, Á., Schlangen, E., and van de Ven, M. (2011). "Induction healing of asphalt mastic and porous asphalt concrete." *Construction and Building Materials*, 25(9), 3746–3752.

Lu, X. (2013). "Investigation of the fracture healing and mechanism of asphalt binders." Doctoral dissertation, Washington State University.

Lundström, R. (2004). "On rheological testing and modelling of asphalt mixtures with emphasis on fatigue characterisation." *TRITA-VT*, (04: 02).

Lyons, P. C., Orem, W. H., Mastalerz, M., Zodrow, E. L., Vieth-Redemann, A., and Bustin, R. M. (1995). "13C NMR, micro-FTIR and fluorescence spectra, and pyrolysis-gas chromatograms of coalified foliage of late Carboniferous medullosan seed ferns, Nova Scotia, Canada: implications for coalification and chemotaxonomy." *International Journal of Coal Geology*, 27(2–4), 227–248.

Lytton, R., Chen, C., and Little, D. (2001). *Microdamage healing in asphalt and asphalt concrete, volume III: A micromechanics fracture and healing model for asphalt concrete*. No. FHWA-RD-98-143.

Lytton, R. L., Uzan, J., Fernando, E. G., Roque, R., Hiltunen, D., and Stoffels, S. M. (1993). *Development and validation of performance prediction models and specifications for asphalt binders and paving mixes*. Strategic Highway Research Program.

Maillard, S., de La Roche, C., Hammoum, F., Gaillet, L., and Such, C. (2004). "Experimental investigation of fracture and healing at pseudo-contact of two aggregates." *3rd Euroasphalt and Eurobitume Congress, Vienna*.

Mamlouk, M., Souliman, M., and Zeiada, W. (2012). "Optimum testing conditions to measure HMA fatigue and healing using flexural bending test." *TRB Annual Meeting 2012*.

Mannan, U. A. (2012). "Effect of Recycled Asphalt Shingles (RAS) on Physical and Chemical Properties of Asphalt Binders." The University of Akron.

Mannan, U. A., Ahmad, M., and Tarefder, R. A. (2017). "Influence of moisture conditioning on healing of asphalt binders." *Construction and Building Materials*, 146, 360–369.

Mannan, U. A., Islam, M. R., and Tarefder, R. A. (2015a). "Effects of recycled asphalt pavements on the fatigue life of asphalt under different strain levels and loading frequencies." *International Journal of Fatigue*, 78, 72–80.

Mannan, U. A., Islam, M., Weldegiorgis, M., and Tarefder, R. (2015b). "Experimental Investigation on Rheological Properties of Recycled Asphalt Pavement Mastics." *Applied Rheology*, 25(2), 7–15.

Masson, J. (2008). "Brief review of the chemistry of polyphosphoric acid (PPA) and bitumen." *Energy & Fuels*, 22(4), 2637–2640.

Masson, J., Pelletier, L., and Collins, P. (2001). "Rapid FTIR method for quantification of styrene-butadiene type copolymers in bitumen." *Journal of Applied Polymer Science*, 79(6), 1034–1041.

Mastalerz, M., Hower, J., and Taulbee, D. (2013). "Variations in chemistry of macerals as reflected by micro-scale analysis of a Spanish coal." *Geologica Acta: an international earth science journal*, 11(4), 483–493.

Matrajt, G., Flynn, G., Brownlee, D., Joswiak, D., and Bajt, S. (2013). "The origin of the 3.4 μm feature in Wild 2 cometary particles and in ultracarbonaceous interplanetary dust particles." *The Astrophysical Journal*, 765(2), 145.

Mazzoni, G., Stimilli, A., and Canestrari, F. (2016). "Self-healing capability and thixotropy of bituminous mastics." *International Journal of Fatigue*, 92, 8–17.

Miao, S., Wang, M. L., and Schreyer, H. L. (1995). "Constitutive models for healing of materials with application to compaction of crushed rock salt." *Journal of Engineering Mechanics*, 121(10), 1122–1129.

Migliori, F., and Corté, J.-F. (1998). "Comparative Study of RTFOT and PAV Aging Simulation Laboratory Tests." *Transportation Research Record: Journal of the Transportation Research Board*, 1638, 56–63.

Mouillet, V., De La Roche, C., Chailleux, E., and Coussot, P. (2011). "Thixotropic behavior of paving-grade bitumens under dynamic shear." *Journal of Materials in Civil Engineering*, 24(1), 23–31.

Nellensteyn, F. (1924). "The constitution of asphalt." *J. Inst. Pet*, 10, 311–325.

Nishizawa, T., Shimeno, S., and Sekiguchi, M. (1997). "Fatigue analysis of asphalt pavements with thick asphalt mixture layer." *Eighth International Conference on Asphalt Pavements*.

Norambuena-Contreras, J., and Garcia, A. (2016). "Self-healing of asphalt mixture by microwave and induction heating." *Materials & Design*, 106, 404–414.

Ouyang, C., Wang, S., Zhang, Y., and Zhang, Y. (2006). "Improving the aging resistance of asphalt by addition of Zinc dialkyldithiophosphate." *Fuel*, 85(7), 1060–1066.

Painter, P. C., Snyder, R. W., Starsinic, M., Coleman, M. M., Kuehn, D. W., and Davis, A. (1981). "Concerning the application of FT-IR to the study of coal: a critical assessment of band assignments and the application of spectral analysis programs." *Applied Spectroscopy*, 35(5), 475–485.

Palvadi, S., Bhasin, A., and Little, D. (2012). "Method to quantify healing in asphalt composites by continuum damage approach." *Transportation Research Record: Journal of the Transportation Research Board*, (2296), 86–96.

Park, S. W., Kim, Y. R., and Schapery, R. A. (1996). "A viscoelastic continuum damage model and its application to uniaxial behavior of asphalt concrete." *Mechanics of Materials*, 24(4), 241–255.

Park, S. W., and Schapery, R. A. (1999). "Methods of interconversion between linear viscoelastic material functions. Part I—A numerical method based on Prony series." *International Journal of Solids and Structures*, 36(11), 1653–1675.

Patrick, R. L. (1981). *Treatise on adhesion and adhesives*. CRC Press.

Perzyna, P. (1966). "Fundamental problems in viscoplasticity." *Advances in applied mechanics*, 9, 243–377.

Pfeiffer, J. P., and Saal, R. (1940). "Asphaltic bitumen as colloid system." *The Journal of Physical Chemistry*, 44(2), 139–149.

Phillips, M. (1998). "Multi-step models for fatigue and healing, and binder properties involved in healing." *Eurobitume workshop on performance related properties for bituminous binders, Luxembourg*.

Prager, S., and Tirrell, M. (1981). "The healing process at polymer–polymer interfaces." *The journal of chemical physics*, 75(10), 5194–5198.

Pronk, A. (2000). "Partial healing model—curve fitting." *Report W-DWW-2000–047*.

Pronk, A., and Cocurullo, A. (2009). "Investigation of the PH model as a prediction tool in fatigue bending tests with rest periods." *Advanced Testing and Characterisation of Bituminous Materials, Loizos, Partl, Taylor & Francis Group, London*.

Pronk, A., and Hopman, P. (1990). "Energy dissipation: the leading factor of fatigue." *Highway Research: Sharing the Benefits. The United States Strategic Highway Research Program*, London, England.

Puig, C., Meijer, H., Michels, M., Segeren, L., and Vancso, G. J. (2004). "Characterization of glass transition temperature and surface energy of bituminous binders by inverse gas chromatography." *Energy & fuels*, 18(1), 63–67.

Qiu, J., Molenaar, A., Van de Ven, M., Wu, S., and Yu, J. (2012). "Investigation of self healing behaviour of asphalt mixes using beam on elastic foundation setup." *Materials and structures*, 45(5), 777–791.

Qiu, J., Van De Ven, M., Wu, S., Yu, J., and Molenaar, A. (2010). "Durable Asphalt Pavements Are Self Healing." *Wuhan Ligong Daxue Xuebao(Journal of Wuhan University of Technology)*, 32(17), 30–34.

Qiu, J., de Ven, M. F. C., Wu, S., Yu, J., and Molenaar, A. A. A. (2009). "Investigating the self healing capability of bituminous binders." *Road Materials and Pavement Design*, 10(sup1), 81–94.

Rabotnov, Y. N., Leckie, F., and Prager, W. (1970). "Creep Problems in Structural Members." *Journal of Applied Mechanics*, 37, 249.

Radke, M., Willsch, H., and Welte, D. H. (1980). “Preparative hydrocarbon group type determination by automated medium pressure liquid chromatography.” *Analytical Chemistry*, 52(3), 406–411.

Raithby, K., and Sterling, A. (1970). “The effect of rest periods on the fatigue performance of a hot-rolled asphalt under reversed axial loading and discussion.” *Association of Asphalt Paving Technologists Proc*.

Raithby, K., and Sterling, A. (1972). “Some effects of loading history on the fatigue performance of rolled asphalt.” *Association of Asphalt Paving Technologists Proc.*

Read, J., and Whiteoak, D. (2003). *The shell bitumen handbook*. Thomas Telford.

Redelius, P., and Soenen, H. (2015). “Relation between bitumen chemistry and performance.” *Fuel*, 140, 34–43.

Reese, R. (1997). “Properties of aged asphalt binder related to asphalt concrete fatigue life.” *Journal of the Association of Asphalt Paving Technologists*, 66.

Richardson, C. (1905). *The modern asphalt pavement*. J. Wiley & sons.

Robertson, R. E., Branthaver, J., Plancher, H., Duvall, J., Ensley, E., Harnsberger, P., and Petersen, J. (1991). *Chemical properties of asphalts and their relationship to pavement performance*. Strategic Highway Research Program, National Research Council Washington, DC.

Rowe, G. M., and Bouldin, M. G. (2000). “Improved techniques to evaluate the fatigue resistance of asphaltic mixtures.” *2nd Eurasphalt & Eurobitume Congress Barcelona*.

Santagata, E., Baglieri, O., Dalmazzo, D., and Tsantilis, L. (2009). “Rheological and chemical investigation on the damage and healing properties of bituminous binders.” *Asphalt Paving Technology-Proceedings*, 28, 567.

Schapery, R. (1984). “Correspondence principles and a generalizedJ integral for large deformation and fracture analysis of viscoelastic media.” *International journal of fracture*, 25(3), 195–223.

Schapery, R. (1989). “On the mechanics of crack closing and bonding in linear viscoelastic media.” *International Journal of Fracture*, 39(1–3), 163–189.

Schapery, R. A. (1975). “A theory of crack initiation and growth in viscoelastic media.” *International Journal of Fracture*, 11(1), 141–159.

Schmets, A. J. M., Kringos, N., Scarpas, A., Duif, C., Schitter, G., and Pauli, T. (2009). “First-principles investigation of the multiple phases in bituminous materials: the case of asphaltene stacking.” *Advanced testing and characterisation of bituminous materials*, 1, 143–150.

Schmidt, R., and Santucci, L. (1966). “A practical method for determining the glass transition temperature of asphalts and calculation of their low temperature viscosities.” *Assoc Asphalt Paving Technol Proc*.

Seo, Y., and Kim, Y. R. (2008). “Using acoustic emission to monitor fatigue damage and healing in asphalt concrete.” *KSCE Journal of Civil Engineering*, 12(4), 237–243.

Shan, L., Tan, Y., Underwood, B. S., and Kim, Y. R. (2011). “Thixotropic Characteristics of Asphalt Binder.” *Journal of Materials in Civil Engineering*, 23(12), 1681–1686.

Shan, L., Tan, Y., Underwood, S., and Kim, Y. (2010). “Application of thixotropy to analyze fatigue and healing characteristics of asphalt binder.” *Transportation Research Record: Journal of the Transportation Research Board*, (2179), 85–92.

Shen, S., Chiu, H.-M., and Huang, H. (2009). "Fatigue and healing in asphalt binders." *Transportation Research Board 88th Annual Meeting*.

Shen, S., Chiu, H.-M., and Huang, H. (2010). "Characterization of fatigue and healing in asphalt binders." *Journal of Materials in Civil Engineering*, 22(9), 846–852.

Si, Z., Little, D. N., and Lytton, R. L. (2002). "Characterization of microdamage and healing of asphalt concrete mixtures." *Journal of materials in civil engineering*, 14(6), 461–470.

Simo, J. C., and Hughes, T. J. (2006). *Computational inelasticity*. Springer Science & Business Media.

Simpson, A., Gardner, T., Evans, M., and Kenwright, J. (2000). "Stiffness, strength and healing assessment in different bone fractures—a simple mathematical model." *Injury*, 31(10), 777–781.

Song, I., Little, D. N., Masad, E. A., and Lytton, R. (2005). "Comprehensive evaluation of damage in asphalt mastics using X-ray CT, continuum mechanics, and micromechanics (with discussion)." *Journal of the association of asphalt paving technologists*, 74.

Speight, J. G. (2014). *The chemistry and technology of petroleum*. CRC press.

Speight, J., and Plancher, H. (1991). "Molecular models for petroleum asphaltenes and implications for asphalt science and technology." 154.

Storm, D. A., Barresi, R. J., and Sheu, E. Y. (1996). "Development of solid properties and thermochemistry of asphalt binders in the 25− 65 C temperature range." *Energy & fuels*, 10(3), 855–864.

Stuart, B. (2005). *Infrared spectroscopy*. Wiley Online Library.

Suresh, S. (1991). "Fatigue of materials, Cambridge solid state science series." *Cambridge (UK)*, 236.

Tarefder, R. A., and Arisa, I. (2011). "Molecular dynamic simulations for determining change in thermodynamic properties of asphaltene and resin because of aging." *Energy & Fuels*, 25(5), 2211–2222.

Tarefder, R. A., Bateman, D., and Swamy, A. K. (2013). "Comparison of fatigue failure criterion in flexural fatigue test." *International Journal of Fatigue*, 55, 213–219.

Tarefder, R. A., and Yousefi, S. S. (2015). "Rheological examination of aging in polymer-modified asphalt." *Journal of Materials in Civil Engineering*, 28(2), 04015112.

Traxler, R. N. (1961). *Asphalt: Its composition, properties, and uses*. Reinhold Pub. Corp.

Ullidtz, P. (1999). "Development of New Bituminous Pavement Design Method: COST 333 Final Report of the Action."

Underwood, B. S. (2016). "A continuum damage model for asphalt cement and asphalt mastic fatigue." *International Journal of Fatigue*, 82, 387–401.

Van Dijk, W., and Visser, W. (1977). "Energy approach to fatigue for pavement design."

Vasconcelos, K. L., Bhasin, A., Little, D. N., and Glover, C. (2012). "Influence of the physical state of water in the diffusion process in asphalt binders." *TRANSPORTES*, 20(4), 12–18.

Verstraeten, J. (1991). "Fatigue of bituminous mixes and bitumen thixotropy." *19th World road congress, AIPCR, Marrakech, Morocco*.

Voyiadjis, G. Z. (2012). *Advances in damage mechanics: metals and metal matrix composites*. Elsevier.

Warren, F. J., Gidley, M. J., and Flanagan, B. M. (2016). “Infrared spectroscopy as a tool to characterise starch ordered structure—a joint FTIR–ATR, NMR, XRD and DSC study.” *Carbohydrate polymers*, 139, 35–42.

Wolf, E. (1970). “Fatigue crack closure under cyclic tension.” *Engineering Fracture Mechanics*, 2(1), 37in345-44in4.

Wool, R., and O’connor, K. (1981). “A theory crack healing in polymers.” *Journal of Applied Physics*, 52(10), 5953–5963.

Wool, R. P. (1991). “Welding, tack, and green strength of polymers.” *Fundamentals of adhesion*, Springer, 207–248.

Wool, R. P. (2008). “Self-healing materials: a review.” *Soft Matter*, 4(3), 400–418.

Yesiltas, M., and Kebukawa, Y. (2016). “Associations of organic matter with minerals in Tagish Lake meteorite via high spatial resolution synchrotron-based FTIR microspectroscopy.” *Meteoritics & Planetary Science*, 51(3), 584–595.

Zhang, M. Q., and Rong, M. Z. (2012). “Theoretical consideration and modeling of self-healing polymers.” *Journal of Polymer Science Part B: Polymer Physics*, 50(4), 229–241.

Zhang, Z., Roque, R., Birgisson, B., and Sangpetngam, B. (2001). “Identification and verification of a suitable crack growth law (with discussion).” *Journal of the Association of Asphalt Paving Technologists*, 70.

Zhu, X., Cai, Y., Zhong, S., Zhu, J., and Zhao, H. (2017). “Self-healing efficiency of ferrite-filled asphalt mixture after microwave irradiation.” *Construction and Building Materials*, 141, 12–22.

APPENDIX A

Separating Viscoelastic Recovery from Healing

Two PG binders (PG 64-22 and PG 70-22) are loaded in the LVE limit (0.75% and 1% strain) and out of the LVE limit (5% strain). The strain within the LVE limit is used to calculate the viscoelastic (VE) recovery and the strain out of LVE limit is used to calculate the healing. The recovery of modulus after loading is plotted in Figure A1. The recovery of modulus shoed in this figure is calculated from the difference between the modulus after rest period and modulus at the end of the loading. It can be seen that for both binders the VE recovery is very small compared to the recovery due to healing. The VE recovery is only 10 to 15% of the overall recovery due to healing at10s of rest period. The percent VE recovery also decreases as the rest period increases, due to the increase in healing. Therefore, the VE recovery is not separated from the healing in the physico-chemical healing model (chapter 5 and 6). However, in the constitutive damage model discussed in chapter 7, both VE recovery and healing is considered.

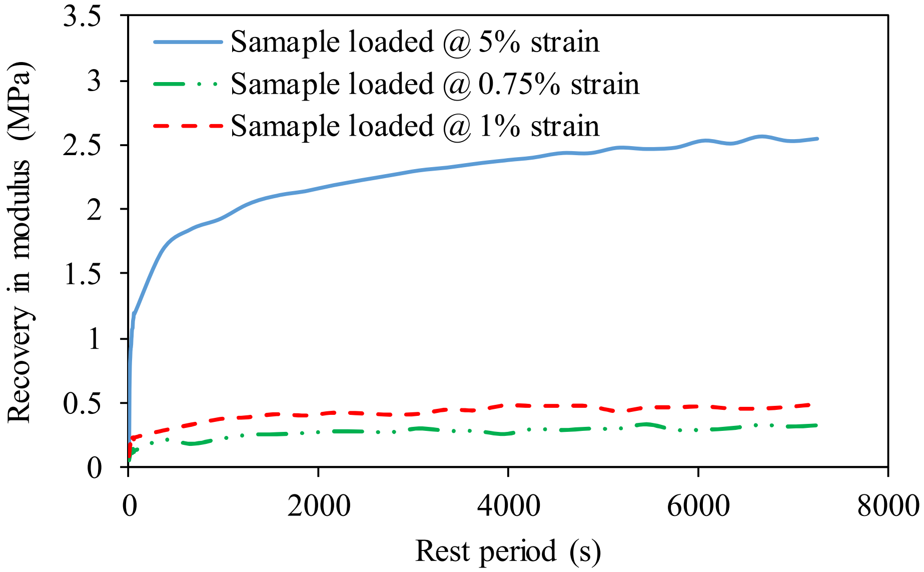

(a) PG 64-22

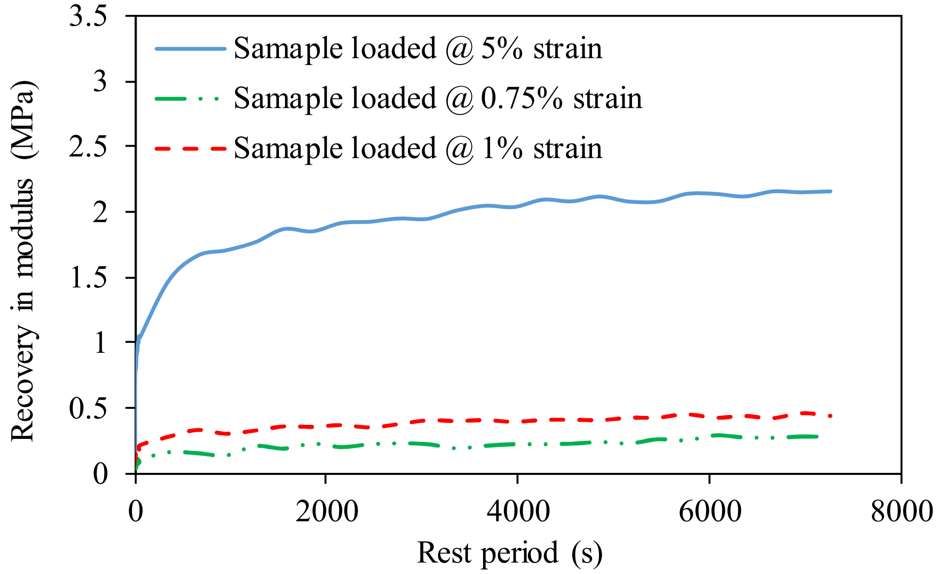

(b) PG 70-22

Figure A1: Recovery of modulus due to healing and VE recovery in binders

APPENDIX B

FTIR Peak Area Calculation

The peak area calculation of FTIR spectrum is conducted by the Spectrum software provided with the FTIR instrument. Figure B1 shows the area for all five PG binders:

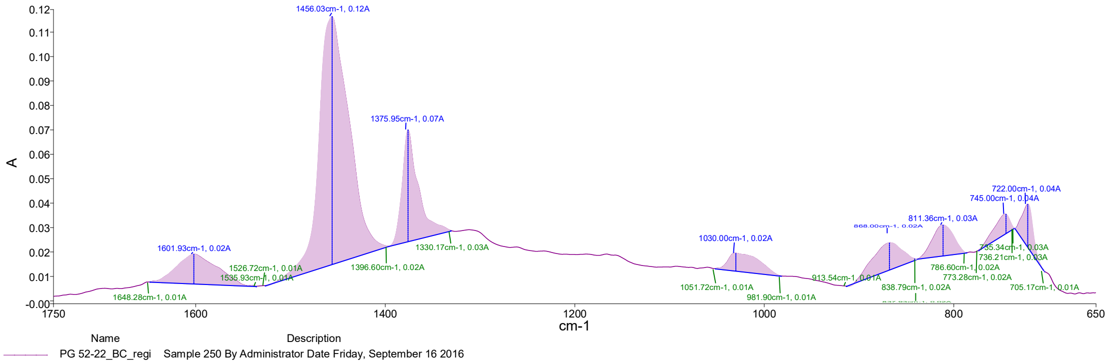

(a) PG 52-22

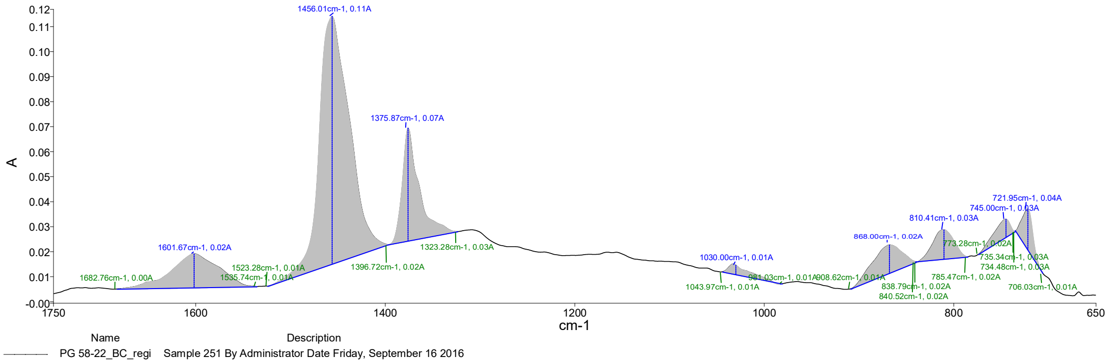

(b) PG 58-22

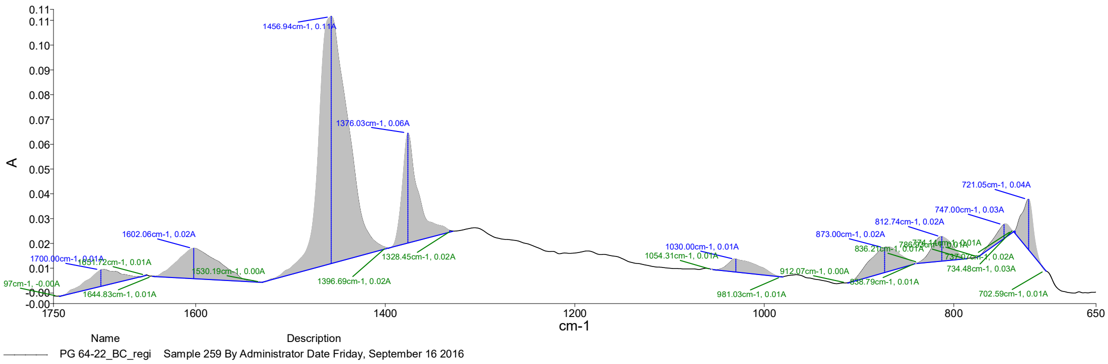

(c) PG 64-22

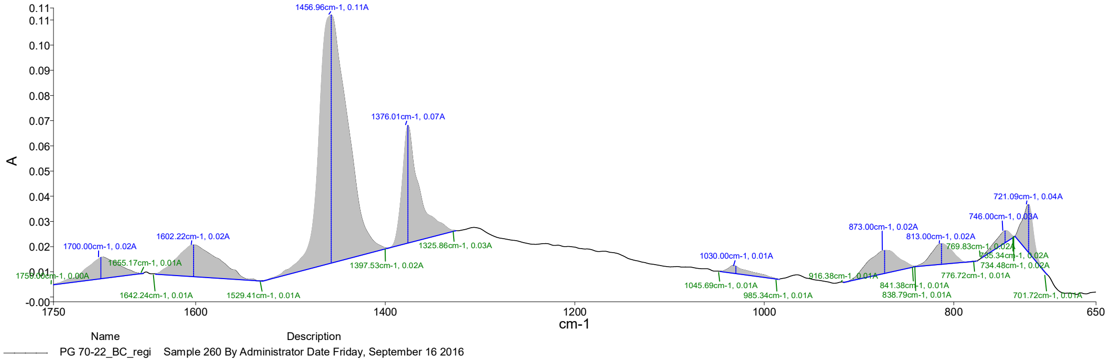

(d) PG 70-22

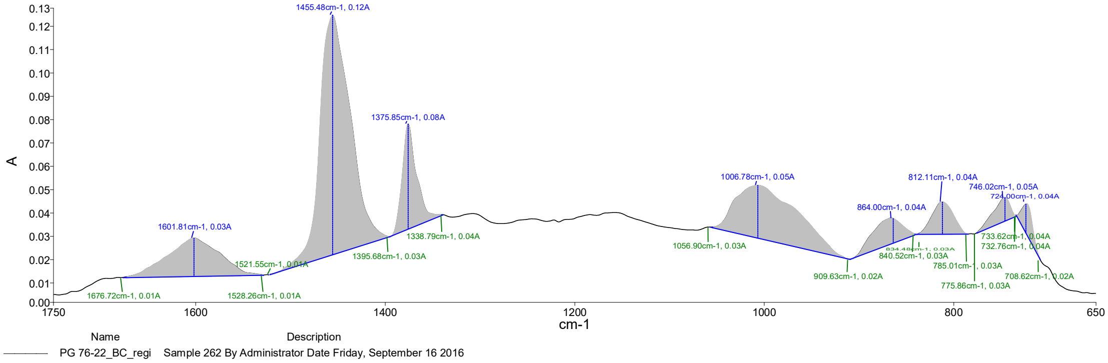

(e) PG 76-22

Figure B1: Peak area calculation for FTIR spectrum of different PG binder